A survey of bubble chamber results on differential cross-sections for high energy π(^+)p quasi two body interactions

Wood, I.

A survey of bubble chamber results on differential cross-sections for high energy π^+p quasi two body interactions.

by

I. Wood, B.Sc.

A Thesis submitted to the University of Durham for the degree of Master of Science.

June 1973.

Errata

P23 line 12	For 'indication of mass' read 'indication of the velocity of the particle, which when taken together with the momentum gives an indication of the particle mass'.
P23	The rule relating to the exchange of the Pomeron, sometimes known as the 'Gribov-Morrison' rule, is by no means firmly established either experimentally or theoretically and so it would be more correct to state that it may possibly hold but is not certain. (Morrison D.R.O. 1968 Phys. Rev. 165 p1690)
P33	It should be clarified that the width of the resonance affects the sharpness of the turnover, and hence this has a bearing on the visibility of the turnover on the graphs.
Figures 14 - 25	There may be a slight error in the calculation for these diagrams, though the equation on which they are based and the form of the graphs are correct. Caution should therefore be exercised when using these graphs. The error is only small and is systematic. It does not affect any of the arguments nor their outcome in the thesis.
P35	Even when a Δ^{++} is produced with $t = 0{\cdot}06\ (\mathrm{GeV/c})^2$, more than 80% of the protons from its decay will have momenta above 100 MeV/c, and therefore the argument as presented does not provide a convincing explanation for the dips observed in figure 33. Hence these dips could be of a physical nature and not the product of experimental techniques.

CONTENTS

ABSTRACT

The thesis is based on a survey of differential cross-sections of quasi two body interactions occurring in $\pi^+ p$ interactions studied in hydrogen bubble chambers. The first two chapters outline the theoretical background for the description of such interactions. The third chapter discusses kinematical and observational effects which can influence the measured shape of the differential cross-section as a function of the four momentum transfer at small values of the latter, and the last chapter surveys, empirically the collected data with particular reference to the discussion of the previous chapter.

It is concluded that in general the differential cross-section falls exponentially with increasing magnitude of four momentum transfer, but that in two reaction channels ($\pi^+ p \to \Delta^{++} A_2^o$ and $\pi^+ p \to \Delta^{++} \eta^o$) there is a significant dip as t approaches zero that cannot be explained by either kinematical effects or experimental bias.

CHAPTER ONE

INTRODUCTION

The following work is concerned with a review of the behaviour of differential cross-sections for high energy collisions of the type

$$\pi^{\pm} p \rightarrow B + M$$

where B and M represent a non-strange baryon and meson system respectively. The results are obtained from bubble chamber experiments, and consideration is given to the possible experimental biases that might cause an apparent reduction in the measured differential cross-section in the region of a zero degree production angle. A compilation of total cross-sections for $\pi^{\pm}p$ interactions in general is given in ref. 1. To see the relevance of the study of such cross-sections chapter two summarises the general theorems concerning the expected behaviour of these, and discusses some of the predictions of simple one particle exchange models. In this first chapter an introduction is given to particle properties, this providing a base for the discussion of their strong interactions. In general the review will only be concerned with non-strange hadrons (see Appendix 1) but for completeness some mention is made in parts of other types of particle and their interactions.

1.1. Particles and their intrinsic properties

Mainly as a result of experiments using proton accelerators many elementary particles other than the proton, neutron and electron have been discovered. The known elementary particles fall naturally into two broad categories according to whether their spin is integer or half-integer, and hence are classified either as Bosons which have integral spin and obey Bose-Einstein statistics, or as Fermions which have half-integral spin and obey Fermi-Dirac statistics. These broad categories can then be subdivided; Fermions are either Leptons or Baryons while the Bosons contain the photon (γ), which is the quantum of the electro-magnetic field, and mesons which can be thought of as quanta responsible for the strong or nuclear interaction.

Four basic interactions are thought to occur between elementary particles:-

(i) the gravitational interaction which is very weak and hence its effects have never been detected in experiments which involve only a small number of elementary particles.

(ii) the electro-magnetic interaction which connects all charged particles, and also those having magnetic dipole moments, via the emission and absorption of photons.

(iii) the weak interaction which is responsible for the majority of the decays of unstable particles and includes β-decay.

(iv) the strong interaction which connects all the baryons via the emission and absorption of mesons, the family of particles involved in this interaction being called quite generally 'hadrons'.

The relative strengths of these interactions are shown in table 1, while table 2 lists the non-strange mesons and baryons that occur in the final states of the interactions that are reviewed later.

Table 1:- Relative strengths of known forces.

Type	Relative strength	Approx. range (cms)
Strong	1	10^{-13}
Electro-magnetic*	10^{-2}	∞
Weak	10^{-14}	$<< 10^{-13}$
Gravitational*	10^{-38}	∞

*Proton-proton interaction
These are compared at a range of 10^{-13} cms.

From table 2 it can be seen that whereas some particles are stable or have lifetimes $>> 10^{-23}$ secs, others have very short lifetimes, and associated with this via the uncertainty principle, masses which are not sharp in value. The very short lived particles (e.g Δ ρ) are known as resonances, the basic physical differences between particles and resonances being the manner in which they can decay. Whereas the shorter lived particles have a strong decay channel open to them, the longer lived particles can only decay by means of the weak interaction, or as in the case of the π^{o} and η decays electro-magnetically.

1.2. Interactions - experimental description

It is found that when two given hadrons interact many different final states involving various types and numbers of particles may be formed. There are constraints however on the transitions that are possible from an initial to final state, these being imposed by the conservation of energy, linear and angular momentum and certain quantum numbers (see appendix 2). For example, interactions in which negative pions react with a proton can lead to numerous possible final states, some of which are:-

Table 2 (i) Hadrons stable against decay by strong interaction.

Particle	$I^G(J^P)C_n$.*	Lifetime (secs)	Mass width
$\pi^{\pm}$	$1^-(0^-)^+$	2.6×10^{-8}	0.0
π^o	$1^-(0^-)^+$	0.84×10^{-16}	7.8 ± 0.9eV
η	$1^-(0^-)^+$	2.53×10^{-19}	2.6 ± 0.6KeV
p	$\frac{1}{2}(\frac{1}{2}^+)$	2.10^{28}years	0.0
n	$\frac{1}{2}(\frac{1}{2}^+)$	935	0.0

(ii) Selection of hadrons unstable against strong decay (resonances).

Particle	$I^G(J^P)C_n$	Lifetime (secs)	Mass width (MeV)
ρ	$1^+(1^-)^-$	5.07×10^{-24}	135 ± 20
ω	$0^-(1^-)^-$	6.58×10^{-23}	10 ± 0.6
A_1	$1^-(1^+)^+$	6.6×10^{-24}	$50 \rightarrow 200$
A_2	$1^-(2^+)^+$	6.58×10^{-24}	100 ± 20
A_3	$1^-(\ \ )^+$	6.6×10^{-24}	$50 \rightarrow 200$
B	$1^+(1^+)^-$	6.58×10^{-24}	100 ± 20
f	$0^+(2^+)^+$	4.30×10^{-24}	156 ± 25
Δ	$^3/_2(^3/_2^+)$	5.98×10^{-24}	$100 \rightarrow 122$

*Footnote:- See Appendix 2 for an explanation of these quantum numbers.

$$\pi^- p \rightarrow \pi^- p \qquad (a)$$
$$\rightarrow \pi^0 n \qquad (b)$$
$$\rightarrow p\, \pi^0 \pi^- \qquad (c)$$
$$\rightarrow p\, \pi^- \pi^0\, \pi^0 \qquad (d)$$

Each of these transitions is called a channel for the reaction. Channel (a) is termed the 'elastic' channel since the same particles are present in the final state as are in the initial one, while channels (b), (c) and (d) are all 'inelastic', as are all interactions in which different particles are present in the final state. (b) is also known as a charge exchange interaction since the particles in the final state differ from those in the initial one merely because they have exchanged an electric charge between themselves.

It is possible for two or more particles in the final state to result from the rapid decay of an intermediate particle which cannot be observed. This has been deduced to occur by studying the so called 'invariant mass' of the combination of two or sometimes more final state particles, which is defined thus*:-

$$m_n^2 = \Big(\sum_{i=1,n} Ei\Big)^2 - \Big(\sum_{i=1,n} \vec{pi}\Big)^2 \qquad (1.1)$$

E_i = energy of i'th particle in an n-particle combination

p_i = 3-momentum " " " " "

Considering reactions (c) and (d); if the combined mass of particular particles, in this case the ($\pi\pi$) or (π p), were calculated a smooth curve for the mass frequency distribution would be expected if this combination were random. In fact various peaks occur indicating that very short lived particles are created these being called

* Unless otherwise stated natural units are used (c = h = 1)

'resonances'. Thus instead of reactions (c) and (d) occurring as they initially appear as shown in fig. 1.

Figure 1 Reaction as seen to occur.

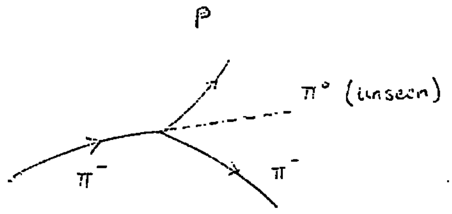

reaction (c)

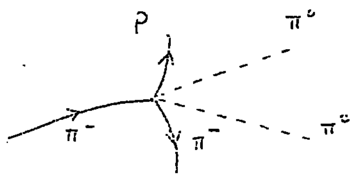

reaction (d)

in a significantly large fraction of cases they arise as shown in fig. 2 where the Δ and ρ are resonances with lifetimes too short to indicate their presence directly.

Figure 2 Reaction as deduced to occur. Note that the lifetimes of Δ and ρ are too short to leave visible evidence of their path.

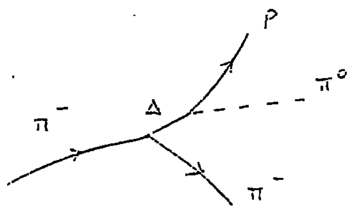

reaction (c)

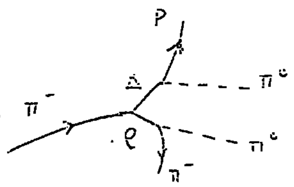

reaction (d)

In the energy range being discussed, resonances are produced very frequently, and in this review only those reactions which can be interpreted as having two particles in the final state will be considered, even though one or both of these may be resonances decaying into a number of particles themselves. These channels are said to be 'quasi two body' interactions.

1.3. Basic description of transitions

The dynamical behaviour of a quantum-mechanical system develops in a manner which is related to its Hamiltonian, though for strong interactions this Hamiltonian is difficult to construct. To describe interactions, generally perturbation theory is used in which the Hamiltonian is split into two parts H_o and H_I such that:-

$$H = H_o + H_I \tag{1.2}$$

where H_o = Hamiltonian of the free particles

H_I = Hamiltonian of the interaction between the particles.

For electro-magnetic interactions the results obtained agree very well with experiment but for strong interactions this method is not successful since their strength makes it invalid to treat the interactive part as a perturbation.

An alternative approach has therefore been used, this being the S-matrix, whose elements are in principle directly observable scattering or decay amplitudes, and hence give the transition probability from a given initial state to one of the possible final states. This matrix is in fact a function of the kinematic variables describing the particles involved in the transition. The S-matrix element $<f'| S |i'>$ is the amplitude for an initially observed free particle state $|i'>$ to be observed as the final free particle state $|f'>$. Included in the S matrix are the elements $<f'|i'>$ representing no interaction. An actual interaction of the particles is described by an amplitude which is i times the T-matrix. (The $i = \sqrt{-1}$ appears solely by convention). Thus:-

$$<f'|S|i'> = <f'|i'> + i<f'|T|i'> \tag{1.3}$$

The T-matrix then depends on the particle momenta, and also on their spin and isospin and any other internal properties. (ref. 2).

The theoretical problem then becomes one of extracting the analytical behaviour of the scattering amplitudes from the experimental measurements, or more usually, exploiting the latter to investigate an assumed theoretical behaviour. Though the transition amplitudes are in general unknown functions of the kinematic variables and internal properties (such as spin), the following chapters are mainly concerned with their dependence on the kinematic quantities which are conveniently summarised by the Mandelstamm variables s, t and u which will now be described.

1.4. The Mandelstamm variables.

The Mandelstamm variables s, t and u are defined in terms of the kinematic quantities shown in fig.3 for the reaction:-

$$a + b \rightarrow c + d \tag{1.4}$$

Figure 3 Kinematic notation for the quasi two body interation a+b→c+d in the centre of mass system

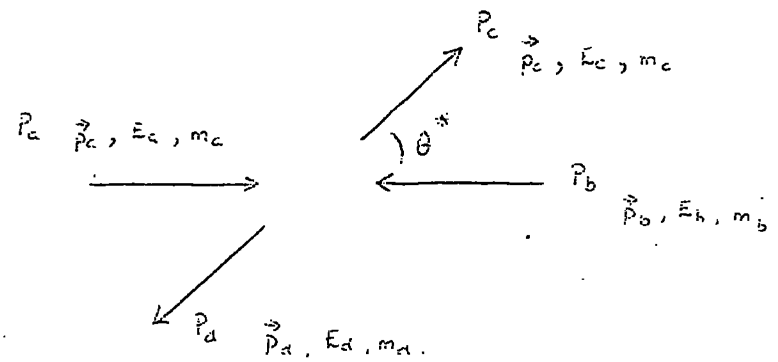

where, $\vec{p}$ = momentum 3-vector
E = Total energy
m = rest mass
P = Energy momentum 4-vector $(E, \vec{p})$
$P_a P_b = E_a E_b \quad \vec{p}_a \cdot \vec{p}_b$

The variables are given by the relations

$$s = (P_a + P_b)^2 = (P_c + P_d)^2 \tag{1.5}$$

$$t = (P_c - P_a)^2 = (P_b - P_d)^2 \tag{1.6}$$

$$u = (P_a - P_d)^2 = (P_c - P_b)^2 \tag{1.7}$$

Thus in the centre of mass where $\vec{p}_a + \vec{p}_b = 0$:-

$$s = (E_a + E_b)^2 = (\text{centre of mass energy})^2 \qquad (1.8)$$

In terms of P_d and P_b

$$\begin{aligned} t &= (P_d - P_b)^2 \\ &= -(\vec{p}_d - \vec{p}_b)^2 + (E_d - E_b)^2 \qquad (1.9) \\ &= (m_d^{\ 2} + m_b^{\ 2}) - 2E_dE_b + 2p_dp_b \cos\theta^* \quad \text{cms system} \\ &= (m_d^{\ 2} + m_b^{\ 2}) - 2E_b^{\ \text{lab}}\, m_d \quad \text{lab system} \end{aligned}$$

where particle b is at rest in the laboratory.

Similarly:-

$$u = (m_a^{\ 2} + m_d^{\ 2}) - 2E_dE_a + 2p_dp_a \cos\theta^* \quad \text{cms system}$$

$$s + t + u = (P_a + P_b)^2 + (P_c - P_a)^2 + (P_a - P_d)^2$$

$$= m_a^{\ 2} + m_b^{\ 2} + m_c^{\ 2} + m_d^{\ 2}$$

Now one of the properties of an equilateral triangle is that the sum of the perpendicular distances from its sides to any point is a constant, and this fact can be utilised, enabling the graphical representation shown in fig. 4 to be drawn.

Figure 4 The plane of the kinematic-invariant variables s, t and u

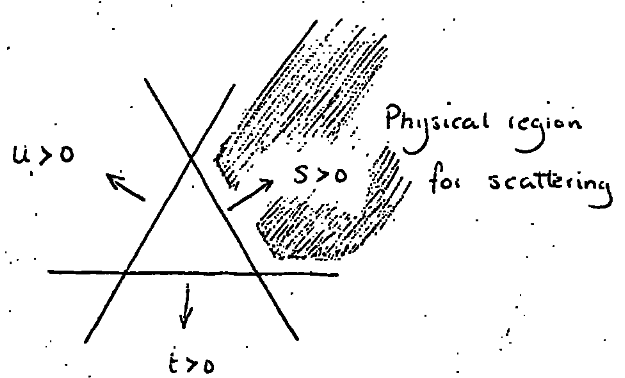

Since $d\Omega = d(\cos \theta^*)$ and $t \alpha \cos \theta^*$ (see equation 1.9), it can be seen that the differential cross-section in the centre of mass $d\sigma / d\Omega$, with which this review is mainly concerned, is easily expressed as $d\sigma/dt$, and in accordance with normal practice in this field, the latter will be employed as a measure of the differential cross-section.

CHAPTER TWO

Introduction.

The results of the many experiments which have studied high energy interactions have indicated that the inelastic production processes are characterised by a number of common features:-

(i) In many cases, the inelastic collisions do not proceed directly to their final state, but rather go through an intermediate one in which strongly decaying particles are produced (eg ρ, ω, η) - the feature of the strong decays being that the resonant states have extremely short lifetimes.

(ii) Up to about 20 GeV/c incident particle momentum, many of these inelastic reactions appear to be quasi two body interactions. The resulting secondary particles have a tendency to go in the forward-backward direction in the centre of mass system, this preference generally becoming more pronounced with increasing primary momentum and less pronounced with increasing number of secondary particles.

This chapter presents some theoretical considerations which are relevant when trying to explain the results obtained from quasi two body interactions occurring at various energies. The first section deals with asymptotic theorems, valid for s (the total interaction energy) tending to infinity. The second part of the chapter deals with peripheral collisions and describes theories which involve a single particle exchange between the two interacting particles. This is subdivided into two sections, the first dealing with one pion exchange, and the second with vector-meson exchange. The last section deals very briefly with Regge theory, this approach being an attempt to provide a more satisfactory theoretical basis for high energy interactions than those described in the preceding sections.

2.1. Asymptotic theorems

At high energies, hadron interactions display certain general properties, such as the energy dependence of their total cross-sections σ_T. For elastic cross-sections, the data indicates that σ_{el}/σ_T (where σ_{el} is the elastic cross-section) tends to a constant as the interaction energy increases. (i.e. $s \to \infty$).

The first of the theorems to describe the asymptotic behaviour of interactions was that postulated by Pomeranchuk in 1958 (ref. 3) which states that if the total cross-section for a-b and $\bar{a}$-b collisions both tend to constants, then these constants must be equal:-

$$\lim_{s \to \infty} \sigma_T (ab, s) = \lim_{s \to \infty} \sigma_T (\bar{a}b, s) \tag{2.1}$$

thus implying common limiting values for $\sigma_T (\pi^+ p)$ and $\sigma_T (\pi^- p)$ etc.

This theorem can be applied to the elastic scattering case since there is a link between this channel and the total cross-section, provided by the Optical Theorem. (ref. 4) It is assumed that for large s and small t, T(s,t), the elastic scattering amplitude, can be expanded in the form:-

$$T(s,t) = \sum_{n=o}^{\infty} b_n (t)\, s^{\alpha_n (t)} \tag{2.2}$$

where $\alpha_n(t)$ are real functions of t ordered such that for fixed, t,

$$\alpha_o > \alpha_1 > \alpha_2 \tag{2.3}$$

and the functions $b_n(t)$ are arbitrary complex functions of t. It can be demonstrated that:-

$$\bar{b}_n^* = b_n e^{i\pi\alpha_n} \tag{2.4}$$

where $\bar{b}^*$ is the complex conjugate of the crossed channel amplitude b. From $|\bar{b}_o| = |b_o|$, one obtains in the asymptotic region $s \to \infty$,

$$\frac{d\sigma}{dt}(s,t) = \frac{d\bar{\sigma}}{dt}(s,t) \tag{2.5}$$

i.e. equality of the elastic differential cross-sections. From the observed constancy of the total cross-sections, at high energy, $\alpha_o(t=0)=1$, in which case 2.4 yields for b_o :-

$$\text{Im } b_o = \text{Im } \bar{b}_o \quad ; \quad \text{Re } b_o = -\text{Re } \bar{b}_o \tag{2.6}$$

This then implies Pomeranchuk's Theorem 2.1. As a particular example, the real part of T(s,t) for $\pi^{\pm}$ p elastic scattering has been obtained from its interference with Coulomb scattering at small angles; for both π^+p and π^-p scattering it is small and negative, and so it may be concluded that Re b_o = 0, i.e. that Re T(t=0) comes from the next term in the expansion.

It would therefore be expected that:-

$$\lim_{s \to \infty} \frac{\text{Re } T(s,t)}{\text{Im } T(s,t)} = 0, \text{ for small } |t| \tag{2.7}$$

Also, since $T(\pi^- p \to \pi^o n) = T - \bar{T}$, the ratio of the charge exchange to the elastic cross-section should tend to zero, in good agreement with experiment.

2.2. Peripheral collisions: one particle exchange

a) One pion exchange

A striking feature of high energy interactions is the peripheral nature of collisions. For meson-nucleon reactions of the type $ab \to cd$, the differential cross-sections have a sharp peak near t = 0, which drops exponentially for increasing $|t|$ (see for example figure 26).

This is most evident for elastic scattering but applies generally to charge exchange and inelastic quasi two body reactions also, the momentum transfer from the initial to the final baryon, or baryon resonance, nearly always preferring small values.

A step in the development of the peripheral model was the introduction of the idea of the exchange of a single pion between the interacting particles (refs. 5, 6, 7, 8, 9, 10 and 11). By the Uncertainty Principle, the longer range interactions are due to particles with lower mass energy (i.e. the lighter particles, since it is these that are the most likely to exist further, from the nucleon. Therefore it is these particles that are the most likely mechanisms to be in operation for peripheral collisions. A diagram representing one particle exchange is shown in fig. 5.

Figure 5:- One particle exchange diagram

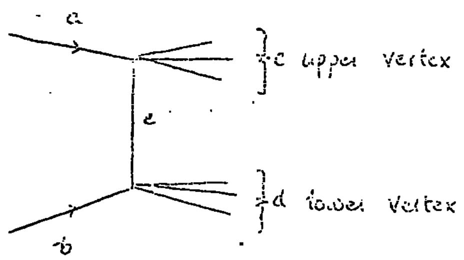

The matrix element T_π of a π-exchange process in momentum space is given by (ref. 12):

$$T_\pi(ab\to cd) = \frac{1}{\mu^2-|t|} T\,(\pi a\to c)\;\; T\,(\bar{\pi}\, b\to d) \qquad (2.8)$$

Where μ is the pion mass

The matrix elements $T(\pi a\to c)$, and $T(\bar{\pi} b\to d)$ refer to collisions of a virtual pion (anti-pion) with a particle a (b).

In the simplest version of the peripheral model (the so-called 'pole-approximation'),the pion is treated as being real, both at the upper and lower vertex (see figure 5). Replacing $|t|$ by μ^2 in $T(\pi a \to c)$ and $T(\pi b \to d)$ in 2.8, the differential cross-section is obtained in the form:-

$$\frac{d\sigma}{d|t|\, ds_{ab}\, ds_{cd}} = \frac{1}{64\, q^2 s} \frac{C(s_{cd})\, C(s_{ab})}{(\mu^2 - |t|)^2} \qquad (2.9)$$

where q is the incident particle momentum in the centre of mass and $C(s_{ab}) = \frac{1}{2\pi} \int d\left[\mathrm{Lips}\,(s_{ab};\, P_a, \ldots P_d)\right] |T(a\pi \to c)|^2$ with a similar relation for $C(s_{cd})$ (ref. 13). The expression $d\left[\mathrm{Lips}(s_{ab} \ldots P_d)\right]$ is a differential element of the Lorentz invariant phase space (ref. 14) and is independent of t.

The main achievment of 2.9 is to reproduce the strong forward peak in $|t|$ due to the pion pole at $|t| = \mu^2$. The exchange of other mesons or meson resonances will also contribute, but the corresponding $d\sigma/d|t|$ will become smaller and less peaked as the exchange particle masses get larger, since the mass appears in the denominator of the expression.

Knowing the spins and parities of the resonances, the pole approximation 2.8 may be improved upon by including the appropriate spin factors, and the Born term model (ref. 12) approximates the invariant amplitude at each vertex to its value at the pole of the exchanged particle; i.e. by the relevant coupling constant. For π-exchange in the reaction $ab \to cd$, the Born terms are then of the general form:-

$$T_\pi^{Born}(s, t, m_a, \ldots m_d) =$$

$$\frac{1}{(\mu^2 - |t|)} B_{a\pi c}(t, m_a, m_c)\, B_{b\pi d}(t, m_b, m_d) \qquad (2.10)$$

where:- $B_{a\pi c}$ and $B_{b\pi d}$ are the vertex functions in the Born approximation and $m_a \ldots m_d$ are magnetic quantum numbers.

Considering the implications of 2.10:-

(i) The dependence on the magnetic quantum numbers allows the decay distributions of the resonances to be computed.

(ii) The s independence of T is predicted. Consequently the differential cross-section should decrease as $(p^{lab})^{-2}$:-

$$\frac{d\sigma}{dt}(s,t) = \frac{\pi}{4q^2 s} \left| \frac{T(t)}{4\pi} \right|^2$$

$$= \frac{\pi}{(2m_b\, p^{lab})^2} \left| \frac{T(t)}{4\pi} \right|^2 \qquad (2.11)$$

It should be noted that finite mass widths of resonances are not included in this treatment.

b) <u>Vector meson exchange</u>

In πp collisions of the quasi two particle type, due to restrictions on the exchange of quantum numbers between the two vertices (see 3-1), single pion exchange is allowed for Δf or $\Delta\rho$ production, but not for $\Delta\omega$ or $\Delta\eta$ channels, which even so are about as peripheral as π-exchange reactions. However for these latter two channels, even though π-exchange is not allowed, vector meson exchange can occur, and it is quite possible that these peripheral reactions are related to such vector meson exchange processes.

In the Born term model, the scattering amplitude is related to the mass of the exchanged meson, and to the quantum numbers of the four particles involved. Quite generally, the number of independent couplings for a given vertex is found from helicity considerations, and is given by the number of independent helicity amplitudes.

It is possible to write the scattering amplitude T as a sum:-

$$T = T_{\pi} + T_{V} + \dots \qquad (2.12)$$

where:- T_{π} is the one pion exchange amplitude

and T_{V} is the vector meson exchange amplitude

The differential transition probability due to vector meson exchange for unpolarised particles, is found to be given by a second degree polynomial in s:-

$$\sum_{m_a \dots m_d} \left| T_V (s, t, m_a \dots d_d) \right|^2 = A(t)\, s^2 + b(t)\, s + C \qquad (2.13)$$

with $A(t) \neq 0$ (ref. 15).

For $s \to \infty$ 2.13 implies constant $d\sigma/dt$ (cf 2.11), but experimentally the cross-sections for inelastic reactions of the type $ab \to cd$ with vector exchange tend to zero with increasing energy, and this energy dependence problem is quite a serious difficulty with the Born term model for Vector exchange.

c) <u>A specific test of the Born term model</u>

As a specific test of the Born term model the detailed shape of the peripheral peak can be studied. In the pole approximation (2.8), the maximum always occurs at the beginning of the physical region (though where c and d are broad resonances, the dependence of this starting point on the particular mass of the exchanged particle must be considered, since this mass can vary between relatively wide limits). However in the Born term model (2.10) the maximum of the peripheral peak is moved to a slightly higher value of $|t|$ since the vertex factors, increase with increasing $|t|$. Experimentally, the peripheral peak has a roughly exponential shape:-

$$\frac{d\sigma}{dt} \approx \text{constant} \times e^{-b|t|} \qquad (2.14)$$

and in many reactions b is of the order $5(\mathrm{GeV}/c)^{-2}$. However, the pole approximation (2.9) gives a flatter $d\sigma/dt$, except possibly for very small t. The Born term model fits even less well, but instead of being abandoned, the general π-exchange matrix element (2.8) is written in the form:-

$$T_\pi(ab \to cd) = T_\pi^{Born}(ab \to cd)\, F(Ma^2, M_c^2, t)\, F(M_b^2, M_d^2, t) \qquad (2.15)$$

where the F 's are 'form factors' associated with the two vertices, which give better agreement, (refs. 16,17, 18).

2.3. Regge Poles

The one particle exchange model, though reasonably successful, has a number of failures; for instance its energy dependence is entirely governed by the spin of the exchanged particle (i.e. the particular t-channel partial wave that is assumed to dominate), and when $s \to \infty$, and the orbital angular momentum ℓ of the exchanged particle is greater than one, this leads to an infinite total cross-section.

A Regge trajectory correlates particles (i.e. bound states and resonances) of the same internal quantum numbers and of the same parity, but with spins that differ by units of two. Provided these requirements are fulfilled, any number of particles may lie on the same trajectory. Regge expanded the partial wave scattering amplitude, which is an analytic function of energy, postulating that the radial Schrödinger Equation should be able to be solved for arbitrary complex ℓ values, providing $\mathrm{Re}\,\ell > -\frac{1}{2}$. A Regge pole is thus a pole or the partial wave amplitude in the complex ℓ plane, and as the energy varies, the pole moves within this plane. The high energy quasi two body reactions are then predicted to be dominated by the exchange of a few of these Regge trajectories (ref. 19,20).

CHAPTER THREE

Introduction

The tendency for the secondary particles from a quasi two body interaction to go in the forward-backward direction in the reaction centre of mass can be observed by studying $d\sigma/dt$ and, as has already been mentioned, experimentally this leads to an approximately exponentially decreasing curve when it is plotted against $|t|$. This curve however sometimes deviates from an exponential behaviour at very low $|t|$, typically $|t| < 0.1$ $(\text{GeV}/c)^2$, in that for some reactions the curve changes the sign of its gradient, causing a dip at low values of $|t|$.

It would not be unreasonable to suppose that such distinctive behaviour might be correlated with the type of exchange particles for each given reaction channel and it is from this point of view that the reaction channels are grouped in chapter four. In this chapter (section 3.1) the approach used for deciding which particles can be exchanged is discussed and the ones relevant to the channels reviewed are tabulated.

The experimental observation of a dip in $d\sigma/d|t|$ may not, however, only arise from the interaction characteristics. Sections 3.2 and 3.3 are concerned with purely experimental and kinematical effects respectively that could lead to such an effect.

3.1 Quantum numbers of the exchanged particle

In this section the various reaction channels which are studied in the next chapter are listed and their possible exchange particles tabulated.

To illustrate the method used to determine the possible exchange particles, the reaction $\pi^+ p \rightarrow \Delta^{++} \pi^0$ is considered. From conservation of quantum numbers (see Appendix one), viz angular momentum, parity, G-parity, isospin and strangeness at each vertex of figure 6, and from the known quantum numbers of the particles, a, b, c and d (which correspond to π^+, p, Δ^{++} and π^0 in this case), a possible exchange particle can be deduced:-

<u>Figure 6</u>:- One meson exchange diagram for the general two-body reaction ab→ cd

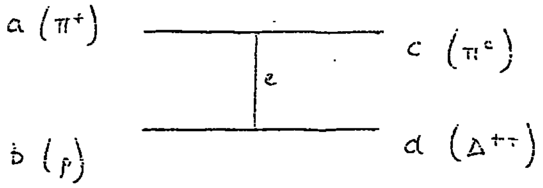

(i) <u>Strangeness</u> Since a, b, c and d all have strangeness number zero, conservation of strangeness at each vertex implies that e must also have strangeness zero.

(ii) <u>G-parity</u> This is a multiplicative quantum number having the values ± 1. Each particle with its baryon number and strangeness both zero is in an eigenstate of the G-operator, i.e. has definite G-parity. The pion has G-parity G = -1, and from G-parity conservation at the meson vertex, where $\pi^+ + e \rightarrow \pi^0$ it follows $G_\pi \cdot G_e = G_\pi$. Hence $G_e = +1$.

(iii) <u>Angular momentum and parity</u> The collision of the exchange particle with the incoming π^+ as seen in the rest system of the outgoing π^0 for the meson vertex is shown in figure 7.

<u>Figure 7</u> :- Meson vertex

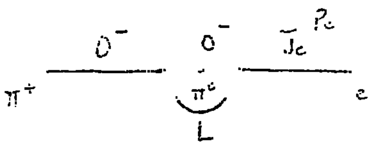

J^P = spin parity

L = relative orbital angular momentum of π and e.

Due to angular momentum conservation, the vectors $\vec{L}$ and $\vec{J}_e$ must be added to give the zero spin of the π^o; therefore $L = J_e$. From parity conservation:-

$$P_\pi . P_e . (-1)^L = P_\pi$$
$$P_e = (-1)^L = (-1)^{J_e}$$

Therefore the exchanged particle must have natural parity (ie $P = (-1)^J$); [P is unnatural if it equals $(-1)^{J+1}$];
ie $J_e^{P_e} = 0^+, 1^-, 2^+, 3^- \ldots$

(iv) Isospin   Isospin conservation at the baryon vertex demands that the isospin I_e of e must be coupled with the nuclear isospin of $\frac{1}{2}$ to give the Δ^{++} isospin 3/2. This is possible if I_e equals either 1 or 2. Similarly for isospin conservation at the meson vertex, $I_e = 0$, 1 or 2, which obviously contains the baryon vertex condition.

If the tables of particle quantum numbers are scanned, the ρ-meson turns out to be the least massive candidate for exchange.

It is possible to find that more than one particle can be exchanged, and in this situation the more probable case may be determined by using Heisenberg's Uncertainty Principle to relate the mass of the exchanged meson to its possible range of influence.

According to the Principle:-

$$\Delta E \, \Delta t \approx \hbar/2$$

Hence if the meson travels with a velocity close to that of light c, a distance r, it will be travelling for a time c/r. Thus equating Δt and (c/r):-

$$\Delta E \sim \frac{r}{c} . \frac{\hbar}{2}$$

But $\Delta E = mc^2$ m = exchanged meson mass

Thus:- $$r \approx c\frac{\hbar}{2} . \frac{1}{mc^2}$$

It follows from this that the range of the nuclear force is inversely proportional to the mass of the exchanged meson, so that the longer range parts of the interaction will be due to the exchange of the lighter mesons. It is therefore expected that the reactions will be dominated by the lower mass exchange particles. Table 3 gives the reactions studied and the possible exchange particles for these reactions.

Table 3:- List of the reactions studied and the possible exchange particles associated with them.

Reaction	Possible exchange particles
$\pi^+ p \to \pi^+ p$	Pomeron, ρ
pA_1^+	Pomeron, ρ
pA_3^+	Pomeron, ρ
$\Delta^{++}\rho^o$	π, A_1, A_2
$\Delta^{++}f^o$	π, A_1, A_2
$p\rho^+$	π, ω, A_1, A_2
pg^+	π, ω, A_1, A_2
$\Delta^{++}\omega^o$	ρ, B
$\Delta^{++}\pi^o$	ρ
$\Delta^{++}A_2^o$	ρ, B
pA_2^+	ρ
$\Delta^{++}\eta^o$	A_2
pB^+	ω, A_1, A_2

Since elastic or diffraction channels do not involve quantum number exchange, to give them the same formal description, the Pomeron was proposed (ref. 20). This does not exist as such, but for its exchange to occur the following relation must hold:-

$$P_f = P_i \, (-1)^{\Delta J}$$

where:- ΔJ = change in spin between incident particle, with parity P_i, and the outgoing resonance with parity P_f.

3.2 Brief account of the handling of data

In all the experiments discussed in this review, the results were obtained from measurements of tracks in a bubble chamber. These tracks correspond to the passage of a charged particle through the fluid contained in the chamber, though the uncharged particles remain undetected unless they decay to produce charged particles. The curvature of the tracks gives the charge to momentum ratio of the particle, and the density of bubbles along the track gives an indication of the mass of the particle, though above 1.5 (GeV/c) the proton and pion, for instance, are indistinguishable so this property cannot always be utilised. If a track is seen to stop in the chamber the initial momentum of the particle can be determined from its range though again this is dependent on the mass of the particle. These tracks are recorded for analysis by taking photographs of them and then using these to reconstruct the original event. The actual sequence of the analysis procedures is shown in figure 8.

Figure 8:- Chart showing basic procedures used in the analysis of an event.

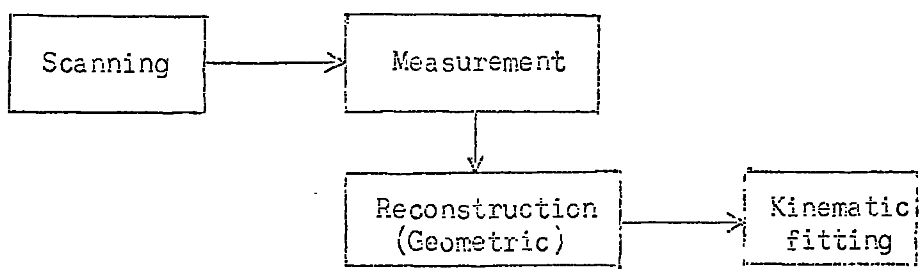

Initially the photograph taken is projected onto a screen and the image scanned for events and tracks leading from these events.

The tracks are then measured by noting the coordinates of several points on the track and also the range and bubble density of the track. These events are then reconstructed using a computer, and those which do not fit are returned for re-scanning. Once the geometry of the events have been reconstructed they are then analysed for particular reaction channels by constraining the measurements to fit the kinematical requirements of conservation of energy and momentum.

3.3 Physical and analytical considerations

The question arises as to whether the dips at low t are of a physical nature or are produced by the techniques used in the analysis of the film and resulting data.

Since in some channels (eg $\pi^+ p \rightarrow \Delta^{++} \pi^0$ see graphs 51 to 59) there is a variation in the shape of the $d\sigma/dt$ versus t curve, at low t, from one graph to another it would seem likely that the curve shape may be affected not only by statistical fluctuations but also by the actual analysis techniques used from one laboratory to another. If the experimental analysis is producing the dip, it could be due to:-

(i) loss of events on the scanning table

(ii) loss of events due to selection techniques used in the obtaining of resonances.

In these cases there is a distinction to be drawn between the two and four prong final states (those in which two and four charged particles are produced respectively). The former could be genuinely missed, particularly for low four-momentum transfers (see figure 9) since the incident and final particle tracks could appear to be one and the same, noticeably when the second track coming from the vertex is short. For four prong interactions the dip could be produced by

Figure 9:- 2 prong interaction involving a low t transfer.

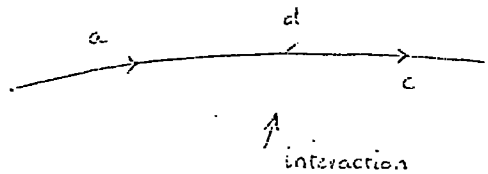

missing a very short track and interpreting the event as a three pronged one. Though these three pronged events are not allowed by charge conservation, nevertheless, some are obtained but are likely to be misidentified four prong events. Obviously if one track is so short that it cannot be seen easily, it indicates that the particle with the short track had a very small four momentum transfer to it, and since the number of interactions within a given t range will be small, the omission of one event will be of significance in determining the shape of the graph. It is very easy to miss a short proton track in the scanning process, since one bubble corresponds to a proton momentum of 85 (MeV/c). Furthermore in two prong interactions associated with small t-transfers, the pion only suffers a small deflection in path direction, making it difficult to see an interaction has occurred, and in four or more pronged interactions short tracks are often obscured by the other tracks coming out from the interaction.

When such events are processed by the various fitting programmes in the computer, either the event is incorrectly fitted or does not fit at all and so are distorted or effectively lost in the subsequent analysis. Since the azimuthal angle distribution with respect to the axis of the bubble chamber should be uniform for all interactions, and for all values of four momentum transfer for any two particular

FIG. 10

t vs. ϕ IN THE REACTION $\pi^0 p \to \pi^0 p$

A. 11·5 GeV/c

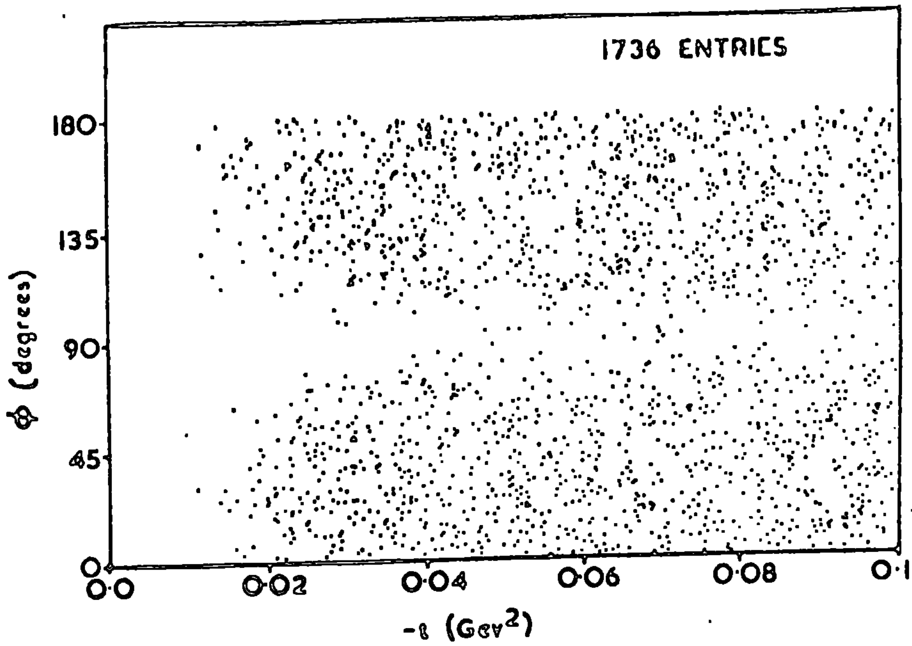

B. 5 GeV/c

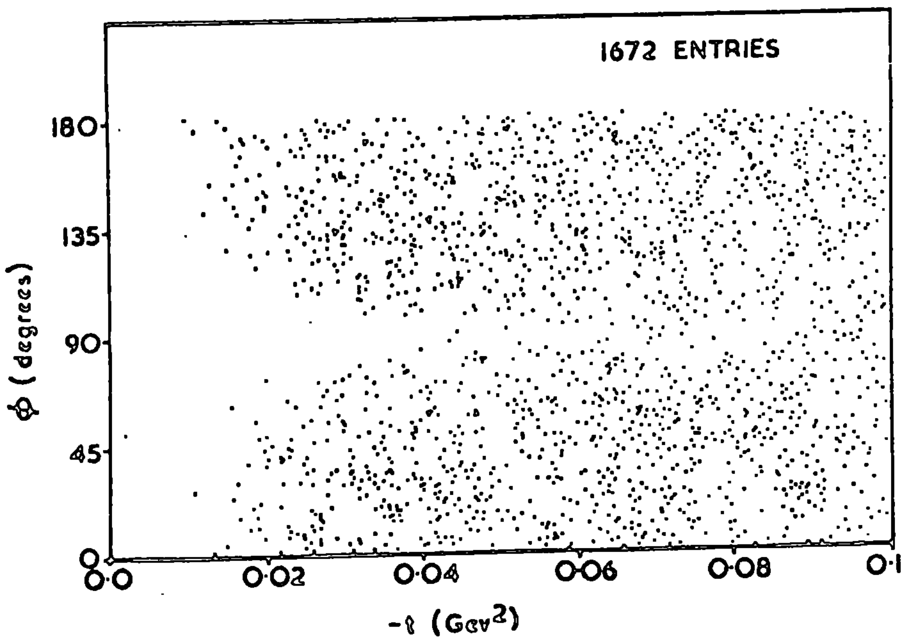

particles (eg proton-proton), it is of interest to see if this is so in the data that is used in the analysis. The results for $\pi^{+}p \rightarrow \pi^{+}p$ fitting elastic scattering are displayed in figure 10 (ref. 21). It is interesting to note that many events are being lost when ϕ, the azimuthal angle, is $\sim 90^{\circ}$ (ie when the tracks are coming towards or away from the cameras), especially for low values of t indicating that the analysis could contribute towards the dip if it were not corrected for. For the elastic channel this correction is easily ascertained empirically and applied to the data.

For $\pi^{+}p$ interactions in which a delta is produced the t-transfer is not only a function of the three-momentum of the delta but also of its mass, and hence there is a lower (and upper) limit on the momenta of the proton and pion resulting from the separation of the delta into its constituent particles. The following calculation was thus used in order to determine the maximum and minimum values of the secondary proton momentum in the laboratory for given values of four momentum transfer from the target proton to the delta, and hence from these momenta it can be determined whether the proton is visible on the scanning table or not.

<u>Figure 11</u>:- Diagram showing the break up of a delta in its centre of mass to a proton (secondary) and pion.

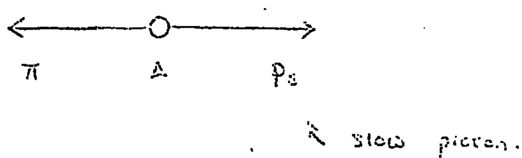

In the centre of mass system of the delta (see fig. 11)

The total energy $E = m_\Delta$

$$= E_\pi + E_{p_s}$$

$$= (m_\pi^2 + p_\pi^2)^{\frac{1}{2}} + (m_{p_s}^2 + p_{p_s}^2)^{\frac{1}{2}}$$

But since it is in the cms. system:-

$$p_\pi = p_{p_s}$$

Hence for a given energy, ie a given delta mass, the momenta of the proton and pion can be calculated. These must then be transformed into the laboratory system.

To calculate p_π and p_{p_s} in the delta cms. system:-

$$E_\Delta = E_\pi + E_{p_s} = m_\Delta$$

Therefore:= $$m_\Delta^2 = (E_\pi + E_{p_s})^2$$

so:- $$m_\Delta^2 - m_\pi^2 - m_p^2 - p_\pi^2 - p_{p_s}^2 = 2E_\pi \cdot E_{p_s}$$

Since $p_\pi = p_{p_s}$, on squaring the above equation and making p_π the subject, this yields:-

$$p_\pi = \left[\frac{(m_\Delta^4 + m_\pi^4 + m_p^4 - 2m_\Delta^2 m_\pi^2 - 2m_\Delta^2 m_p^2 - 2m_\pi^2 m_p^2)}{4m^2} \right]^{\frac{1}{2}}$$

Now transforming to the laboratory system using the conventional Lorentz transforms:-

$$\gamma = \frac{1}{(1-\beta^2)^{\frac{1}{2}}}$$

$\beta =$ momentum of delta/energy of delta

The maximum momentum of the proton in the laboratory is given by

$$P_{max} = \gamma \left[p_{p_s} + (\beta \cdot E_{p_s}) \right]$$

and its minimum momentum by:-

$$p_{min} = \gamma \left[-p_{p_s} + (\beta \times E_{p_s}) \right]$$

Similarly the maximum and minimum momenta of the pion in the laboratory are given by the same relationships, with the energy of the pion inserted in place of that of the proton.

The results of this calculation are shown in figure 12. It can be seen from this graph that the minimum value of the t-transfer from the proton to the delta in order for the secondary proton to be seen is dependent on the mass of the delta but for the lighter deltas the secondary protons would have a range <3mm (<100 MeV/c) for t-transfers below 0.05 $(\mathrm{GeV/c})^2$.

Now considering events in which a proton is one of the two final state particles, as opposed to a delta, figure 13 (i) and (ii) shows the laboratory momentum of the secondary proton, and its range resulting from a given t-transfer. The calculation for this utilises directly the definition of t (see section 1.4) putting $\theta = 0^\circ$, to obtain the minimum p_c

$$-t = (P_a - P_c)^2$$
$$= m_a^2 + m_c^2 - 2E_a E_c + 2p_a p_c$$

and the results are shown in figure 13(i).

This graph shows that a value of $|t| = 0.007$ $(\mathrm{GeV/c})^2$ is obtained for a proton momentum of 85 MeV/c - at which momentum the track is 1 mm. long. Since in most reactions which involve a proton in the intermediate state the dip starts to occur at $|t| \approx 0.04$ to 0.06 $(\mathrm{GeV/c})^2$ (which corresponds to a secondary proton momentum of 200 to 250 MeV/c or a track length of 3 to 10 cms), it seems extremely unlikely that a significant proportion of these tracks will be missed, or be badly measured.

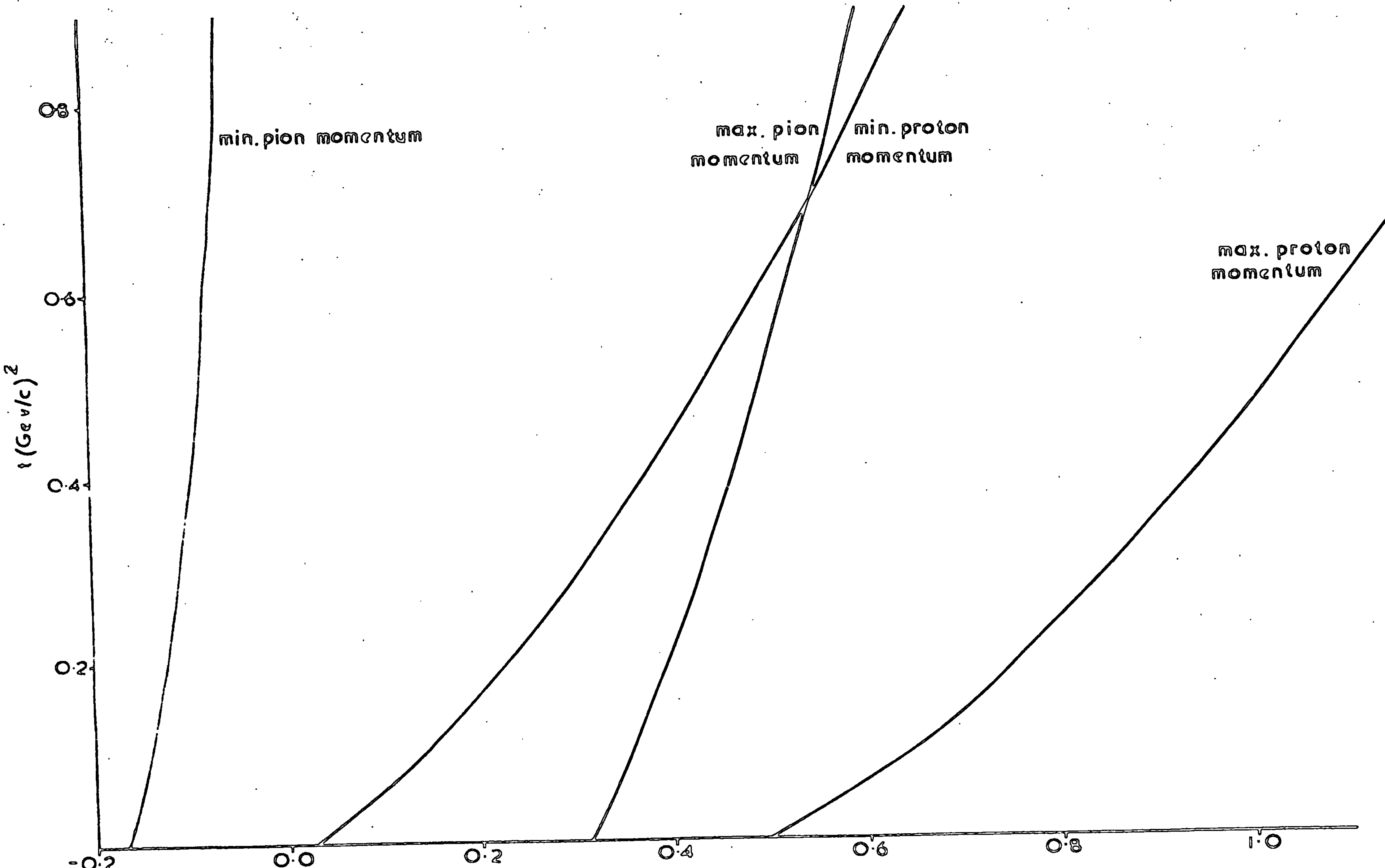

min. pion momentum
max. pion momentum
min. proton momentum
max. proton momentum
0·8
0·6
0·4
0·2
t (Gev/c)²
-0·2
0·0
0·2
0·4
0·6
0·8
1·0
LAB MOMENTUM (Gev/c) ALONG DELTA DIRECTION

FIG.12

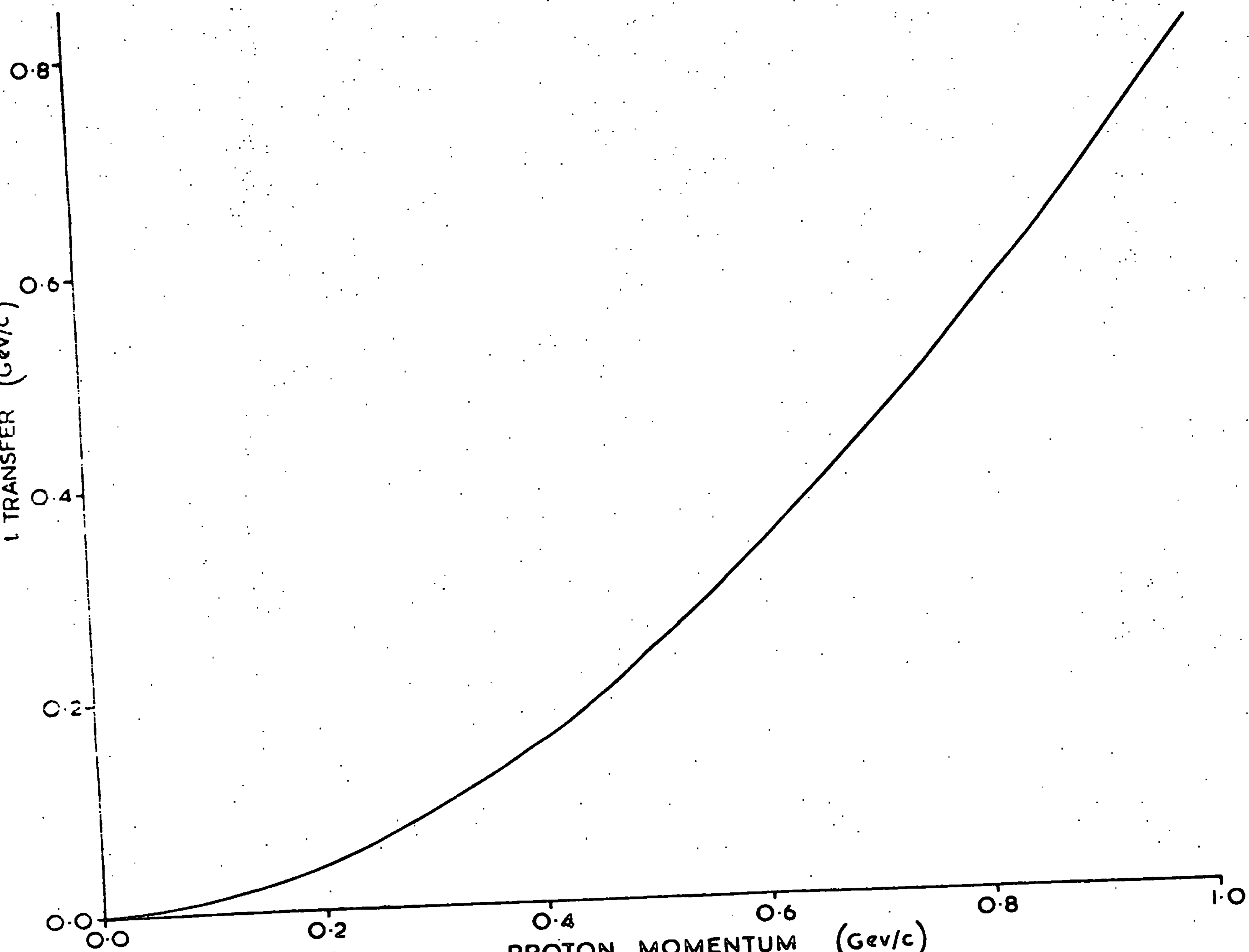
0·8
0·6
0·4
0·2
0·0
t TRANSFER $(Gev/c)^2$
0·0
0·2
0·4
0·6
0·8
1·0
PROTON MOMENTUM (Gev/c)

FIG. 13 i

RANGE AND ENERGY LOSS IN LIQUID HYDROGEN

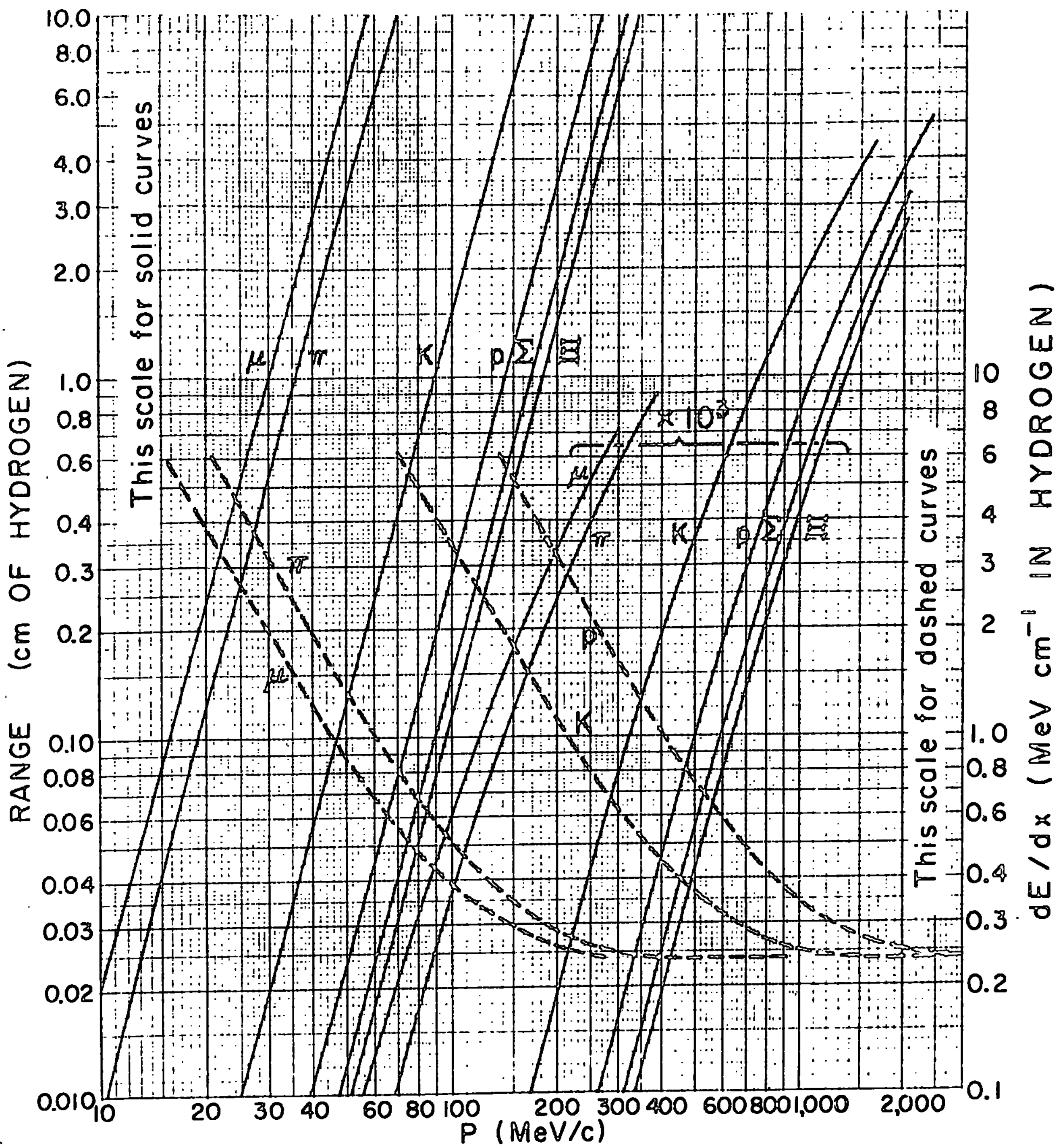

Range and energy loss in liquid hydrogen bubble chamber, determined by a μ^+ range of 1.103 ± 0.003 cm from the $\pi^+ \to \mu^+\nu$ decay. Liquid hydrogen conditions: $T = 27.6 \pm 0.1$°K; $P = 48 \pm 5$ psia; $\rho = (5.86 \pm 0.06) 10^{-2}$ g/cm^3. (Data by Clark and Diehl, UCRL-3789, 1957.) Bubble chamber physicists: note that the number of bubbles per cm is proportional to $1/\beta^2$, not to dE/dx.

FIG. 13 ii

Another possible cause of the dip at low t is that the masses of the secondary particles have a large width, though in the case of particles such as the proton this will obviously not apply. This effect can be compensated for by calculating the minimum value of t-transfer that can occur for a given resonance mass, thus:-

Since $t = m_a^2 + m_c^2 + 2p_a p_c \cos\theta^* - 2E_a.E_c$

a maximum and minimum value of t can be determined,

i.e. when $\cos\theta^* = \pm 1$. This gives:-

$$t_{\substack{min\\max}} = \left(\left[\left(\frac{E^2 + m_c^2 - m_d^2}{2E} \right)^2 - m_c^2 \right]^{\frac{1}{2}} \mp \left[\left(\frac{E^2 + m_a^2 - m_b^2}{2E} \right)^2 - m_a^2 \right]^{\frac{1}{2}} \right)^2$$

$$- \left[\frac{(m_c^2 - m_a^2) - (m_d^2 - m_b^2)}{2E} \right]^2$$

The results of this calculation for the channels considered are shown in figures 14 to 25. Now since t is mass dependent, its minimum value t_{min} will vary from one interaction to another, within a particular reaction channel, depending on the particular mass of the resonance in question. Hence the graph of $d\sigma/dt$ versus t will not contain a unique resonance mass for a given value of t, but rather a unique mass is spread over a range of t. It follows then that at low values of t, when t' (t' being defined to be $t - t_{min}$) is nearly zero, for some masses and at zero for the remainder, there will be no contribution to the distribution from the larger masses and higher momenta since there will be insufficient energy to allow them to occur. Therefore a dip will occur in graphs of $d\sigma/dt$ versus t.

However if t' is used instead of t in these graphs this dip should be lost if it is the resonance width which is the cause. Though to a certain extent this loss of the dip does occur, it is still noticeable in some of the interactions studied.

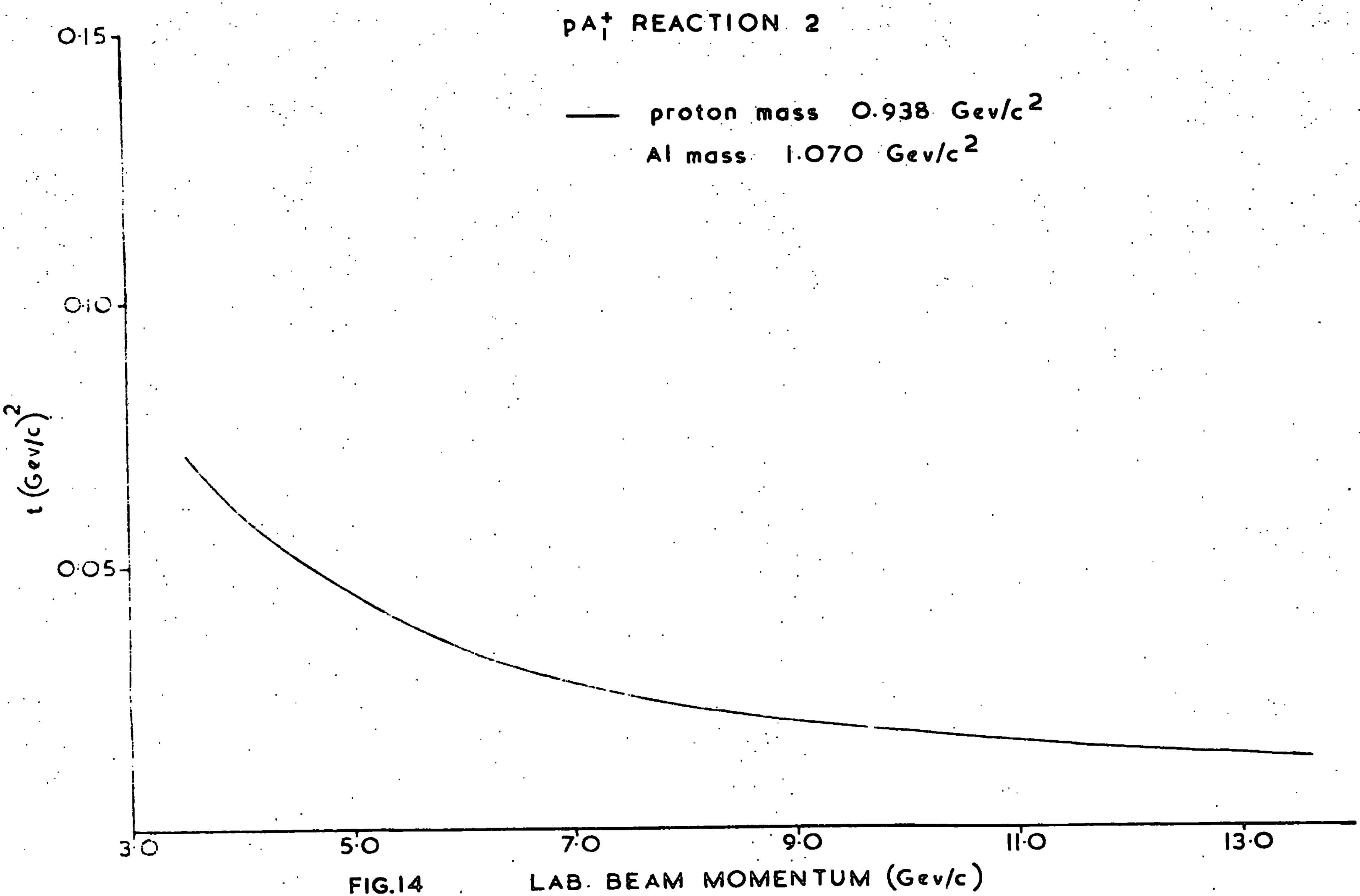

pA_1^+ REACTION 2
proton mass 0.938 Gev/c^2
Al mass 1.070 Gev/c^2
0.15
0.10
0.05
t (Gev/c)^2
3.0
5.0
7.0
9.0
11.0
13.0
LAB. BEAM MOMENTUM (Gev/c)

FIG.14

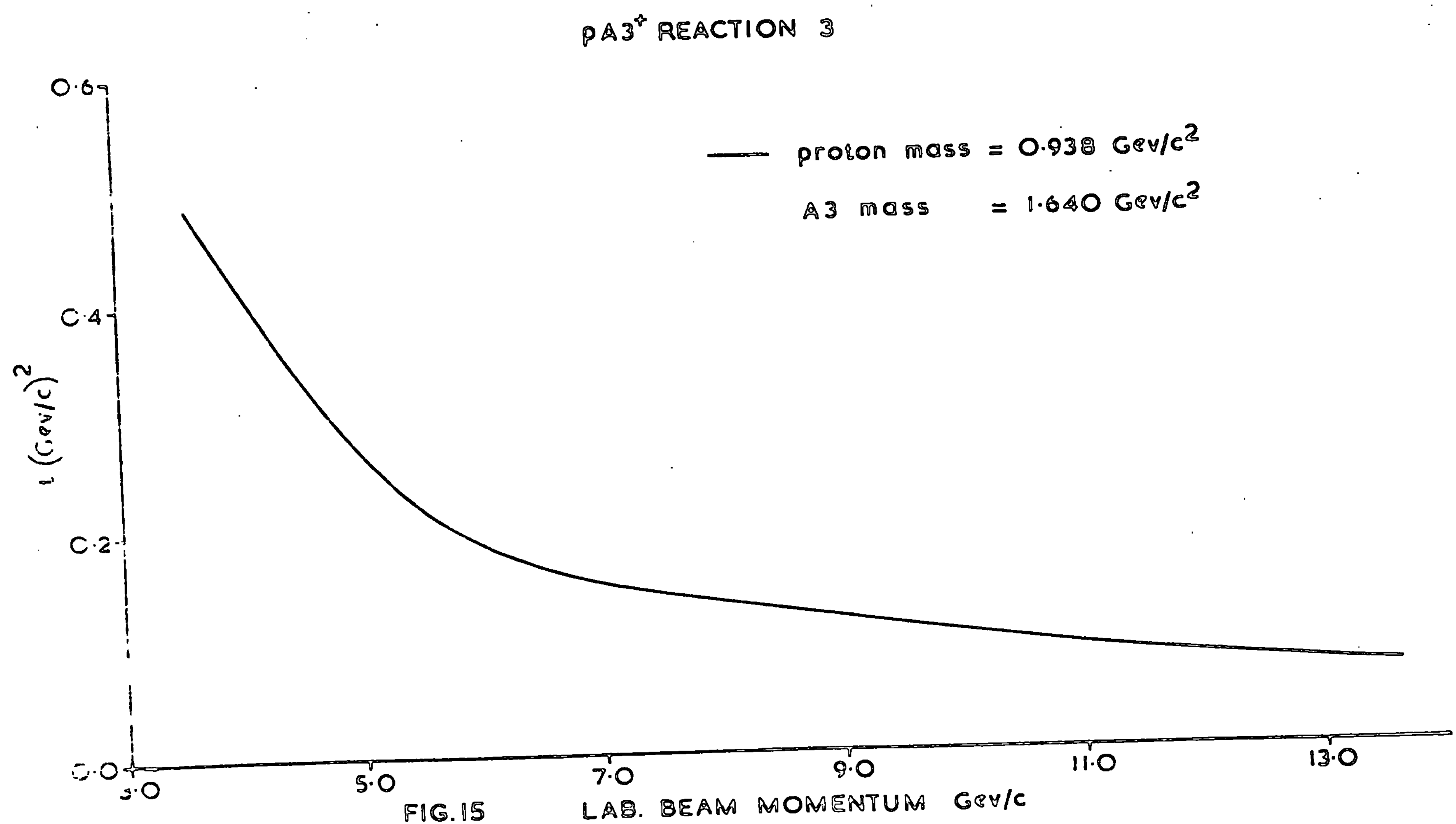
pA3+ REACTION 3
proton mass = 0·938 Gev/c²
A3 mass = 1·640 Gev/c²
0·6
0·4
0·2
0·0
t (Gev/c)²
3·0
5·0
7·0
9·0
11·0
13·0
LAB. BEAM MOMENTUM Gev/c

FIG. 15

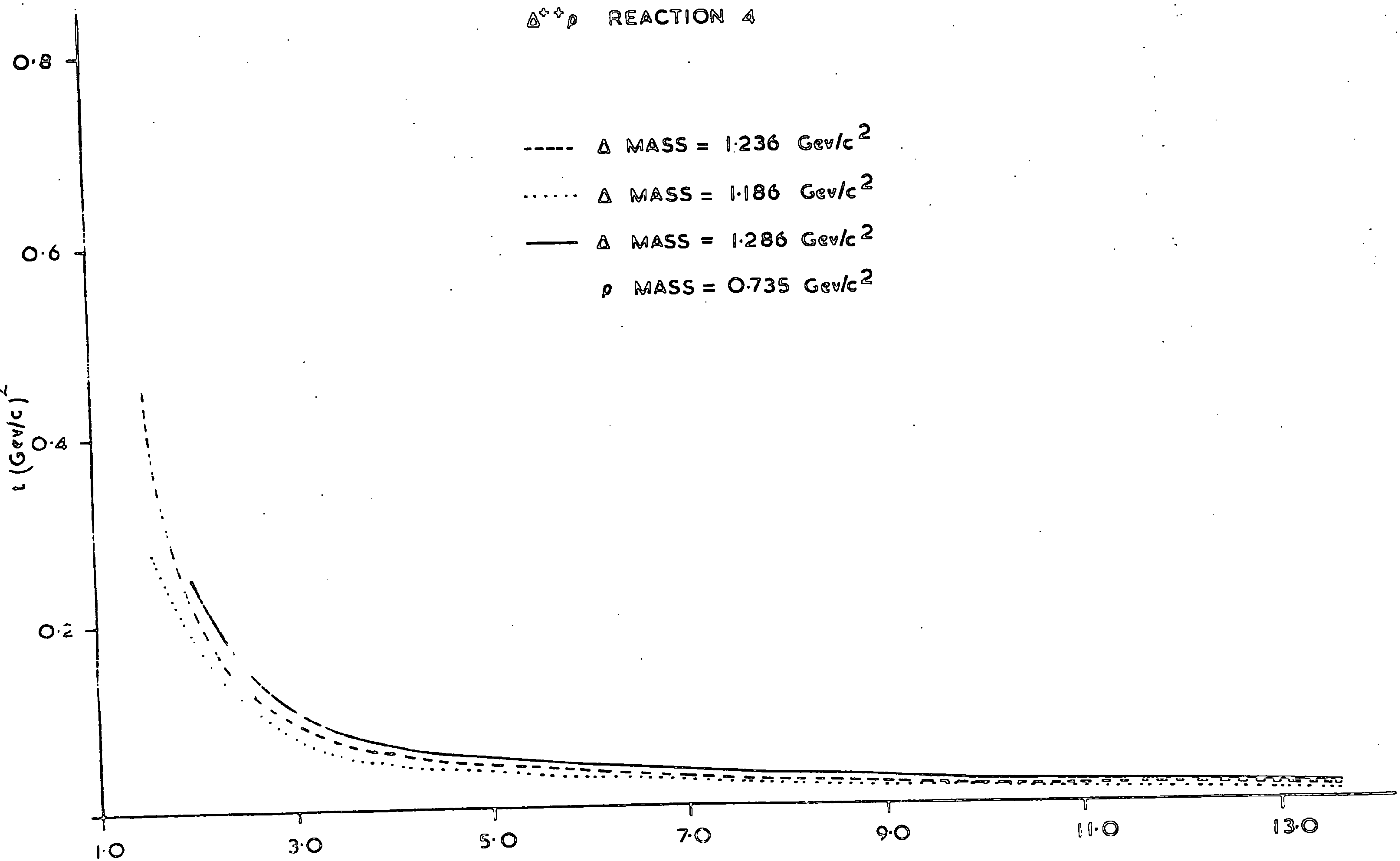

Δ⁺⁺ρ REACTION 4
Δ MASS = 1·236 Gev/c²
Δ MASS = 1·186 Gev/c²
Δ MASS = 1·286 Gev/c²
ρ MASS = 0·735 Gev/c²
0·8
0·6
0·4
0·2
t (Gev/c)²
1·0
3·0
5·0
7·0
9·0
11·0
13·0
BEAM MOMENTUM Gev/c

FIG.16

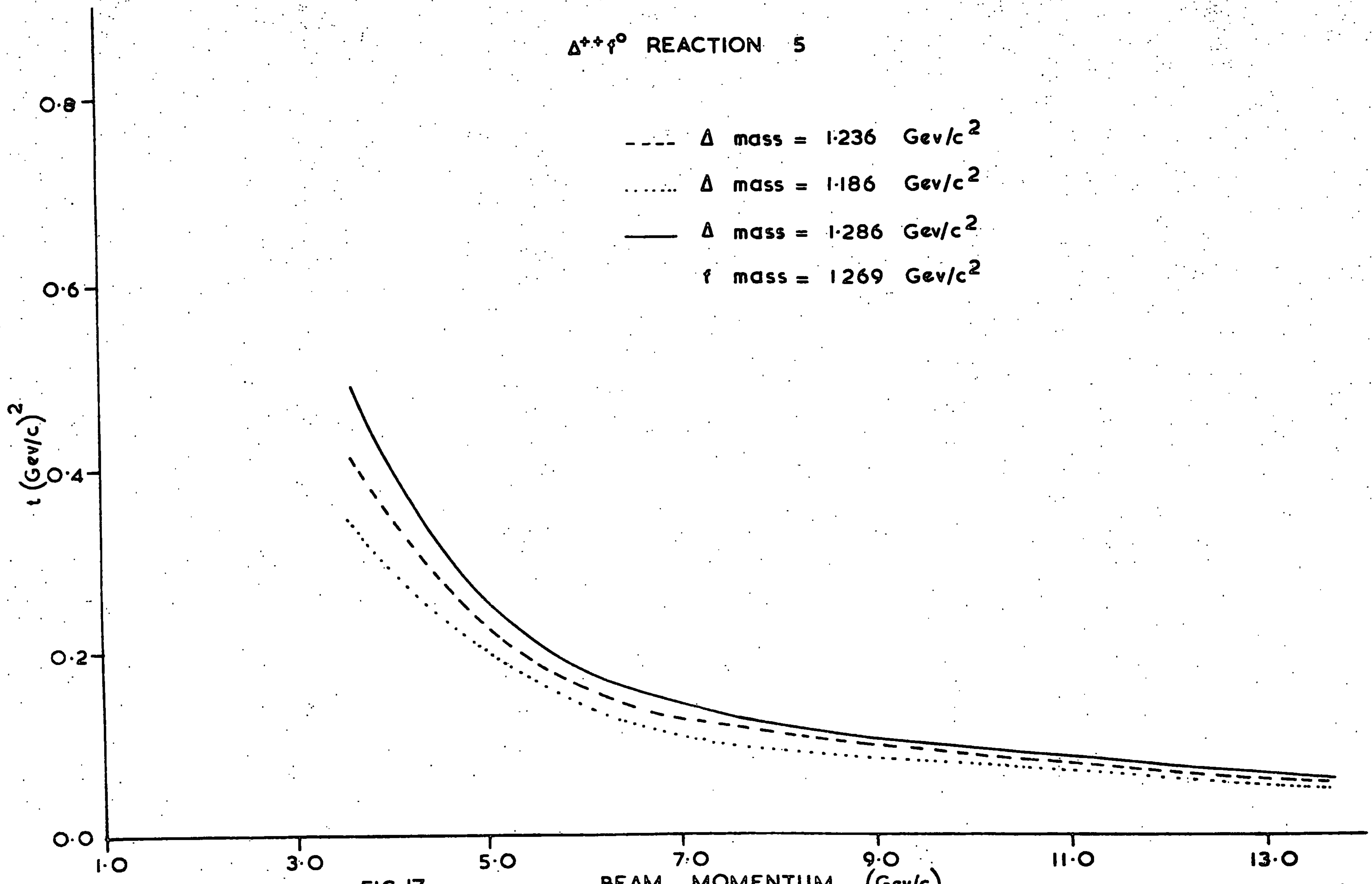

$\Delta^{++} f^0$ REACTION 5
Δ mass = 1·236 Gev/c^2
Δ mass = 1·186 Gev/c^2
Δ mass = 1·286 Gev/c^2
f mass = 1269 Gev/c^2
t (Gev/c)^2
0·8
0·6
0·4
0·2
0·0
1·0
3·0
5·0
7·0
9·0
11·0
13·0
BEAM MOMENTUM (Gev/c)

FIG 17

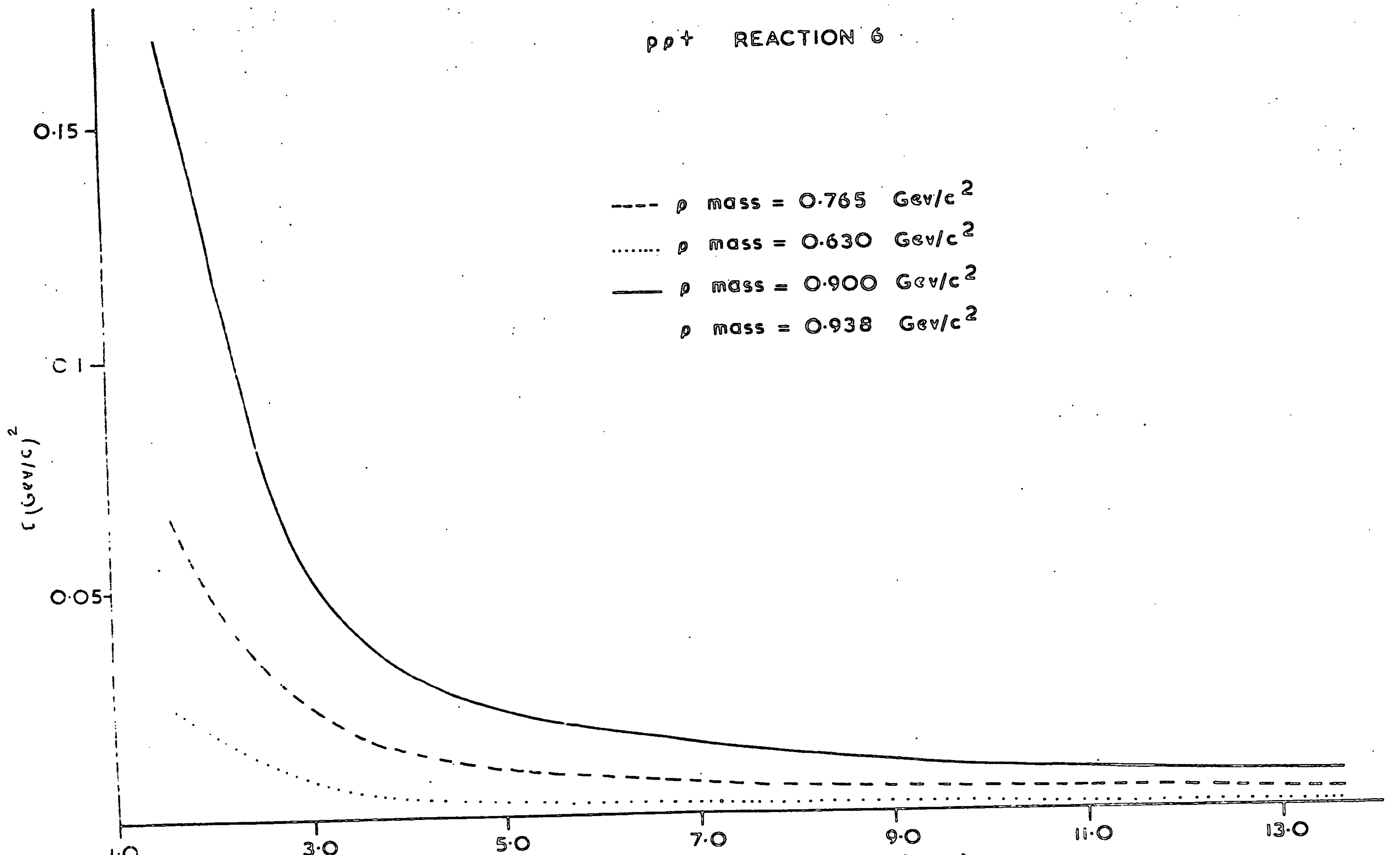

ρρ+ REACTION 6
ρ mass = 0·765 Gev/c²
ρ mass = 0·630 Gev/c²
ρ mass = 0·900 Gev/c²
ρ mass = 0·938 Gev/c²
0·15
0·1
0·05
t (Gev/c)²
1·0
3·0
5·0
7·0
9·0
11·0
13·0
BEAM MOMENTUM (Gev/c)

FIG. 18

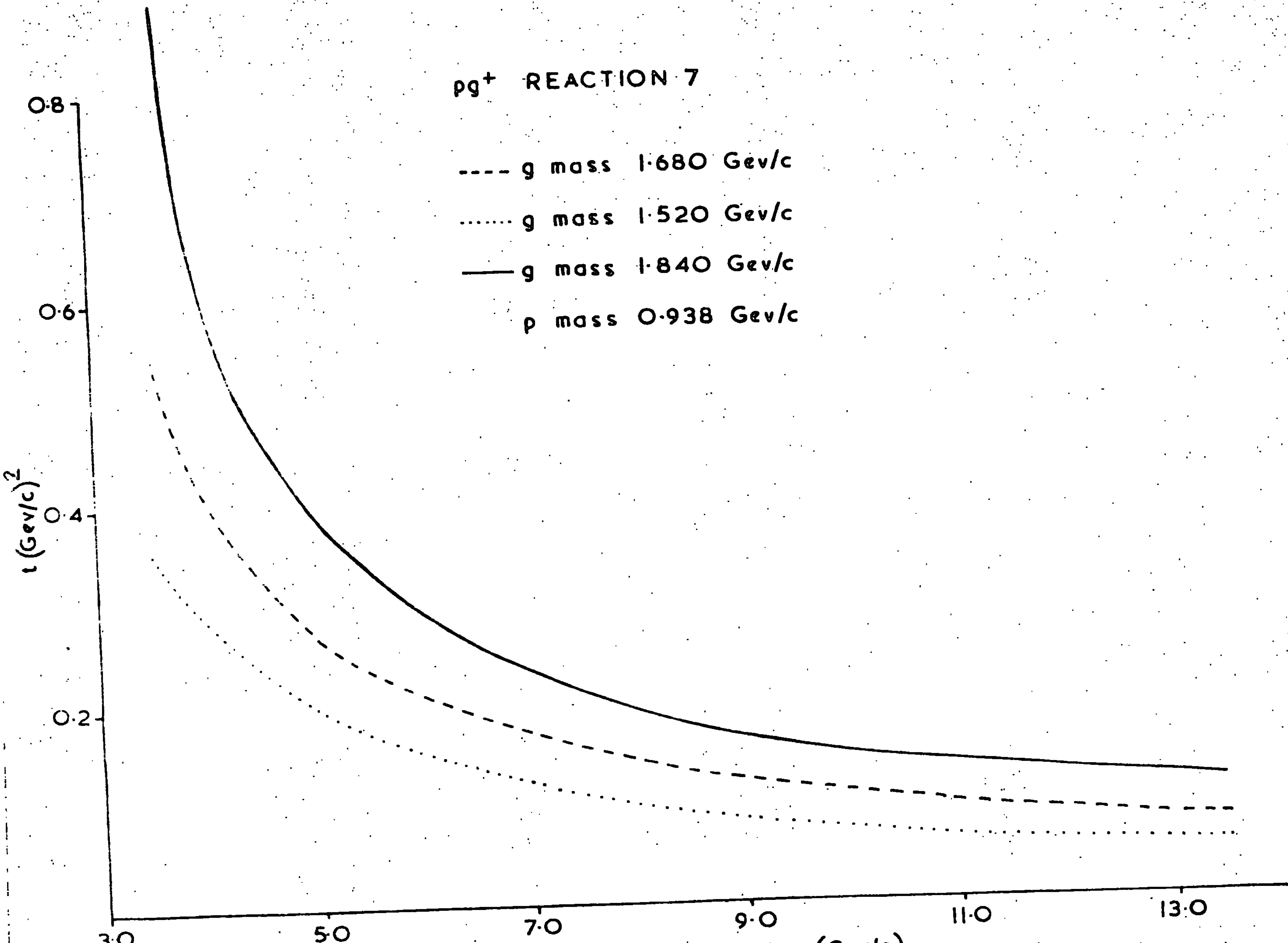
pg+ REACTION 7
g mass 1·680 Gev/c
g mass 1·520 Gev/c
g mass 1·840 Gev/c
p mass 0·938 Gev/c
0·8
0·6
0·4
0·2
t (Gev/c)²
3·0
5·0
7·0
9·0
11·0
13·0
BEAM MOMENTUM (Gev/c)

FIG.19

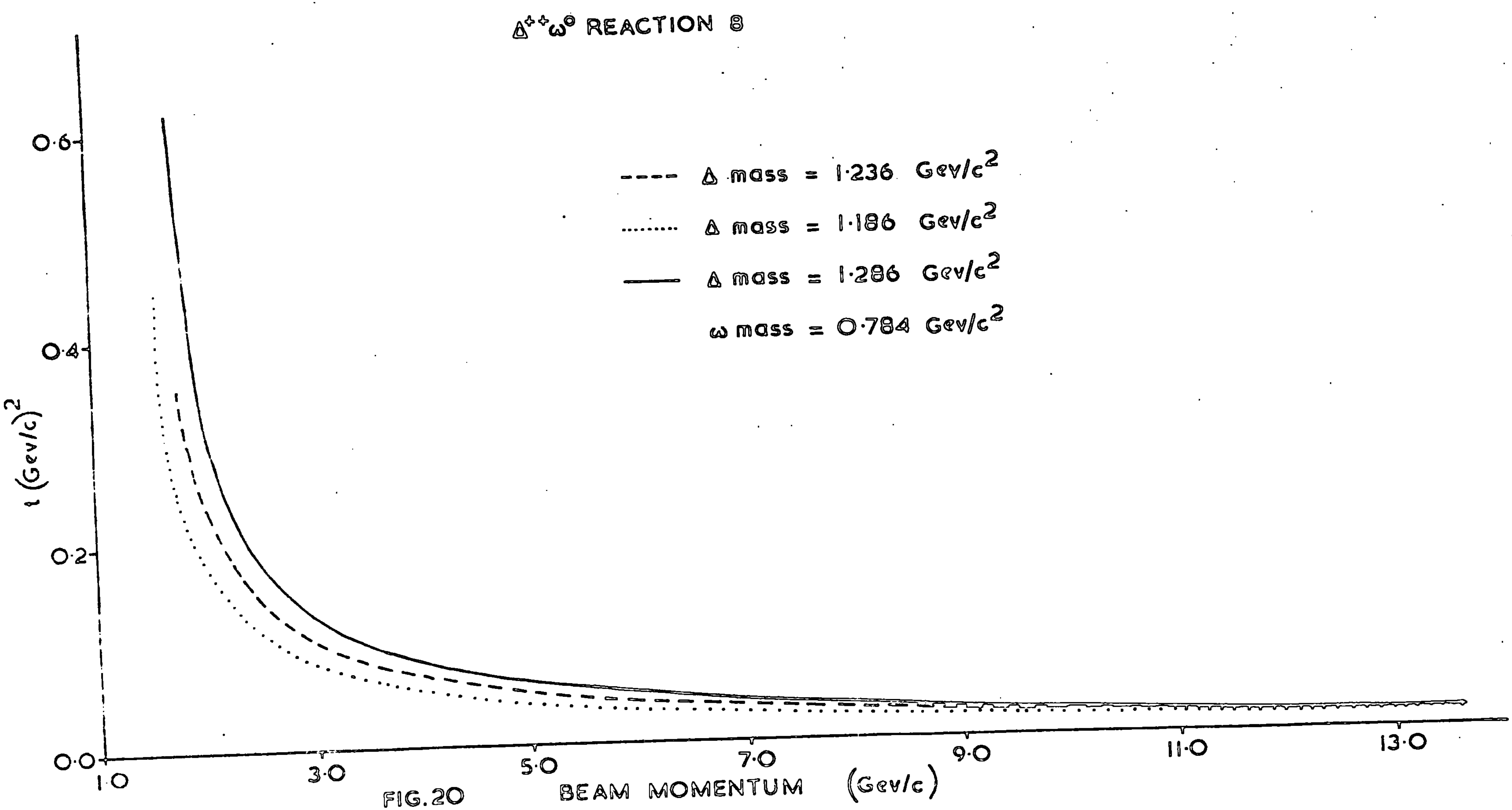

$\Delta^{++}\omega^{0}$ REACTION 8
Δ mass = 1·236 Gev/c^2
Δ mass = 1·186 Gev/c^2
Δ mass = 1·286 Gev/c^2
ω mass = 0·784 Gev/c^2
t (Gev/c)^2
0·0
0·2
0·4
0·6
1·0
3·0
5·0
7·0
9·0
11·0
13·0
BEAM MOMENTUM (Gev/c)

FIG. 20

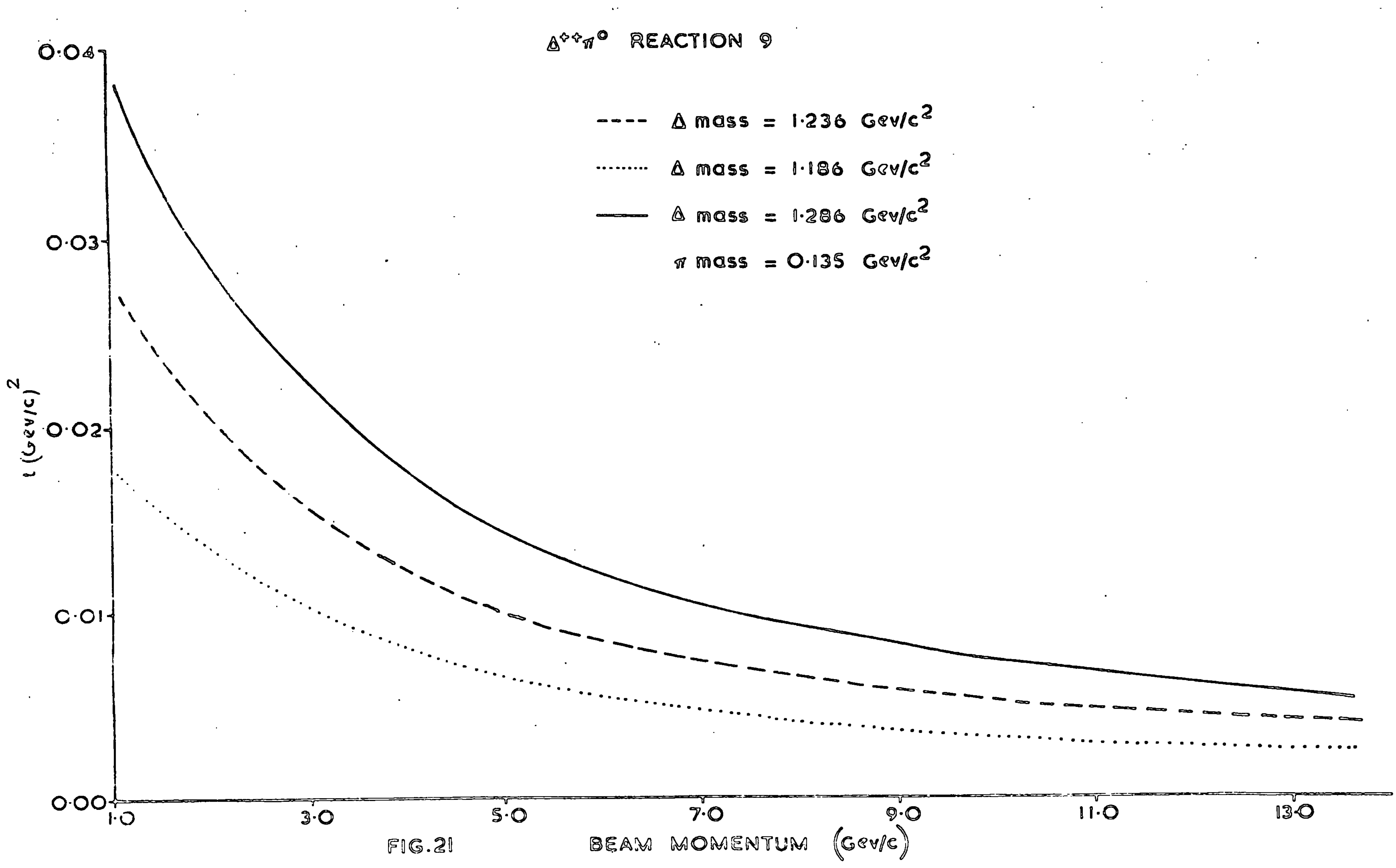

$\Delta^{++}\pi^0$ REACTION 9
Δ mass = 1·236 Gev/c²
Δ mass = 1·186 Gev/c²
Δ mass = 1·286 Gev/c²
π mass = 0·135 Gev/c²
t (Gev/c)²
0·04
0·03
0·02
0·01
0·00
1·0
3·0
5·0
7·0
9·0
11·0
13·0
BEAM MOMENTUM (Gev/c)

FIG.21

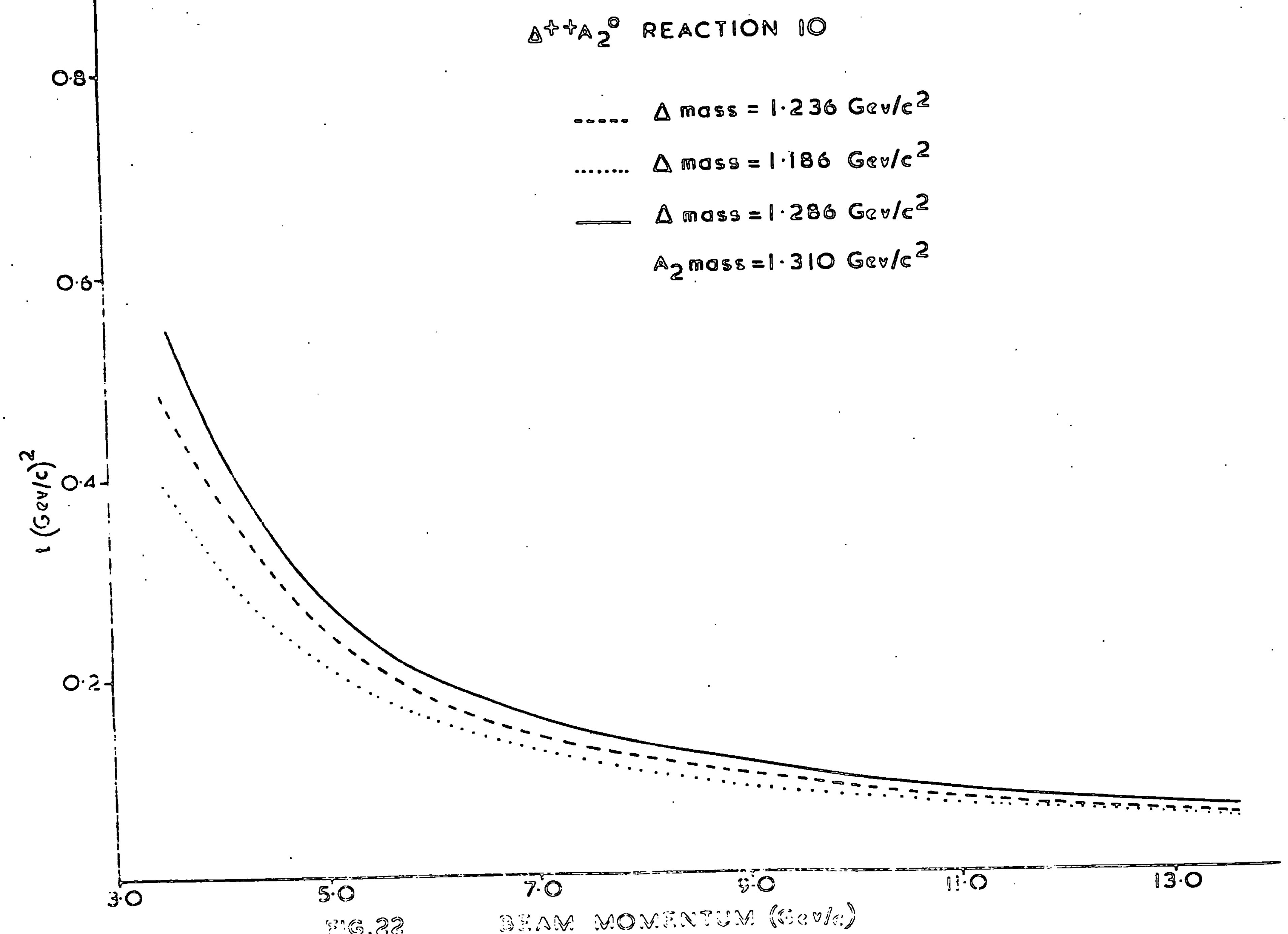

$\Delta^{++}A_2^0$ REACTION 10
Δ mass = 1·236 Gev/c^2
Δ mass = 1·186 Gev/c^2
Δ mass = 1·286 Gev/c^2
A_2 mass = 1·310 Gev/c^2
0·8
0·6
0·4
0·2
t (Gev/c)^2
3·0
5·0
7·0
9·0
11·0
13·0
BEAM MOMENTUM (Gev/c)

FIG. 22

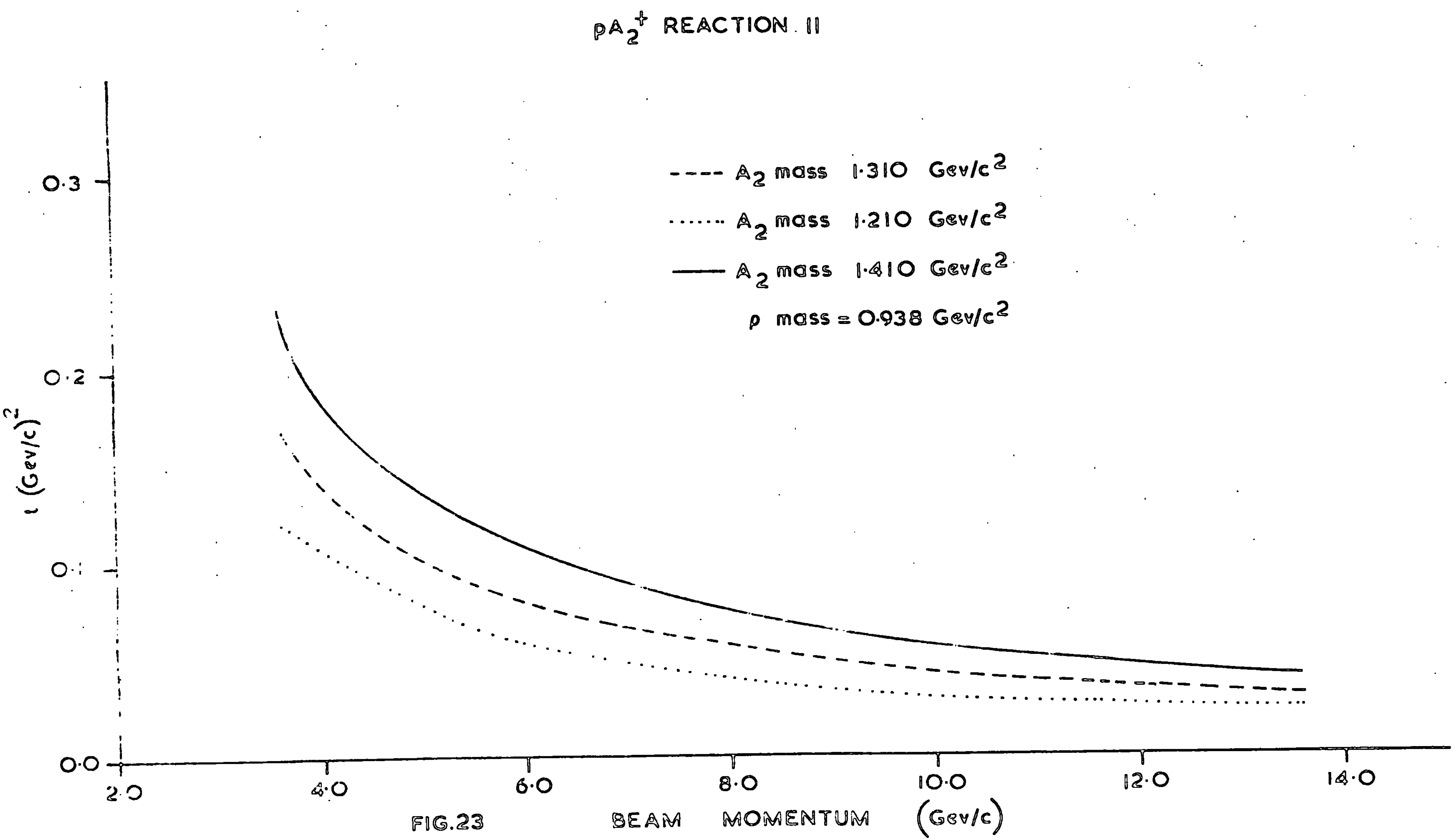

pA$_2^+$ REACTION II
A$_2$ mass 1·310 Gev/c^2
A$_2$ mass 1·210 Gev/c^2
A$_2$ mass 1·410 Gev/c^2
ρ mass = 0·938 Gev/c^2
0·3
0·2
0·1
0·0
t (Gev/c)^2
2·0
4·0
6·0
8·0
10·0
12·0
14·0
BEAM MOMENTUM (Gev/c)

FIG.23

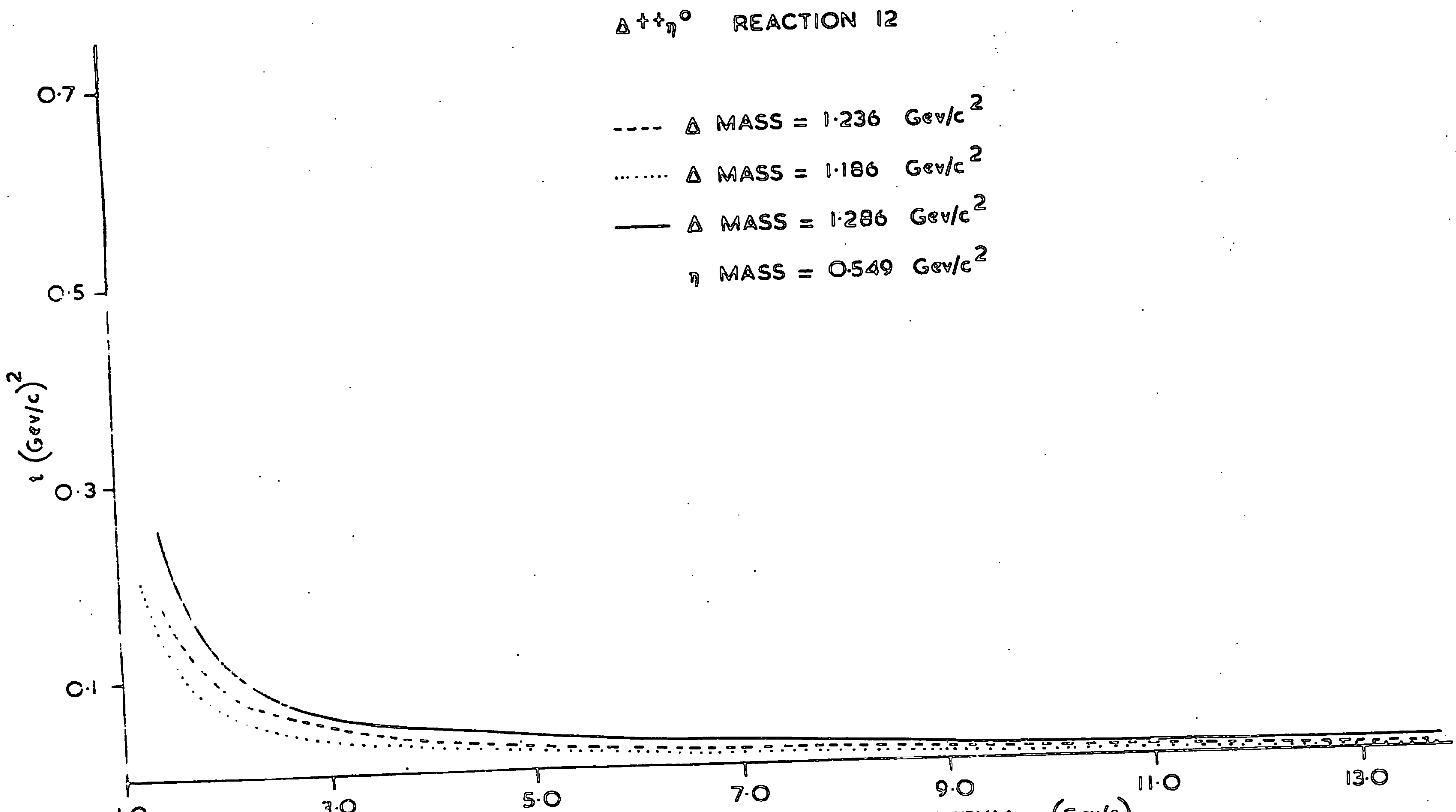
$\Delta^{++}\eta^{0}$ REACTION 12
Δ MASS = 1·236 Gev/c^{2}
Δ MASS = 1·186 Gev/c^{2}
Δ MASS = 1·286 Gev/c^{2}
η MASS = 0·549 Gev/c^{2}
0·7
0·5
0·3
0·1
t (Gev/c)^{2}
1·0
3·0
5·0
7·0
9·0
11·0
13·0
BEAM MOMENTUM (Gev/c)

FIG. 24

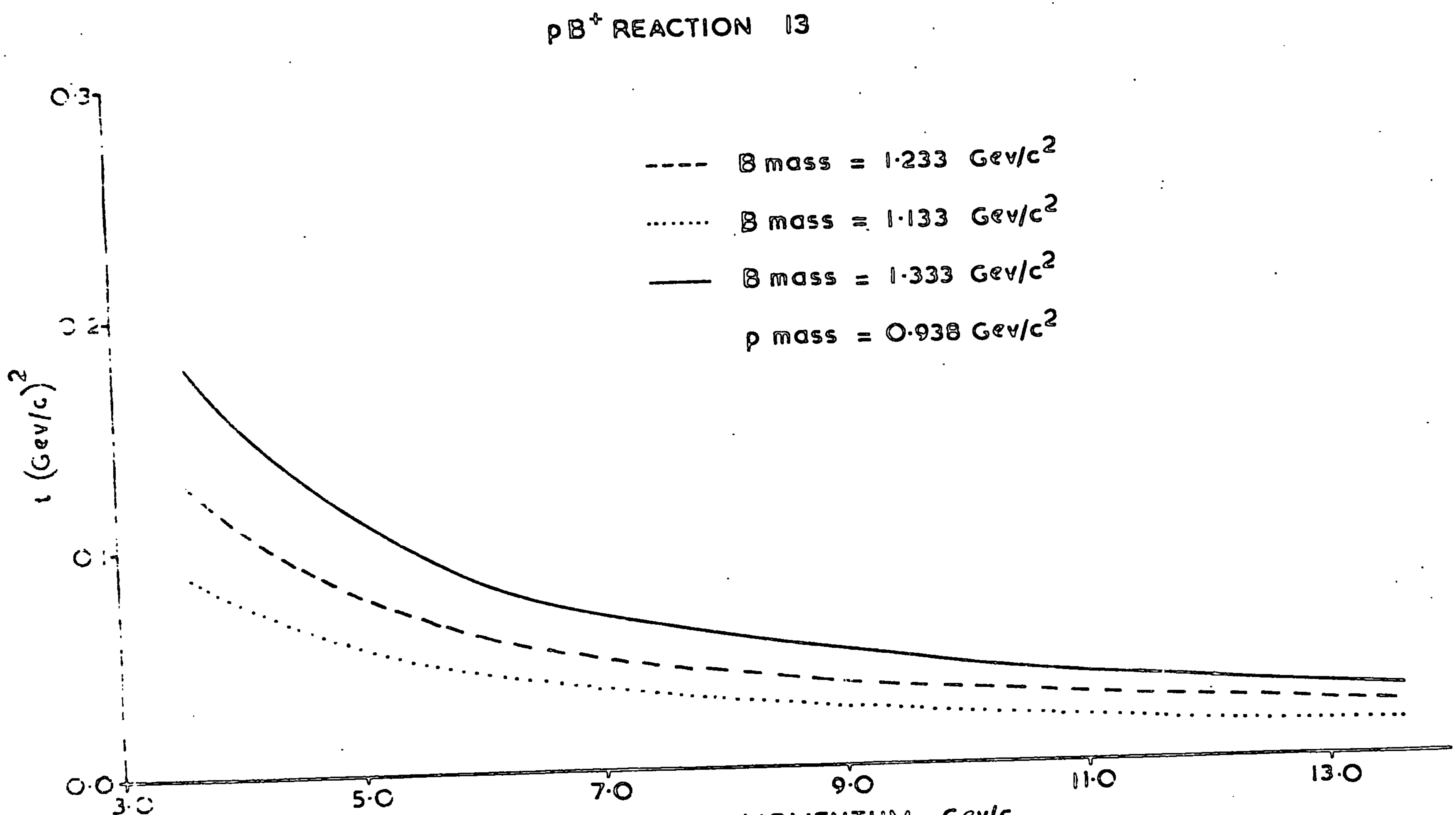
pB⁺ REACTION 13
B mass = 1·233 Gev/c²
B mass = 1·133 Gev/c²
B mass = 1·333 Gev/c²
p mass = 0·938 Gev/c²
t (Gev/c)²
0·3
0·2
0·1
0·0
3·0
5·0
7·0
9·0
11·0
13·0
LAB. BEAM MOMENTUM Gev/c
FIG. 25

CHAPTER FOUR

Introduction

In this chapter the graphs obtained from various experiments for $d\sigma/dt$ versus t, and $d\sigma/dt'$ versus t' will be compared, taking each particular reaction in turn, though the channels with the same lowest mass exchange particles will be grouped together for comparison. Where there are a number of experiments dealing with one channel, the results are displayed in the text in the form of summary graphs, but all the original data is collected together in Appendix III.

Appendix III shows that for all the channels, the differential cross-section falls sharply with increasing t (or t'). Of special concern in this chapter is whether there is a physically meaningful dip in the differential cross-section as t (or t') approaches zero. A final section summarises the conclusions. The approach is entirely empirical and the conclusions are based on the experimental data alone with no consideration given to the detailed fits with theoretical models some of which predict decreasing cross-sections at low values of t. Where possible the conclusions arrived at are compared with those of Collins (ref. 22), which are based on a review of theoretical fits to a much wider selection of interaction channels.

4.1. Channels in which Pomeron exchange can occur

The dominant channel in this category is $\pi^{\pm}p$ elastic scattering, but the transitions to the pA_1 and pA_3 final states can also occur via the same exchange. The graphs corresponding to these channels are shown in figures 26 and 27.

$\pi^{\pm}p \rightarrow \pi^{\pm}p$ channel.

In this, the elastic channel, t_{min} is identically zero, and hence there is no distinction between t and t'. The results for this channel

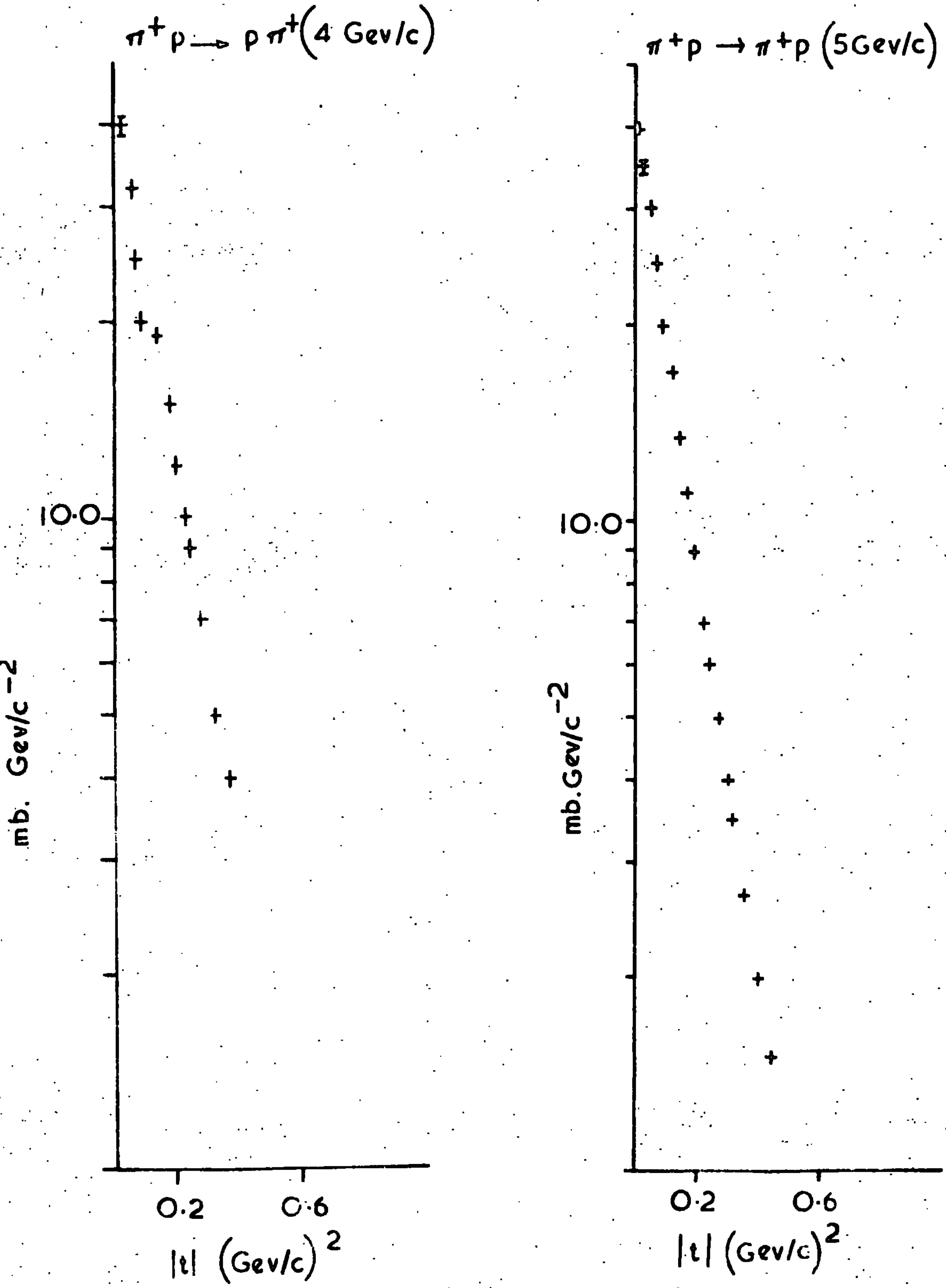

π⁺p → pπ⁺(4 Gev/c)
10.0
mb. Gev/c⁻²
0.2
0.6
|t| (Gev/c)²
π⁺p → π⁺p (5Gev/c)
10.0
mb.Gev/c⁻²
0.2
0.6
|t| (Gev/c)²

FIG. 26 (i)

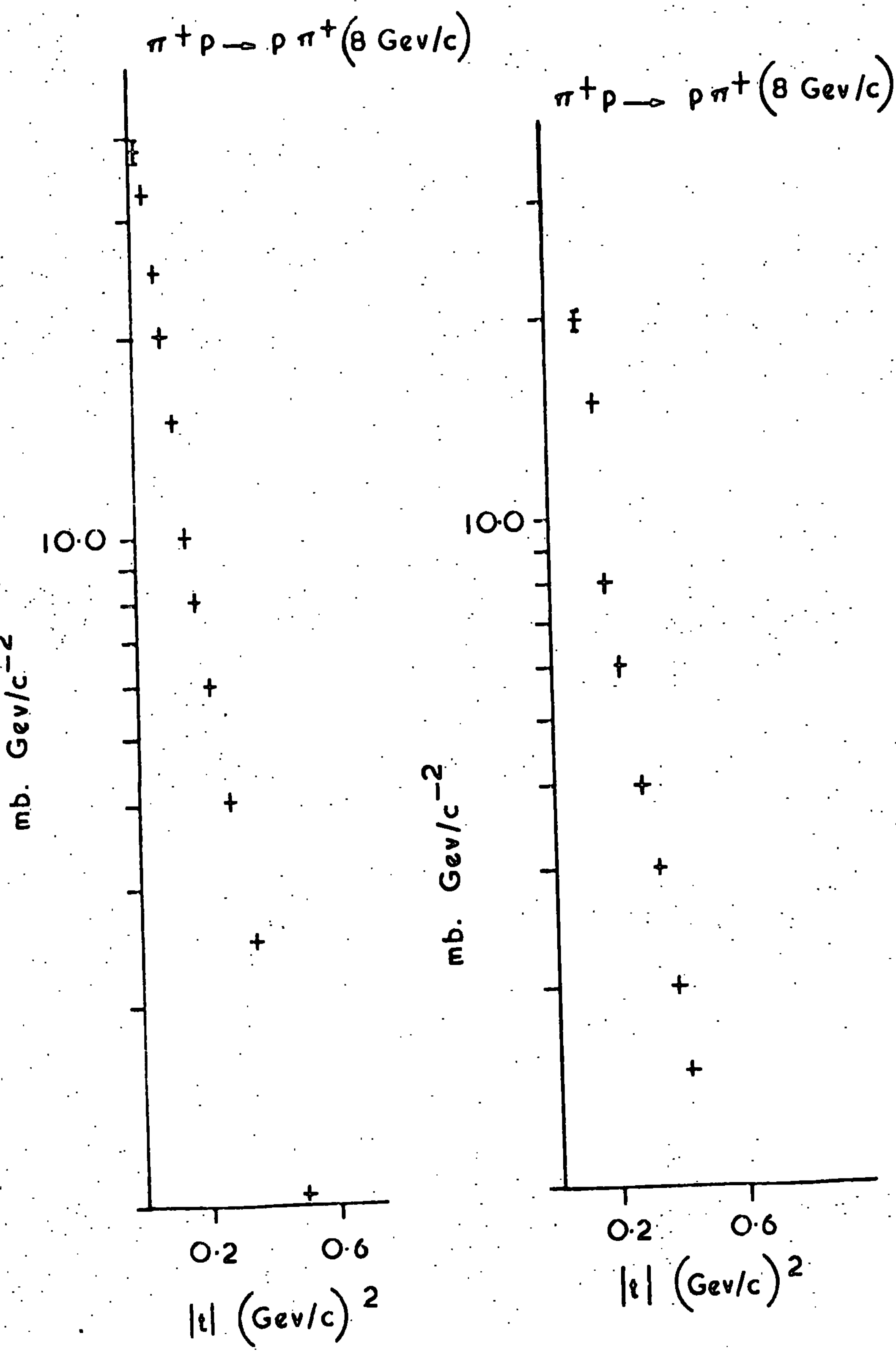

$\pi^+ p \to p \pi^+$ (8 Gev/c)
10·0
mb. Gev/c^{-2}
0·2
0·6
|t| (Gev/c)^2
$\pi^+ p \to p \pi^+$ (8 Gev/c)
10·0
mb. Gev/c^{-2}
0·2
0·6
|t| (Gev/c)^2

FIG. 26 (ii)

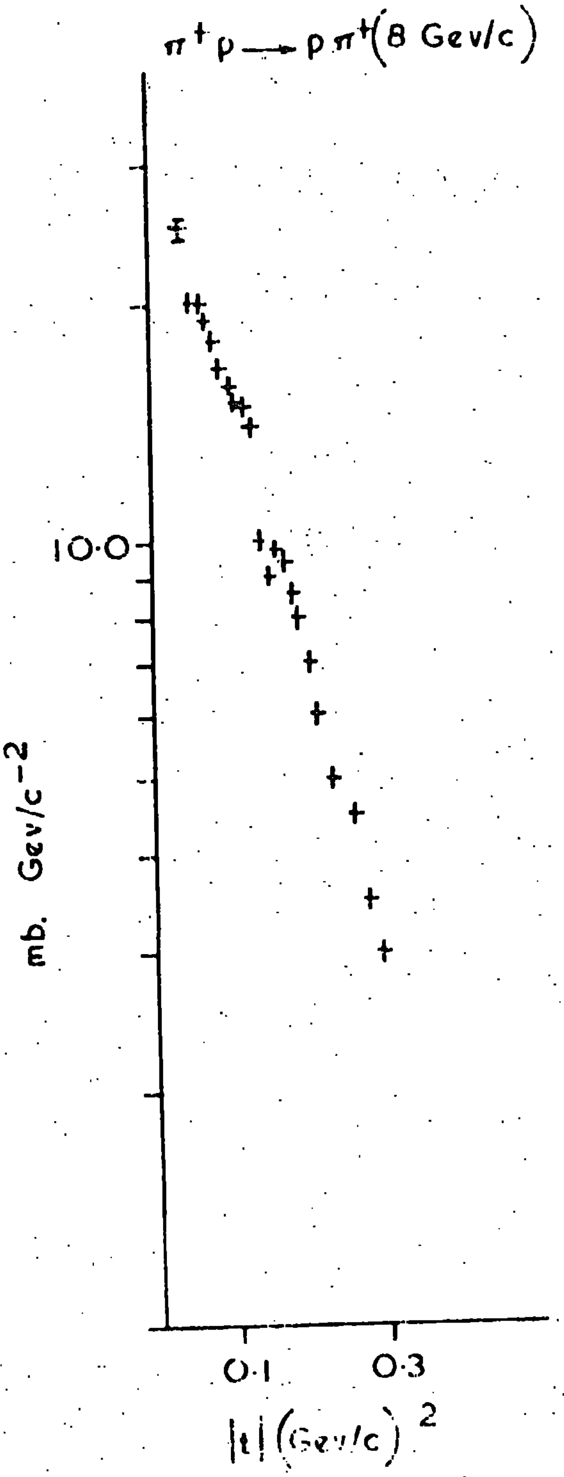

FIG. 27 (a)

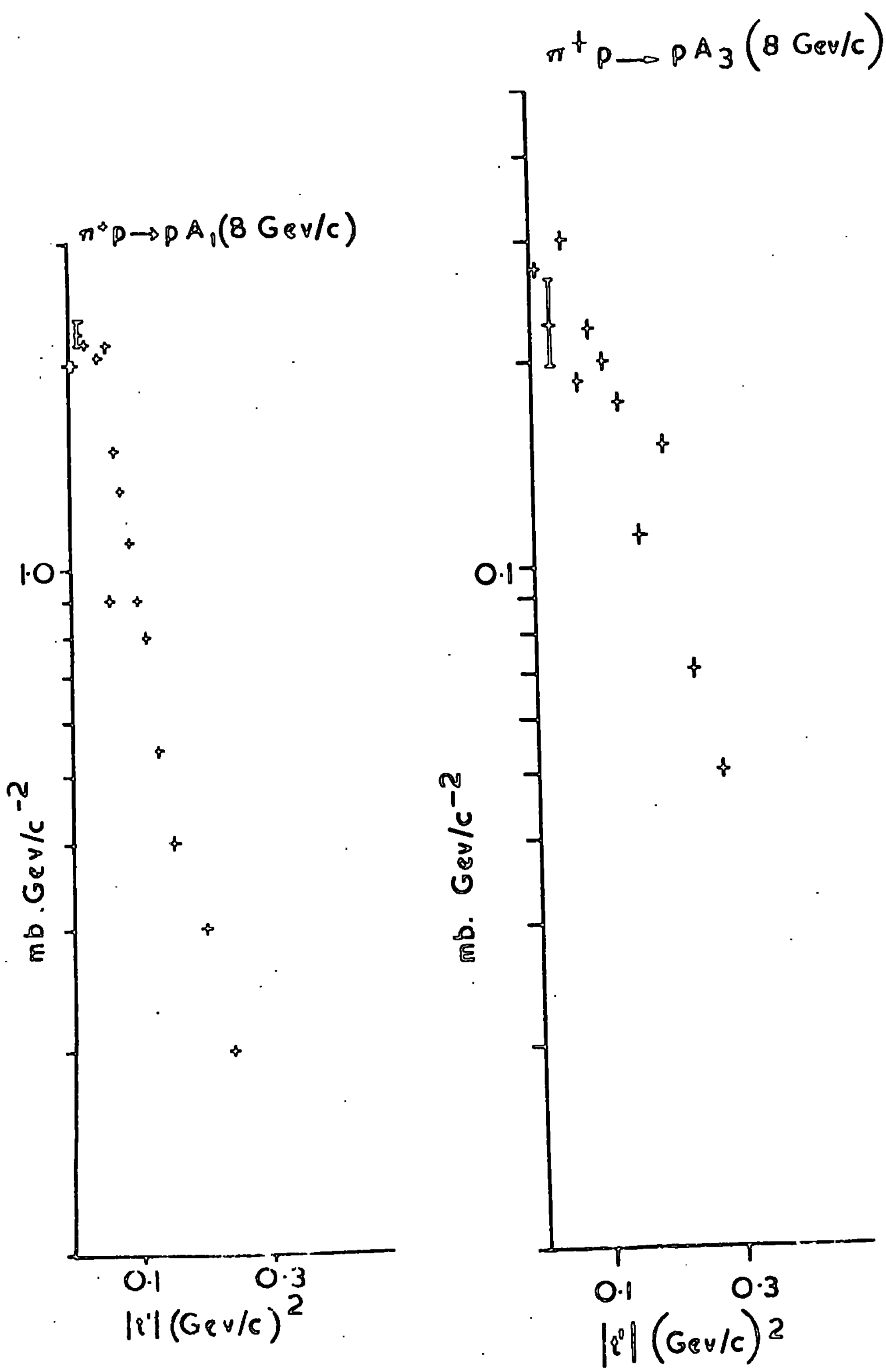

π⁺p → p A₁(8 Gev/c)
1·0
mb.Gev/c⁻²
0·1
0·3
|t'| (Gev/c)²
π⁺p → p A₃ (8 Gev/c)
0·1
mb. Gev/c⁻²
0·1
0·3
|t'| (Gev/c)²

FIG. 27 (b)

are based on very high statistics and as can be seen from figure 26 there is very good agreement from one experiment to another in that no dip appears at low t, and $d\sigma/dt$ seems to tend to the same value as t tends to zero, these results being obtained for incident pion momenta in the range 3.63 to 8.0 GeV/c. The difficulties of detecting and measuring the low momentum protons associated with small values of t, discussed in section 3.4 do not appear to distort the behaviour of $d\sigma/dt$ in this channel, since a correction for the effect can be easily applied.

$\underline{\pi^+ p \rightarrow pA_1 \text{ and } pA_3}$ channels.

Both these channels are studied in only one experiment, at an incident pion momentum of 8 GeV/c. Figure 27b shows the t' distribution of both channels, using a narrow bin width, and in neither case is there evidence of a significant dip. Figure 27a shows the elastic channel with the same t bin widths and a comparison of figures 27a and 27b shows that for these Pomeron exchange channels, the graphs have similar gradients, but the differential cross-sections at t' = 0 are very different.

It would appear then that there is no evidence of a dip at low t in either the $\pi^+ p \rightarrow pA_1$ or pA_3 channel.

4.2 Channels in which π-exchange can occur.

Of the channels studied in which the lightest exchange particle is the π and the initial state contains a proton and π^+, final states containing $\Delta^{++}\rho^o$, $\Delta^{++} f^o$, $P\rho^+$ and pg^+, are obtained, the first two involving charge exchange.

$\underline{\pi^+ p \rightarrow \Delta^{++}\rho}$ channel.

In this channel, generally speaking a dip occurs in the $d\sigma/dt$ versus t distributions for small values of t, but not in those where t' is used instead of t (see figure 28).

Considering first the t distributions, all the curves have the same basic shape, though the higher the momentum of the incident pion,

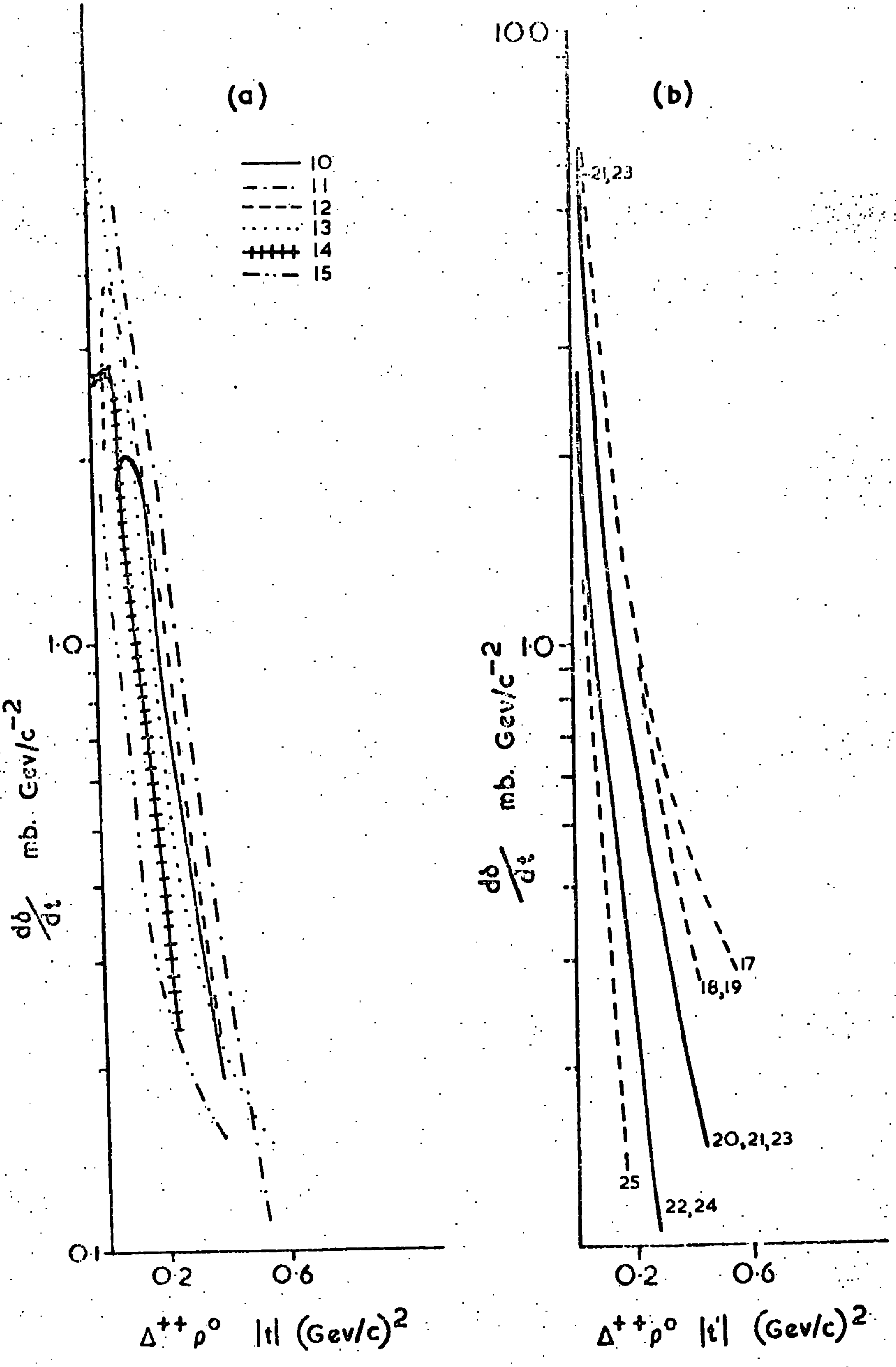

(a)
10
11
12
13
14
15
1·0
0·1
0·2
0·6
dδ/dt mb. Gev/c^-2
Δ^++ρ^o |t| (Gev/c)^2
(b)
100
10
21,23
17
18,19
20,21,23
25
22,24
0·2
0·6
dδ/dt mb. Gev/c^-2
Δ^++ρ^o |t'| (Gev/c)^2

FIG. 28 (a,b)

the narrower the peak of the curve, near $t = 0$, becomes. Graph 10 (corresponding to incident pion momenta of 2.95, 3.2, 3.5, 3.75 and 4.08 GeV/c), 12 (4 GeV/c), 13 (5.45 GeV/c), 14 (8 GeV/c) and 15 (11.7 GeV/c) all have a statistically significant turnover near $t = 0$. Graph 11 (4 GeV/c) possibly starts to turn over, though the points only carry on down to $t = 0.075$ $(GeV/c)^2$, which is not as low as the other graphs obtained for this channel. Graph 10 starts turning over at $t = 0.15$ $(GeV/c)^2$, whereas t_{min} for the corresponding incident pion momentum is approximately 0.06 $(GeV/c)^2$, this depending on the mass of the delta produced. At this value of t_{min}, the secondary proton tracks will be easily visible, since the protons will have a minimum and maximum momentum of 0.1 GeV/c and 0.6 GeV/c respectively, assuming that they are travelling co-linearly with the incident pion, and the delta formed has a mass of 1.236 GeV/c^2. The proton track lengths corresponding to these momenta are 0.04 cm and 20 cm.

Table 4 summarises the basic characteristics of these graphs;

Table 4 $\Delta^{++}\rho$ channel t graph summary

Graph no.	Incident pion momentum GeV/c	t_{min}	Posn. dip starts to occur t $(GeV/c)^2$
1	2.95→ 4.08	-	0.15 [1]
2	4.0	0.06	0.1 [2]
3	4.0	0.06	0.06
4	5.45	0.04	0.04
5	8.0	0.025	0.08 [3]
6	11.7	0.02	0.02

1. Low momenta are used in this graph, and so t_{min} can have large values (see figure 16).
   Hence it would be expected that the graph turns over as it does.
2. A large t bin width is used and hence a dip would not be noticed.
3. The position the dip starts to occur corresponds to a minimum and maximum proton path length of 0.8cm and 22cm respectively, meaning that it is likely that the particles will be seen, i.e. a significant dip.

However on examination of the t'graphs (figure 28b) none display a dip.

It would appear then that, looking at the position the graphs turn over and the position of t_{min}, the turnover in the t graphs in this particular reaction is due to the width of the resonance masses, and not to a physical mechanism connected with low t transfers. The possible non-visibility of protons associated with low t transfers could be reasonably supposed to be unimportant.

$\pi^+ p \rightarrow \Delta^{++} f^o$ channel

In this channel, the t distributions (figure 29a) give strong evidence for the occurrence of a dip. However the corresponding t' graphs (figure 29b) do not show a dip. The graphs are based on experiments at incident pion momenta of 3.5 GeV/c to 8 GeV/c, and for these values, t_{min} is large and corresponds to the value at which the dip occurs in the t graphs. A further experiment at 13.1 GeV/c also shows no evidence of a dip in the t' graph.

Since t_{min} is so large for this channel, there will be no problems concerning the visibility of low momentum protons, and so it would appear

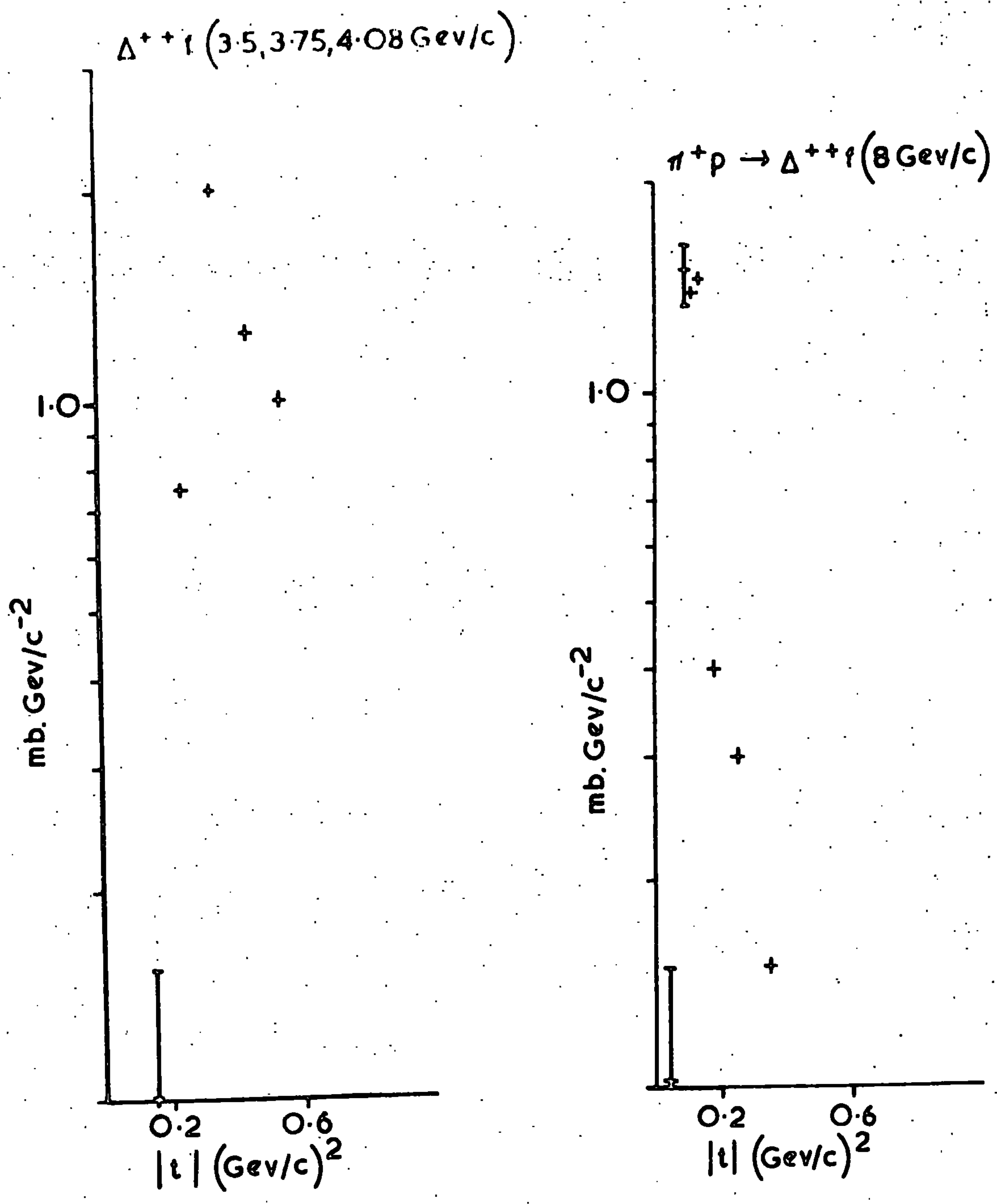

Δ⁺⁺f (3.5, 3.75, 4.08 Gev/c)
1.0
mb. Gev/c⁻²
0.2
0.6
|t| (Gev/c)²
π⁺p → Δ⁺⁺f (8 Gev/c)
1.0
mb. Gev/c⁻²
0.2
0.6
|t| (Gev/c)²

FIG. 29 (a)

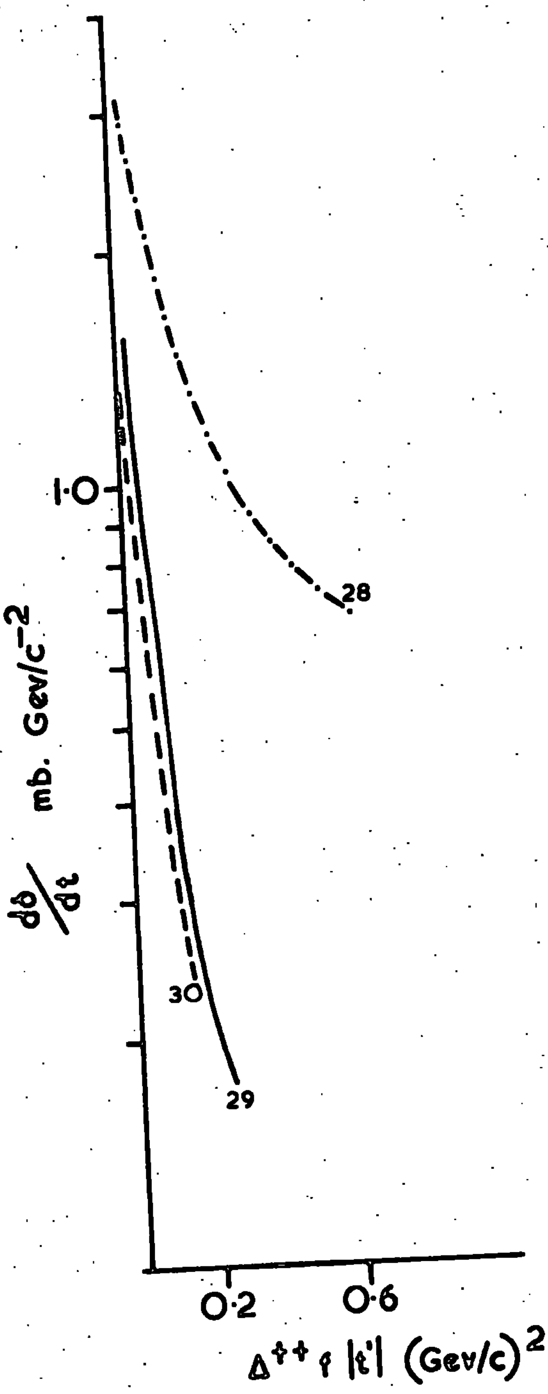

FIG. 29 (b)

then that in this channel there is no evidence for a dip at low t, other than that associated with the resonance widths.

$\pi^+p \rightarrow p\rho^+$ channel

Considering the t graphs, which are based on incident pion momenta of 4 GeV/c and 8 GeV/c, and are summarised in figure 30a, the graphs of the 4.0 GeV/c data do not show a statistically significant dip, while those at 8.0 GeV/c do, the dip occurring at $t = 0.06\ (GeV/c)^2$. Since t_{min} is so small relative to the position the dip occurs, it would be expected that the t' graphs (5 GeV/c and 8 GeV/c) (figure 30b) would also show the dip and indeed a dip occurs in all but one of them. Since the dip corresponds to a proton track length of 3mm, or less, it seems possible that it may be caused by difficulties associated with short proton tracks and is not due to some physical effect.

$\pi^+p \rightarrow p\sigma^+$ channel

The t graph (figure 31) for an incident pion momentum of 8 GeV/c shows a dip starting at $t = 0.1\ (GeV/c)^2$, for which t transfer the proton tracks are long enough to be seen. However, this dip occurs near t_{min}, and since the corresponding t' graph has no dip it indicates that there is no dip of physical origin in this channel, though the experimental evidence is not strong enough to be certain since it is based on only one experiment.

4.3. Channels in which ρ-exchange can occur

Of the channels studied in which the lightest exchange particle is the ρ and the initial state contains a proton and π^+, final states containing $\Delta^{++}\omega^o$, $\Delta^{++}\pi^o$, $\Delta^{++}A_2^{\ o}$ and $pA_2^{\ +}$ are obtained, the first three involving charge exchange.

$\pi^+p \rightarrow \Delta^{++}\omega^o$ channel

In this channel the t graphs (2.92 GeV/c to 8 GeV/c) which are shown in figure 32a, and the t' graphs (2.92 GeV/c to 8 GeV/c), which are shown

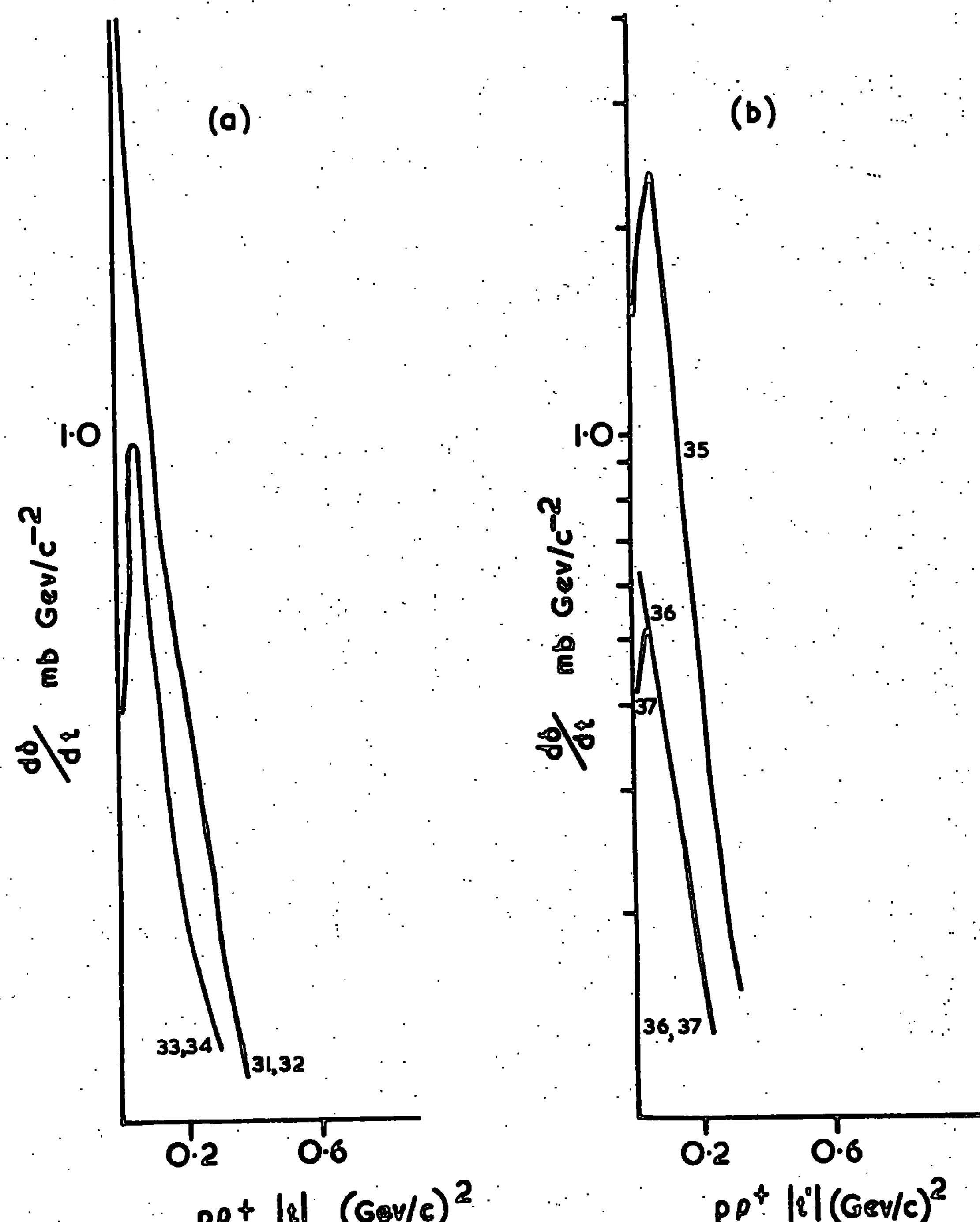

(a)
1·0
dσ/dt mb Gev/c^-2
33,34
31,32
0·2
0·6
pρ+ |t| (Gev/c)^2
(b)
1·0
35
36
37
36,37
dσ/dt mb Gev/c^-2
0·2
0·6
pρ+ |t'| (Gev/c)^2

FIG.30 (a,b)

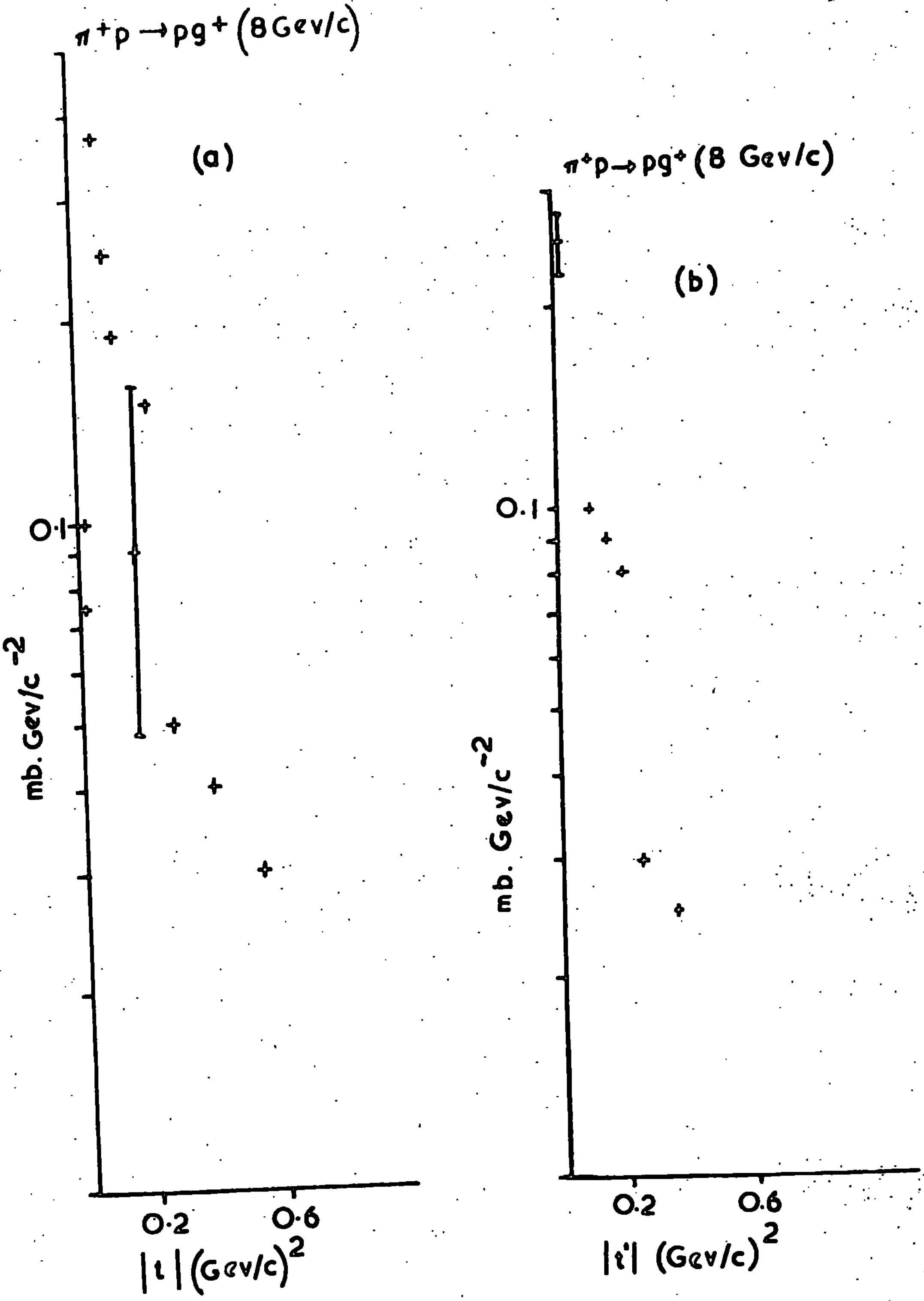

$\pi^+p \rightarrow pg^+$ (8 Gev/c)
(a)
0·1
mb. Gev/c^{-2}
0·2
0·6
$|t|$ (Gev/c)^2
$\pi^+p \rightarrow pg^+$ (8 Gev/c)
(b)
0.1
mb. Gev/c^{-2}
0.2
0.6
$|t'|$ (Gev/c)^2

FIG. 31 (a,b)

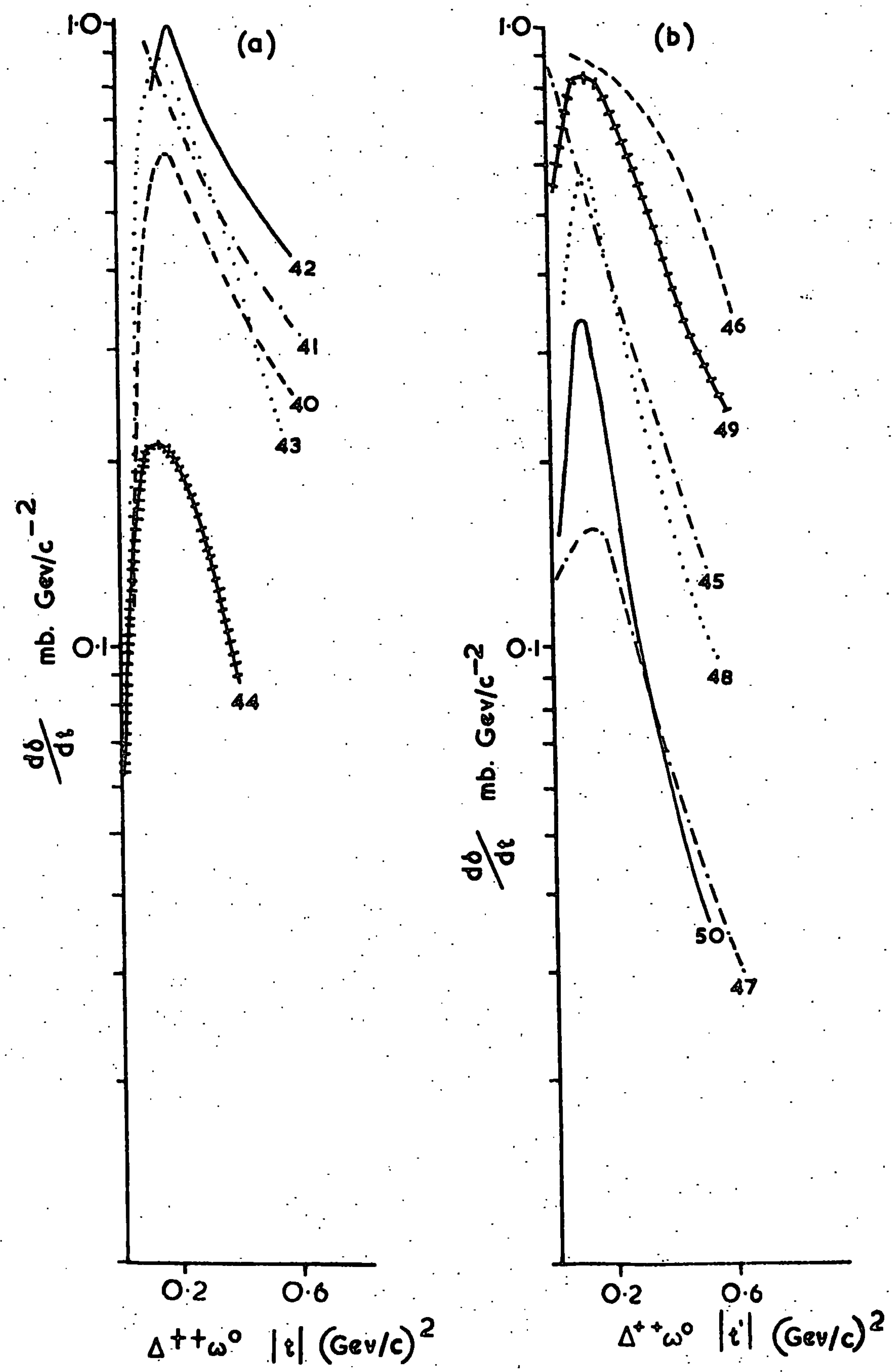

(a)
1·0
0·1
dσ/dt mb. Gev/c^-2
42
41
40
43
44
0·2
0·6
Δ++ω° |t| (Gev/c)^2
(b)
1·0
0·1
dσ/dt mb. Gev/c^-2
46
49
45
48
50
47
0·2
0·6
Δ++ω° |t'| (Gev/c)^2

FIG. 32 (a,b)

in figure 32b, in many cases show a pronounced, statistically significant dip. This dip occurs in all the t graphs except those at 4.0 GeV/c (graph 41) and appears in the t' graphs as the incident pion momenta increases, becoming significant above 5.0 GeV/c (graphs 48, 49, 50). Since the dip appears at $t \approx 0.2$ $(\mathrm{GeV}/c)^2$ for all the graphs in which it occurs, which represents a minimum secondary proton track length of 4 cm., it would seem likely that the turnover is caused by some physical mechanism of the interaction. There may be a momentum dependence for the effect since it is clear from figure 32b, that below 5 GeV/c (graphs 45, 46, 47) there is not much evidence of a dip. The t' curves do not appear to drop to a constant value of $d\sigma/dt'$ at $t' = 0$ even though there are reasonable statistics at this value of t', indicating that the normalisation of this channel has not been completely successful. Even so, this does not alter the significance of the dip in this channel above 5 GeV/c which cannot be accounted for either by the width of the resonance nor by the visibility of the secondary proton.

$\pi^+ p \rightarrow \Delta^{++}\pi^0$ channel

The results for this channel are based on incident pion momenta of 3.54 GeV/c to 13.1 GeV/c for the t graphs (figure 33a) and 5 and 8 GeV/c for the t' graphs (figure 33b). Generally the t graphs exhibit a dip but the evidence from the t' graphs is not so strong.

In five of the six t graphs (the exception being the one at 13.1 GeV/c) a dip occurs, and is in the region $t \approx 0.06$ $(\mathrm{GeV}/c)^2$. This is well above t_{min}, but more significantly corresponds to a proton range of 3mm., which is about the minimum track length to be measured on the scanning table. Of the five graphs with some evidence for dips it should be noted that the one at 4 GeV/c as published, exhibits an anomalously high cross-section. The sixth t graph for 13.1 GeV/c is at a significantly higher momentum than the others, and no dip occurs, possibly indicating

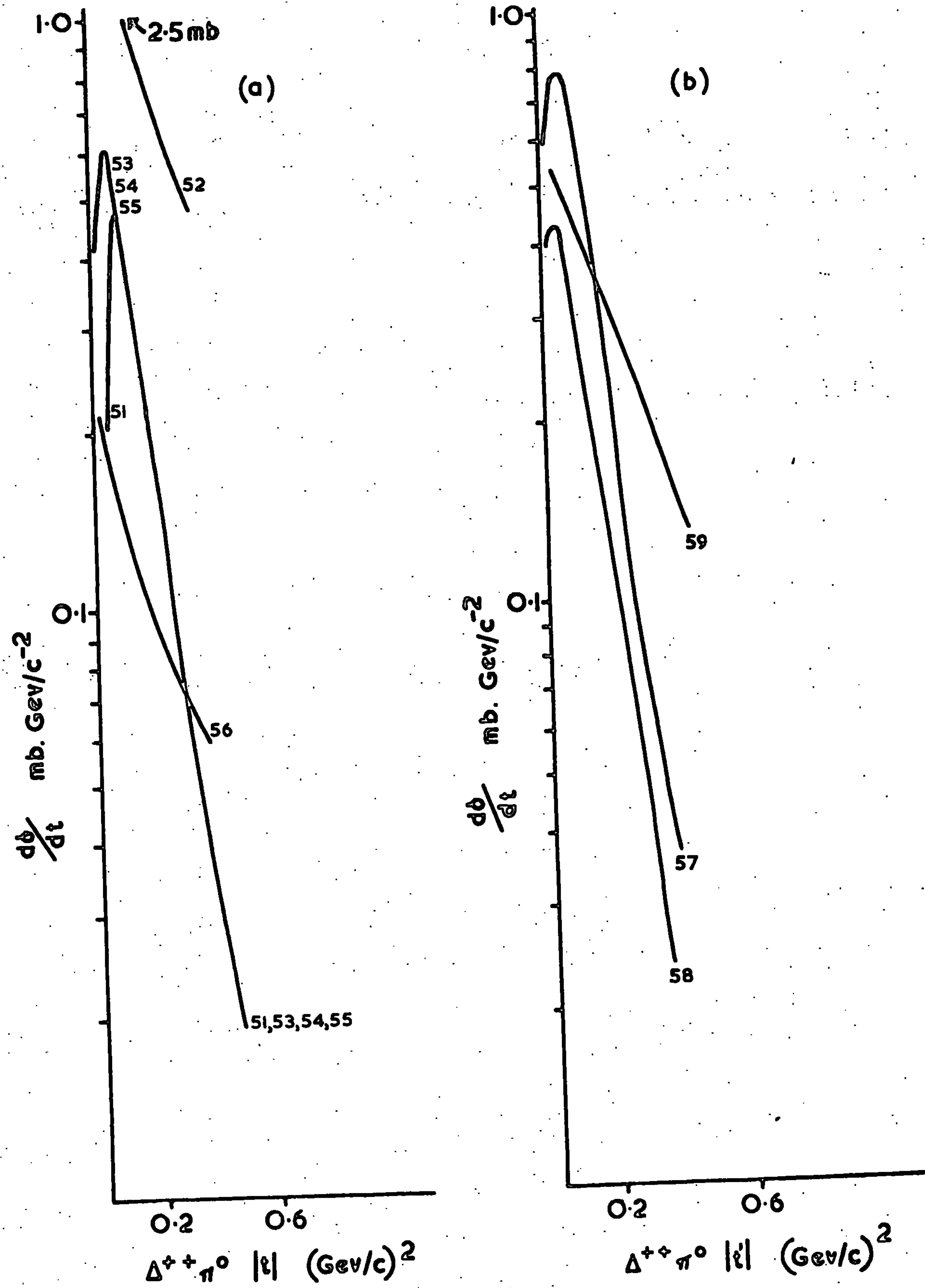

1·0
2·5mb
(a)
53
54
55
52
51
0·1
56
51,53,54,55
dσ/dt mb. Gev/c^-2
0·2
0·6
Δ++π° |t| (Gev/c)^2
1·0
(b)
59
0·1
57
58
dσ/dt mb. Gev/c^-2
0·2
0·6
Δ++π° |t| (Gev/c)^2

FIG. 33 (a,b)

that the effect is momentum dependent.

Since t_{min} is so small relative to the position the dip occurs, it would be expected that the t' graphs would be almost exactly the same as the t graphs, and this is in fact so.

It would appear then that both the t and the t' graphs turnover, but they do so at a value of t which corresponds to a region of difficulty for measuring proton tracks, and so it is unlikely that this dip is a feature of the interaction mechanism.

$\pi^{+}p \rightarrow \Delta^{++}A_2^{o}$ channel

The t' graphs (figure 34) obtained for this channel is based on an experiment at 8 GeV/c, and does not show a statistically significant dip. At this energy $t_{min} \approx 0.15$ $(\mathrm{GeV}/c)^2$ so the secondary protons have reasonably long ranges.

$\pi^{+}p \rightarrow pA_2^{+}$ channel

The results for this channel are based on incident pion momenta of 4 GeV/c and 8 GeV/c for the t graphs (fig. 35a) and 5 GeV/c and 8 GeV/c for the t' graphs (fig. 35b). Both t graphs have the same general shape above $t \approx 0.05$ $(\mathrm{GeV}/c)^2$ but the one at 8 GeV/c, which has a point below this value of t shows a significant dip. However this point is near t_{min}, and neither of the two t' graphs show a dip.

It would appear then that this channel does not show a dip. Visibility considerations are not important in this channel at the energies considered.

4.4 Channels in which other exchanges occur

In this category are two channels, the $\Delta^{++}\eta^{o}$ final state firstly which has as its lightest exchange particle the A_2, and also involves charge exchange. The second is the pB^{+} final state which has ω exchange.

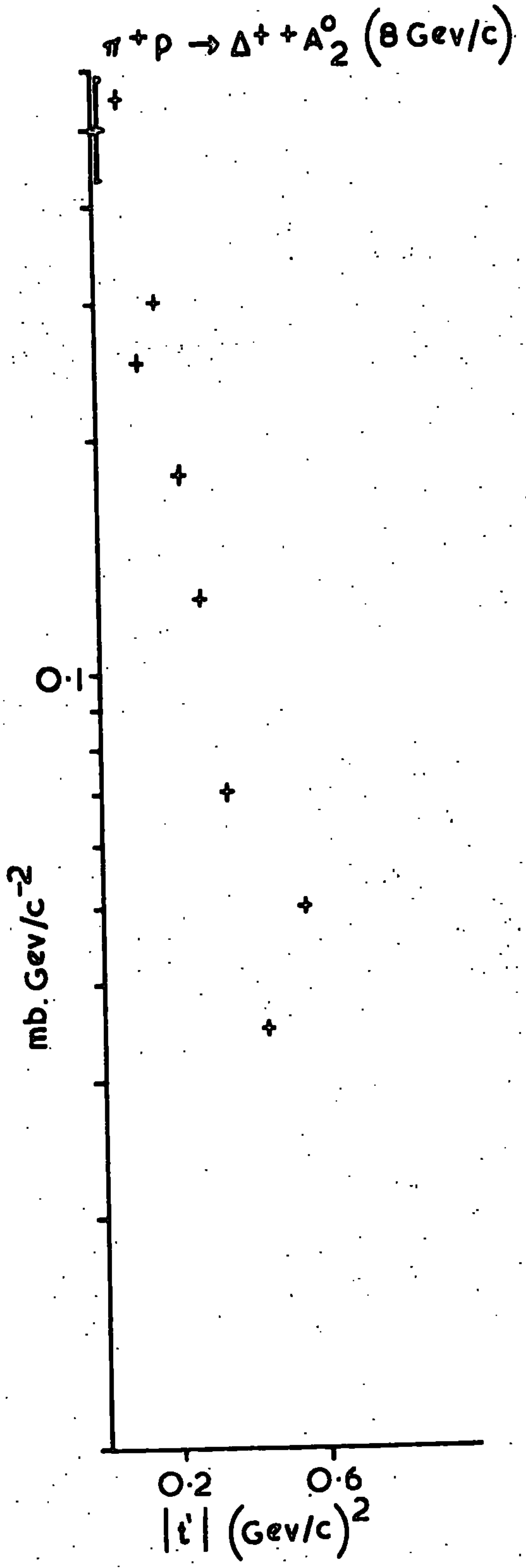

FIG. 34

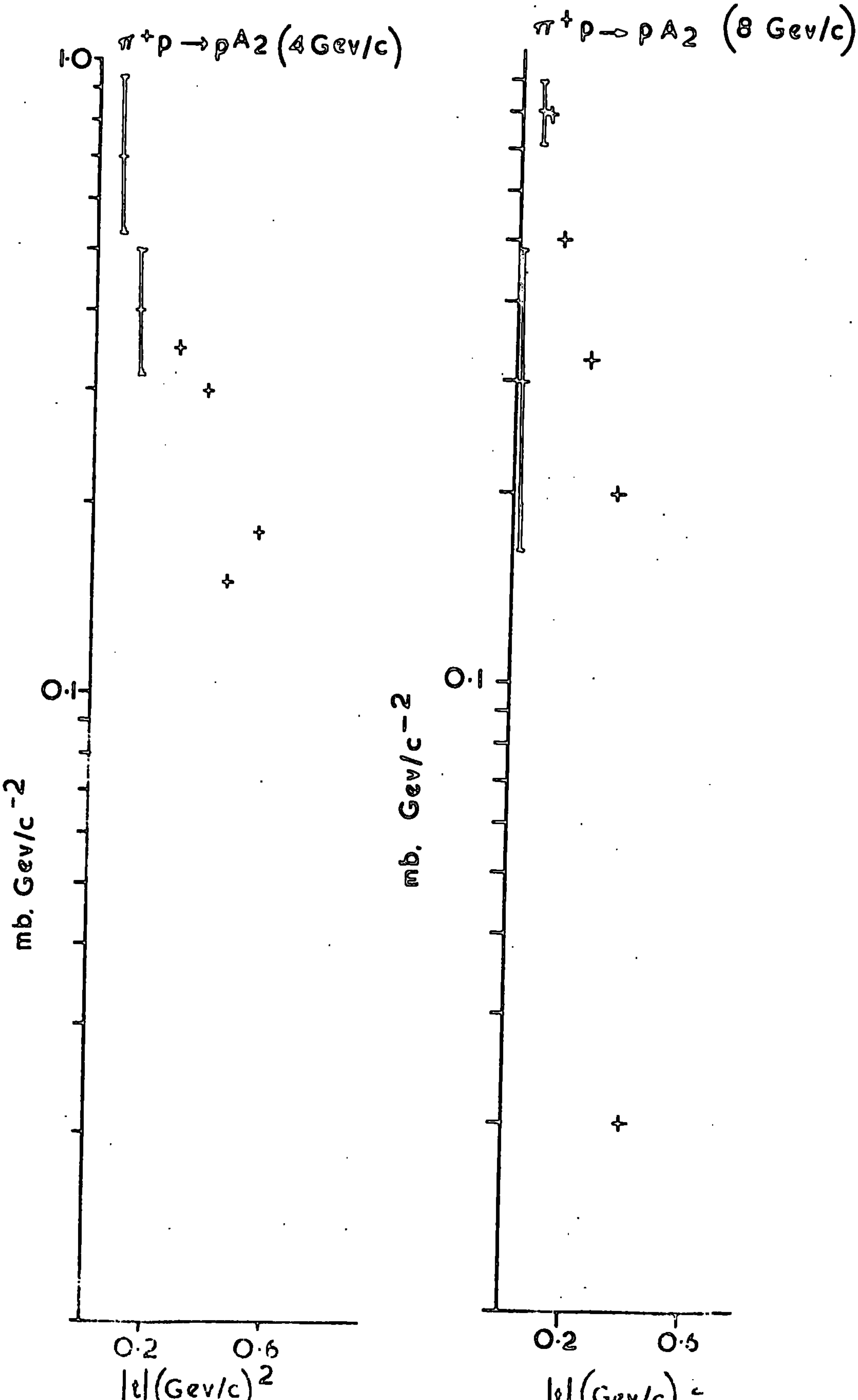

π⁺p → pA2 (4 Gev/c)
1·0
0·1
mb. Gev/c⁻²
0·2
0·6
|t| (Gev/c)²
π⁺p → pA2 (8 Gev/c)
0·1
mb. Gev/c⁻²
0·2
0·6
|t| (Gev/c)

FIG.35 (a)

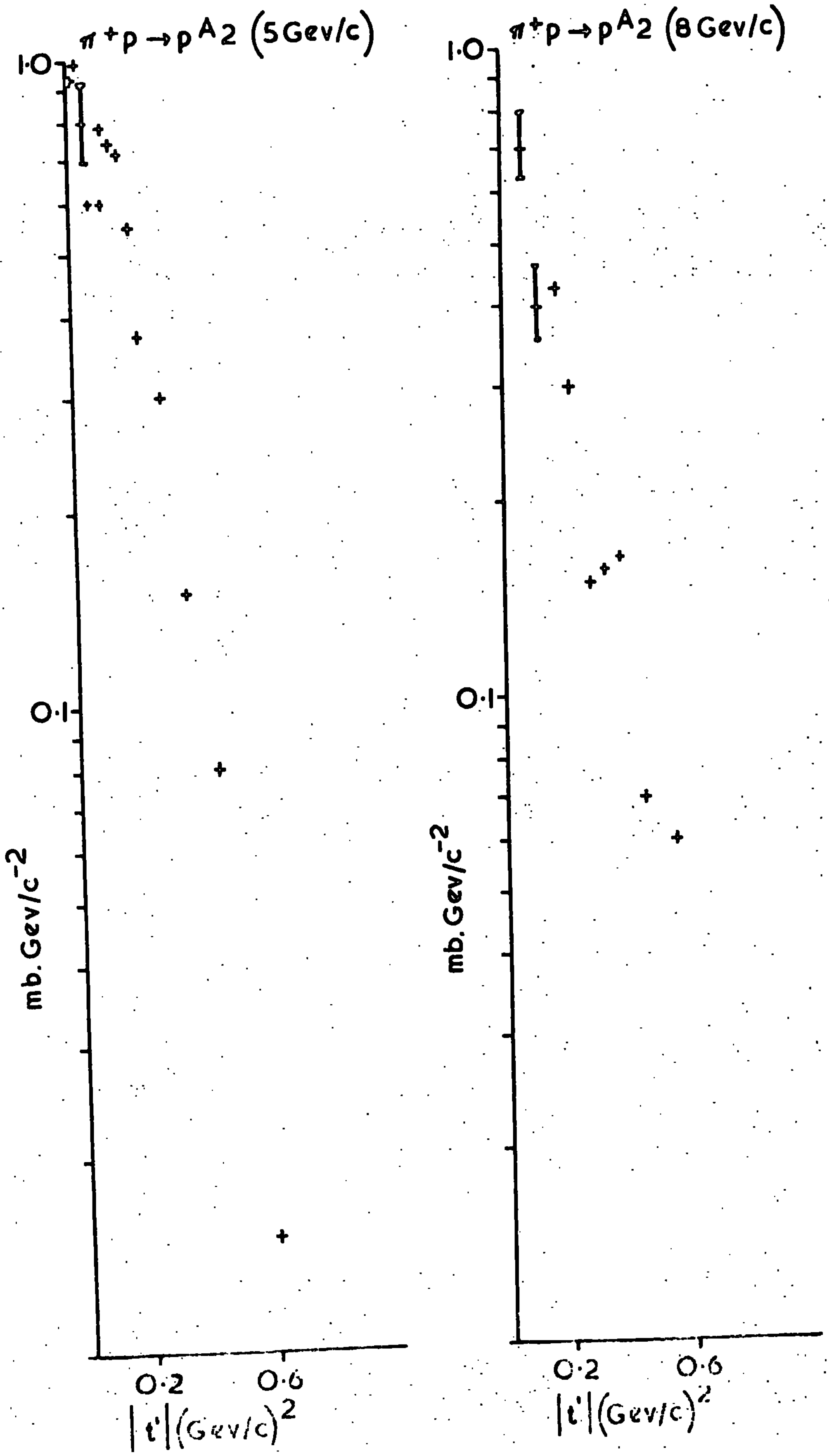

$\pi^+p \to pA_2$ (5Gev/c)
1.0
0.1
mb.Gev/c^{-2}
0.2
0.6
|t'|(Gev/c)^2
$\pi^+p \to pA_2$ (8Gev/c)
1.0
0.1
mb.Gev/c^{-2}
0.2
0.6
|t'|(Gev/c)^2

FIG. 35 (b)

$\pi^+ p \rightarrow \Delta^{++} \eta^o$ channel

This channel is based on experiments at incident pion momenta of 2.95 GeV/c to 8 GeV/c. For both the t graphs (figure 36a) a curious curve shape is obtained since $d\sigma/dt$ is nearly constant from $t = 0.02$ to 0.45 $(GeV/c)^2$. For an incident pion momentum of 4 GeV/c, the minimum secondary proton track length is 2.5cm, and for lower momenta this minimum increases so it is unlikely that events will be lost due to difficulties of measurement. The dip on the lower momentum t graph is partly due to the width of the delta resonance since it occurs at a value of t which is below t_{min} for all but the highest momentum concerned, ie 4.08 GeV/c. On the 8 GeV/c t graph; the curve tends to flatten out rather than to dip.

However considering the t' graphs (figure 36b), all the curves show a statistically significant dip, the two at 5 GeV/c (68,69) dipping at $t' \approx 0.15 (GeV/c)^2$, while the remaining two dip at $t' \approx 0.25$ $(GeV/c)^2$.

It would appear that the dip in the t' graphs in this channel cannot be accounted for either by short ranges of the secondary proton tracks, nor by the effect of the resonance widths, and so appears to be physically caused.

$\pi^+ p \rightarrow pB^+$ channel

Only t' graphs are available for this channel and are displayed in figure 37. One is at an energy of 5 GeV/c and the other at 8 GeV/c. The points on neither graph indicate a dip. There is not likely to be a problem with short range tracks for t transfers in the region of t_{min} since it is large $(> 0.6 (GeV/c)^2)$.

4.5 Conclusions

(i) It would appear that bubble chambers are not ideal for the determination of the presence or absence of a dip in the majority of quasi two body final states resulting from $\pi^+ p$ interactions since difficulties

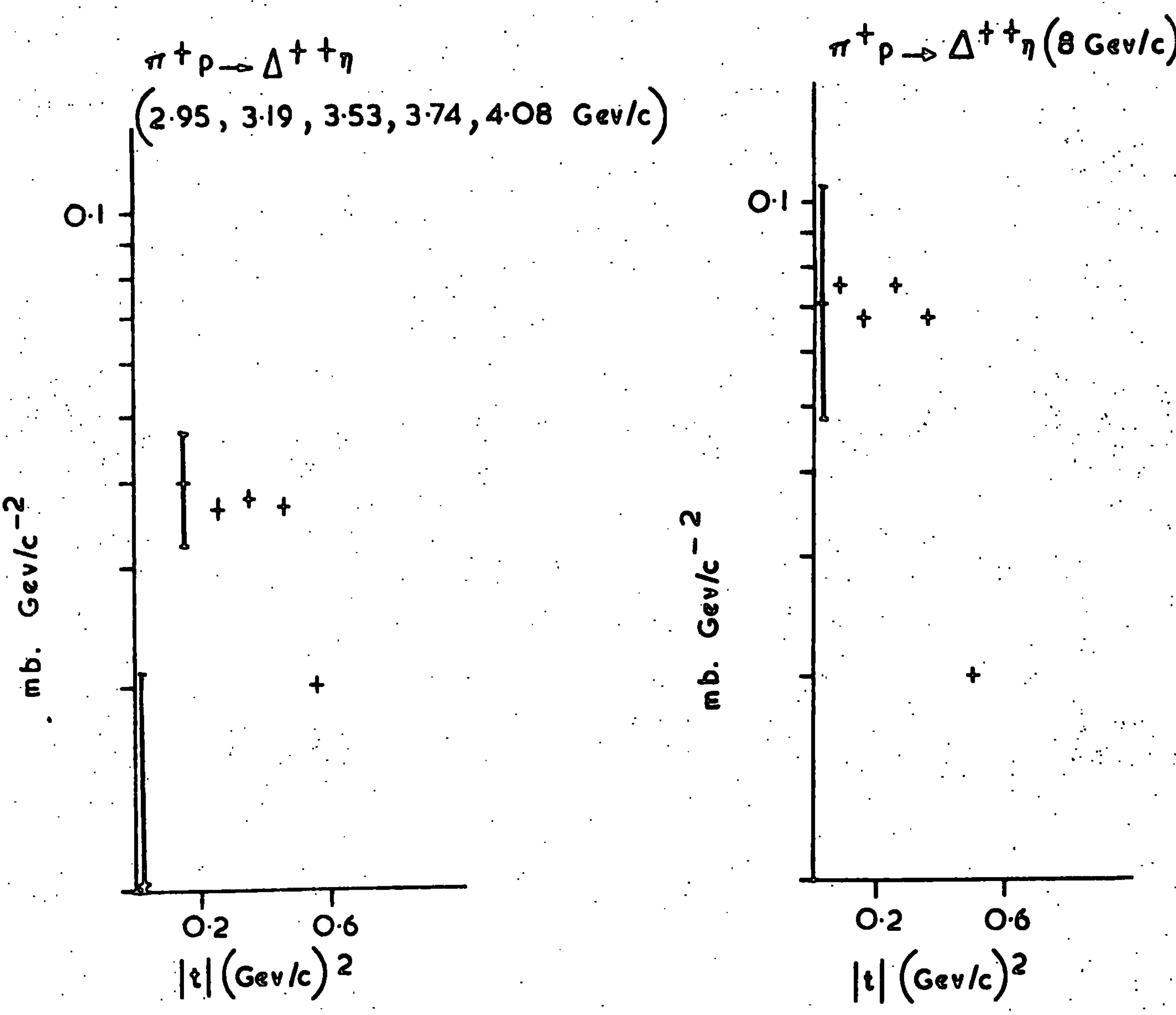

$\pi^+ p \rightarrow \Delta^{++} \eta$
(2·95, 3·19, 3·53, 3·74, 4·08 Gev/c)
0·1
mb. Gev/c^{-2}
0·2
0·6
$|t|$ (Gev/c)^2
$\pi^+ p \rightarrow \Delta^{++} \eta$ (8 Gev/c)
0·1
mb. Gev/c^{-2}
0·2
0·6
$|t|$ (Gev/c)^2

FIG. 36 (a)

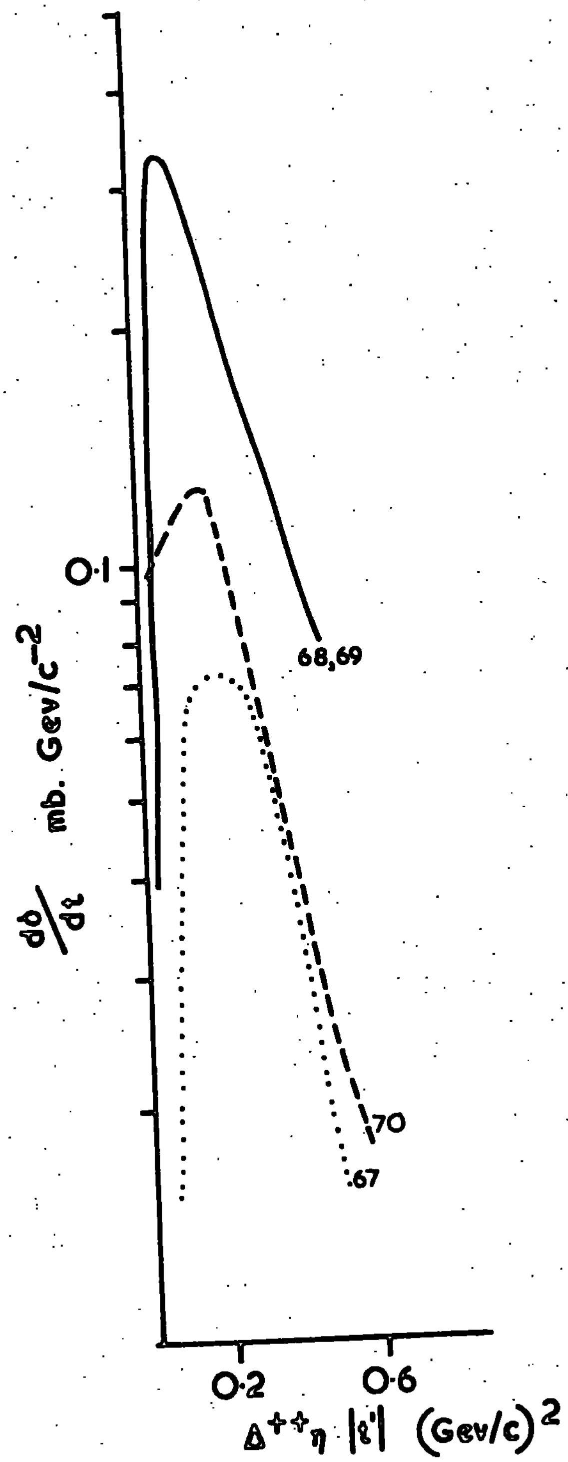

FIG. 36 (b)

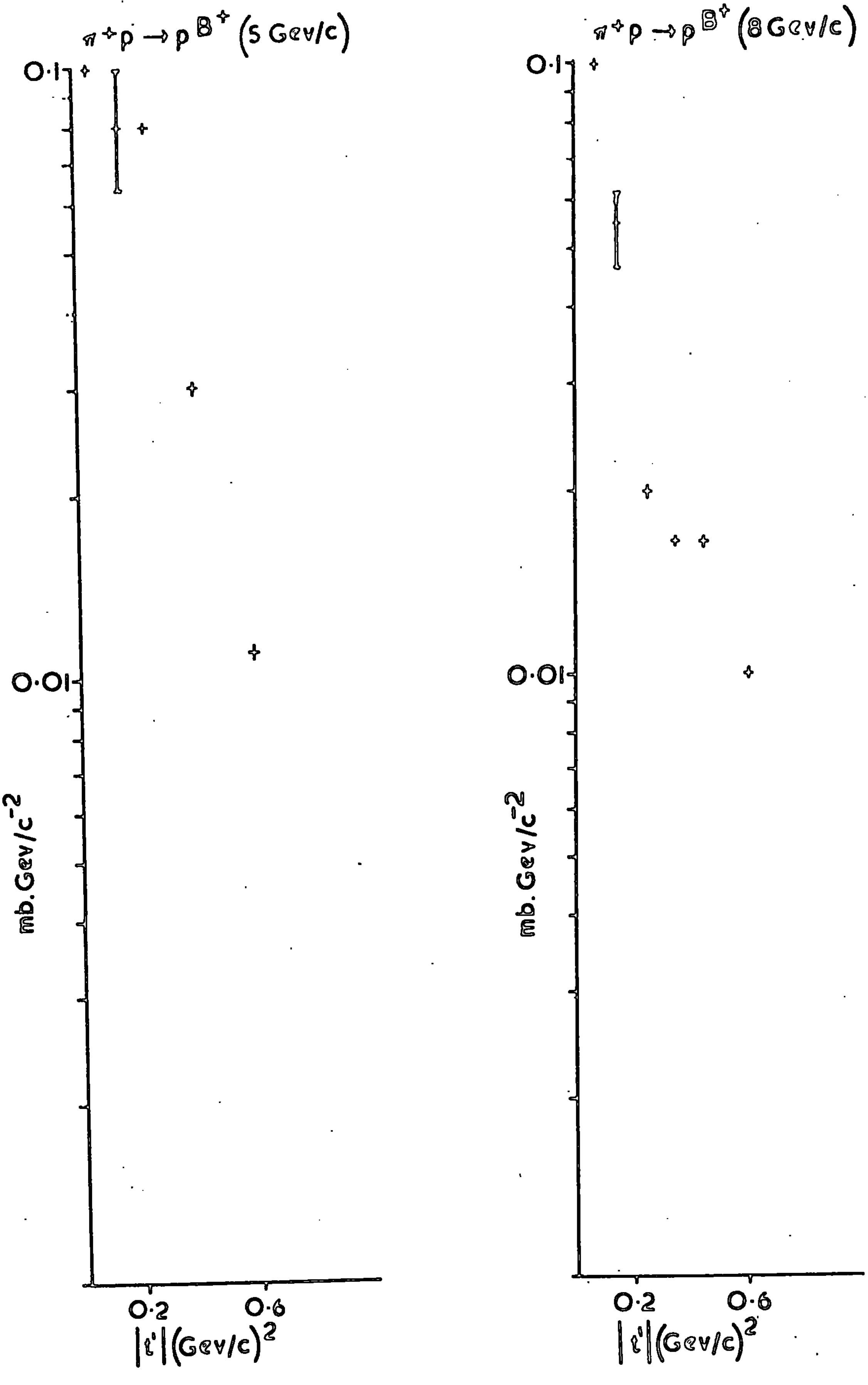

π⁺p → p B⁺ (5 Gev/c)
0·1
0·01
mb.Gev/c⁻²
0·2
0·6
|t'|(Gev/c)²
π⁺p → p B⁺ (8 Gev/c)
0·1
0·01
mb.Gev/c⁻²
0·2
0·6
|t'|(Gev/c)²

FIG. 37

may arise from the handling and fitting of short proton tracks resulting from low t-transfers and the total statistics available in any one channel are limited.

(ii) There is no evidence to suggest a dip in the $\pi^{+}p$, pA_1^{+}, pA_3^{+}, $\Delta^{++}\rho^{o}$, $\Delta^{++}f^{o}$, pg^{+}, pA_2^{+} and pB^{+} final states.

(iii) There is a statistically significant dip in the $p\rho^{+}$, $\Delta^{++}\pi^{o}$ and $\Delta^{++}A_2^{o}$, final states but this can be at least partially accounted for in each case. Collins (ref 22) suggests that in the $p\rho^{+}$ channel there should be a dip. In the $\Delta^{++}f^{o}$ channel, which is the only other channel common to this survey and his article, he suggests there should be a spike at low t.

(iv) In the $\Delta^{++}\omega^{o}$ and $\Delta^{++}\eta^{o}$ channels, a statistically significant dip occurs, these channels having exchange particles ρ and B, and A_2 respectively. Both the ω and η have isospin T = 0, and at the meson vertex charge exchange has occurred.

Of the other final states which involve ρ and charge exchange, namely $\Delta^{++}A_2^{o}$ $\Delta^{++}\pi^{o}$, both these channels have a dip which can at least partially be accounted for. The other ρ exchange channel which leads to the pA_2^{+} final state does not involve charge exchange and does not show a dip.

No channels are considered other than the $\Delta^{++}\eta^{o}$ one, which have as their lightest exchange particle the A_2.

APPENDIX ONE

Quantum numbers and conservation laws

Besides the classical conservation laws which govern energy, momentum and angular momentum, in nuclear physics others become apparent also, and these control the number of baryons and leptons allowed in any given state. There are also more conservation laws which govern the strong interaction.

(i) Isospin (I)

This is also known as isotopic spin. The observations of charge independence in proton-proton and proton-neutron interactions (ie the observation that the interaction cross-sections depend on the orbital angular momentum and spins and not the charge) indicated that the inter-nucleon forces are equal, the proton and neutron being the charged states of a basic particle called the nucleon, the charge depending on the z-component of the isospin I (the isospin behaving like angular momentum ℓ in ordinary space, I being quantised along the charge axis I_z, equivalent to ℓ_z). Isospin is an additive quantum number.

Since the nucleon has two charged states (ie the proton and neutron), therefore $I = \frac{1}{2}$, and $I_3 = \pm \frac{1}{2}$. The charge Q of the nucleon is given by:-

$$Q = I_3 + B/2$$

Where B = the baryon number.

Similarly the pion exists in three charged states so I = 1, and $I_3 = +1$, 0 and -1.

(ii) Parity (P)

The property of the parity operator is that, when it operates on a function, it changes each of the position variables to its negative. Obviously if a function is operated on twice, the original function is left, and hence an eigenfunction corresponding to the eigenfunction +1 for the parity operator is said to be a function of even parity and an eigenvalue -1 of odd parity. In strong interactions, the parity of a system must remain unchanged; ie parity is conserved. Since the orbital angular momentum part of the total wave function has even parity for even ℓ and odd parity for odd ℓ, the parity is $(-1)^{\ell}$.

Since strong interactions involve the creation and annihilation of particles, the intrinsic parity of the particles must be introduced (this is defined to be even for the nucleon and determined experimentally for other particles) and hence the parity of a two particle system, with the particles having intrinsic parities P_1 and P_2 and relative orbital angular momentum ℓ is given by:-

$$P = P_1 . P_2 . (-1)^{\ell}$$

(iii) Charge conjugation (C)

The action of C is to transform a particle into its own anti-particle, such that the quantum numbers (such as those corresponding to electric charge, baryon number and strangeness) all take on their opposite values. Only neutral particles can have a definite C-parity (**NB** C-parity is multiplicative).

(iv) G-parity

In strong interactions both C and I are simultaneously conserved and this forms the basis for the definition of G thus:-

$$G = C.\exp\,(i\pi I_2)$$

where $\exp(i\pi I_2)$ represents a rotation of 180° about the second I-spin axis.

(v) Strangeness (S) and hypercharge (Y)

As the range of known strongly interacting particles increased, it was found that a whole series of transitions which would be expected to occur as strong interactions and which did not violate any of the known conservation laws either did not take place, or if they did occur did so only via the weak or electromagnetic processes.

Therefore a new additive quantum number S, was introduced, this being conserved in strong interactions. The hypercharge is then defined as:-

$$Y = B + S$$

Since all strong interactions conserve the quantities I, G, J and P, all particles produced in strong interactions can be assigned these numbers, and this is usually done in the form $I^G (J^P)$.

APPENDIX TWO

Crossing symmetry

The scattering amplitude T, introduced in chapter two, can be expressed generally and symmetrically by the three Mandelstamm variables s, t and u (through only two of them are independent). It follows from general symmetry laws that:-

$$T\ (s,t,u) = T\ (s,u,t)$$
$$= T\ (u,t,s)$$

Since that only means that some change in the direction of flight of the particles is involved, this type of symmetry of the scattering amplitude is called the 'crossing symmetry'.

APPENDIX THREE

Collection of all the individual t and t' graphs for the reactions studied.

Note: the large number below each diagram indicates the number of the graph, while the small super script indicates the reference from which it was obtained.

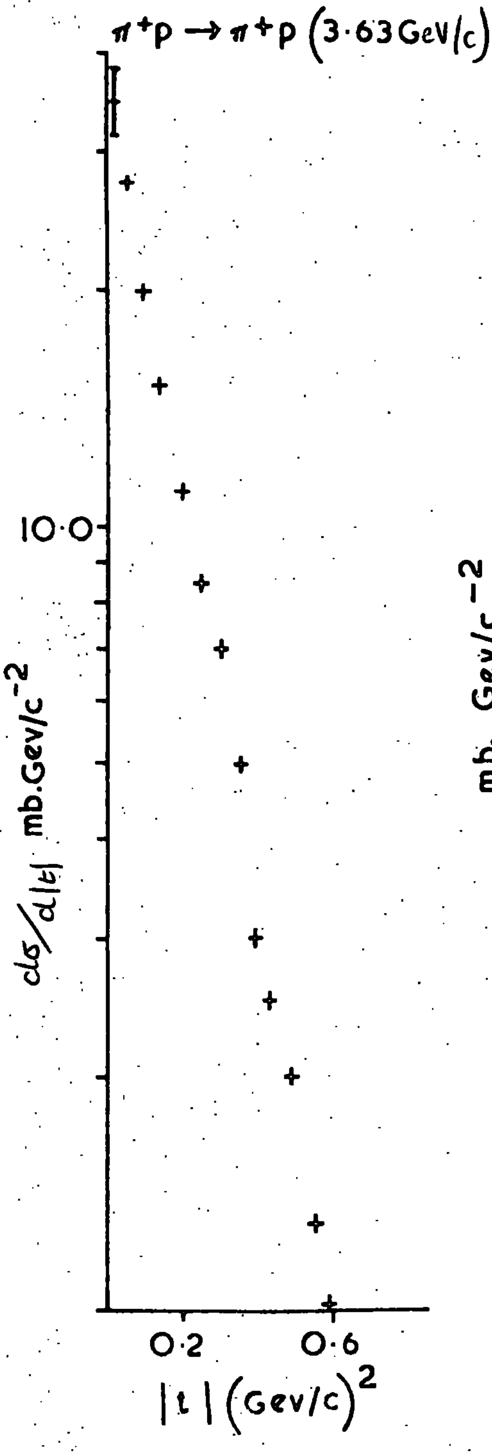
π⁺p → π⁺p (3·63 GeV/c)
10·0
dσ/d|t| mb.Gev/c⁻²
0·2
0·6
|t| (Gev/c)²

1[37]

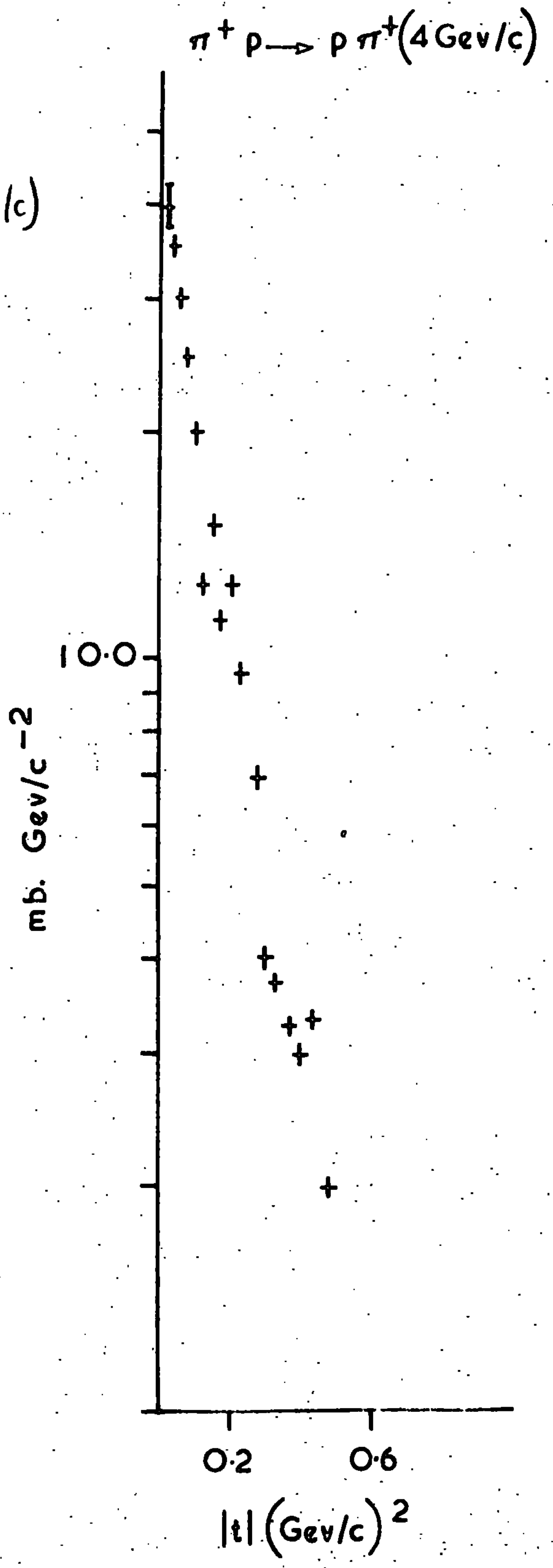
π⁺ p → p π⁺ (4 Gev/c)
10·0
mb. Gev/c⁻²
0·2
0·6
|t| (Gev/c)²

2[25]

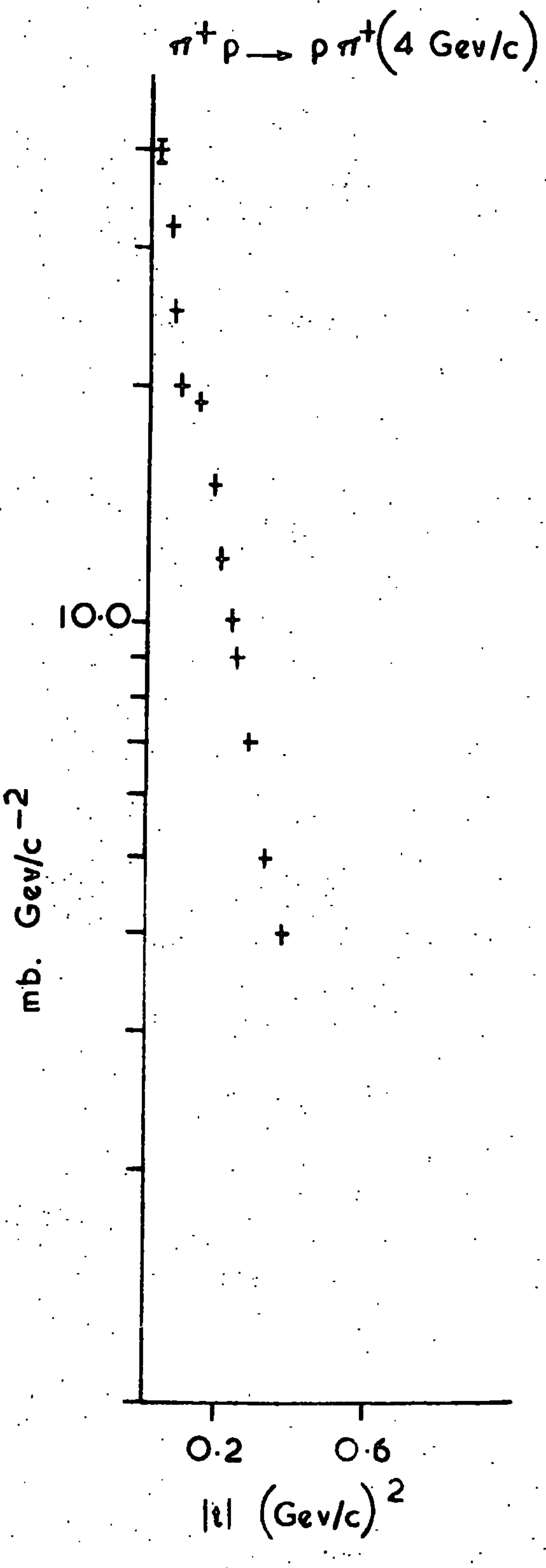
$\pi^+ p \to p \pi^+$ (4 Gev/c)
10.0
mb. Gev/c^{-2}
0.2
0.6
|t| (Gev/c)^2

3[38]

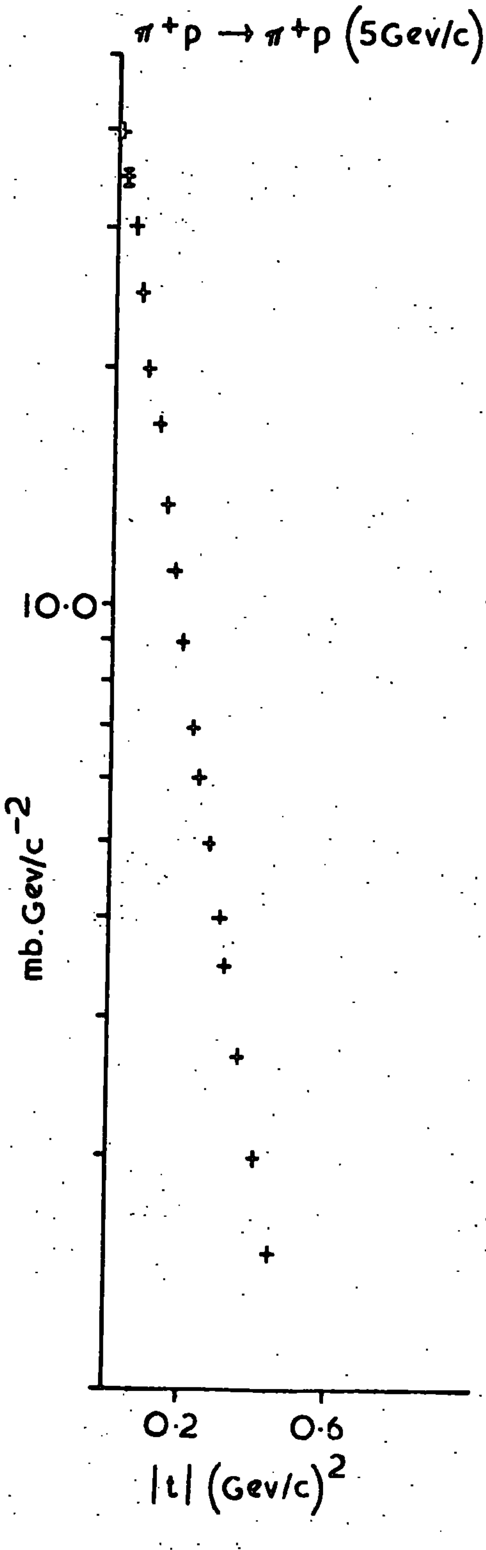
$\pi^+ p \to \pi^+ p$ (5Gev/c)
10.0
mb. Gev/c^{-2}
0.2
0.6
|t| (Gev/c)^2

4[35]

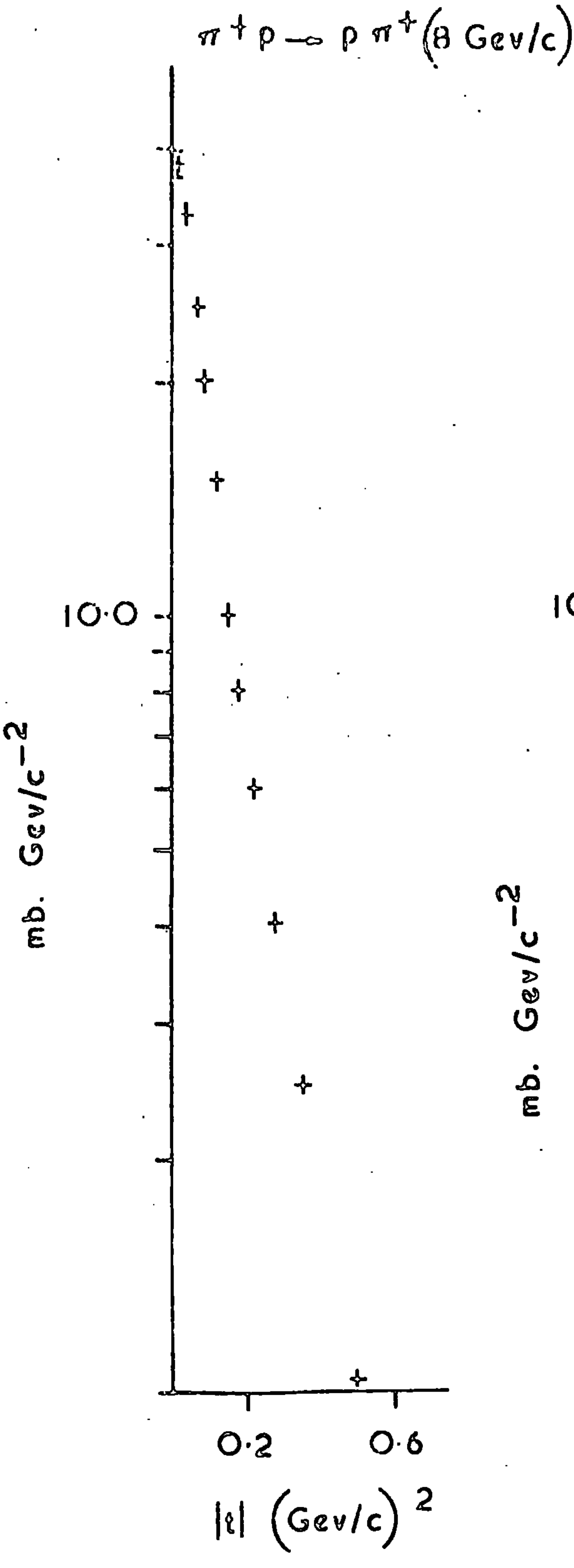

π⁺p → pπ⁺ (8 Gev/c)
10·0
mb. Gev/c⁻²
0·2
0·6
|t| (Gev/c)²

5[28]

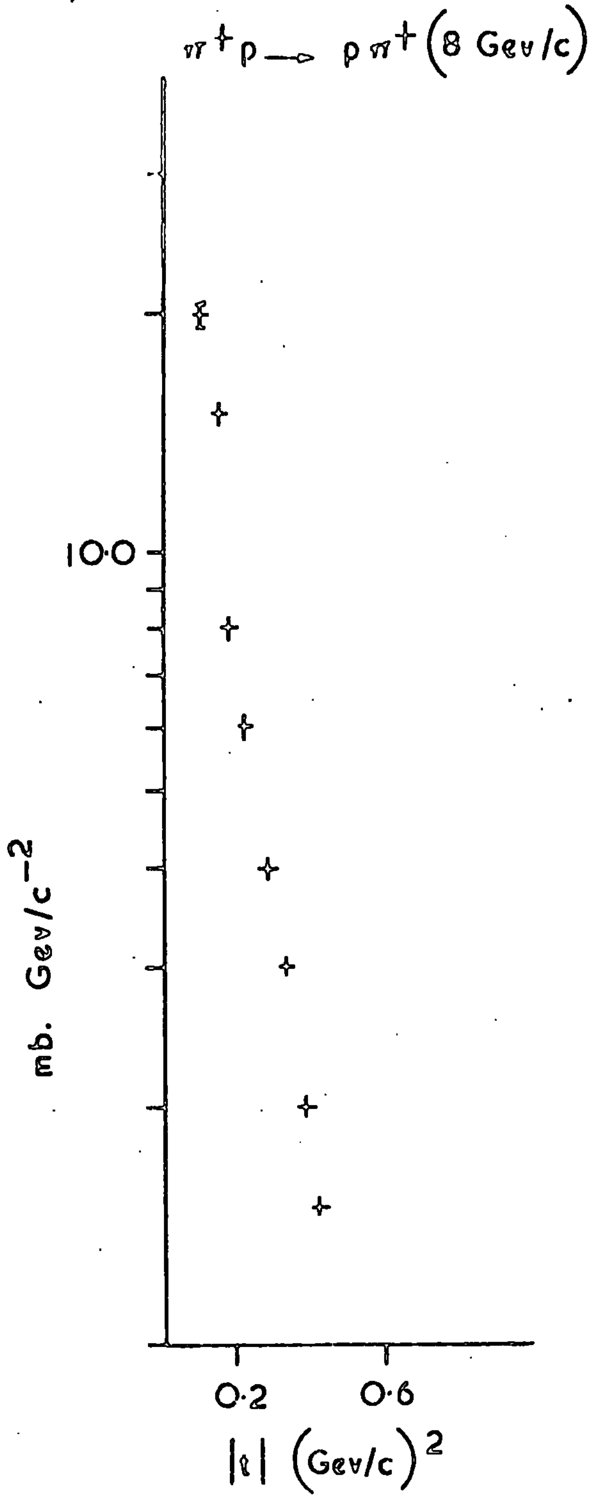

π⁺p → pπ⁺ (8 Gev/c)
10·0
mb. Gev/c⁻²
0·2
0·6
|t| (Gev/c)²

6[33]

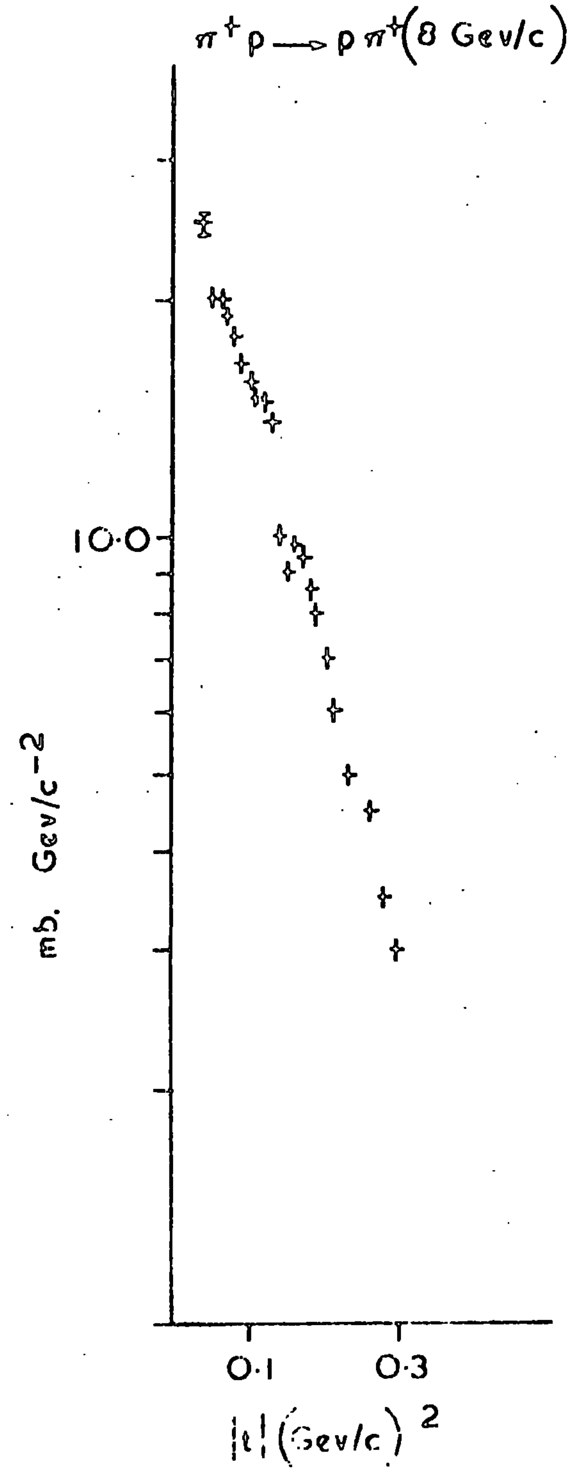

7[33]

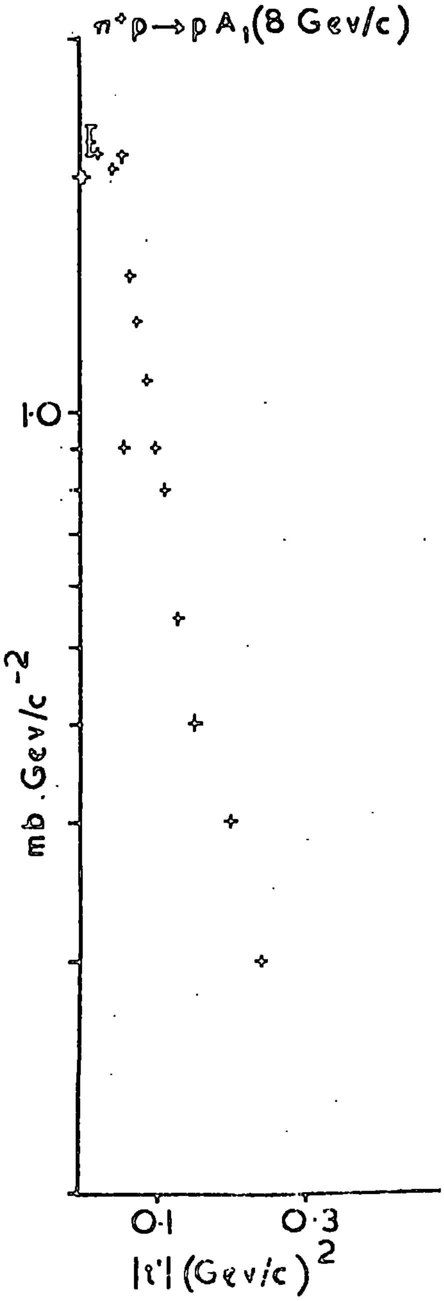
$\pi^+ p \rightarrow p A_1$ (8 Gev/c)
1·0
mb . Gev/c^{-2}
0·1
0·3
$|t'|$ (Gev/c)^2

8[33]

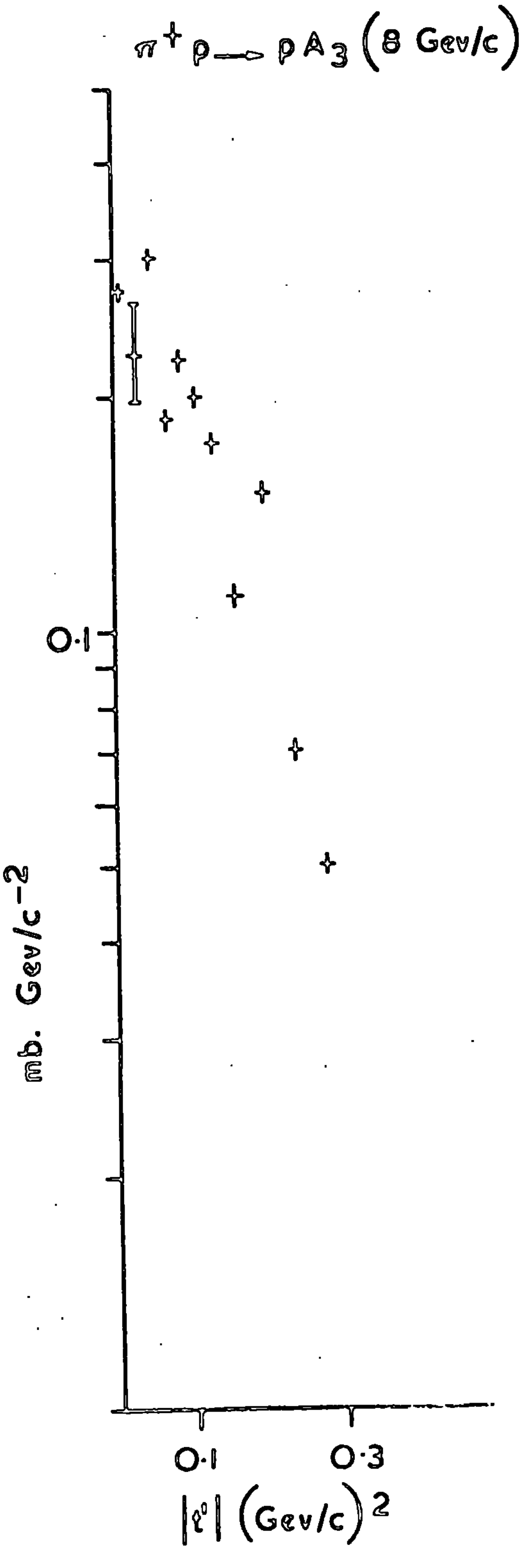
$\pi^+ p \rightarrow p A_3$ (8 Gev/c)
0·1
mb. Gev/c^{-2}
0·1
0·3
$|t'|$ (Gev/c)^2

9[33]

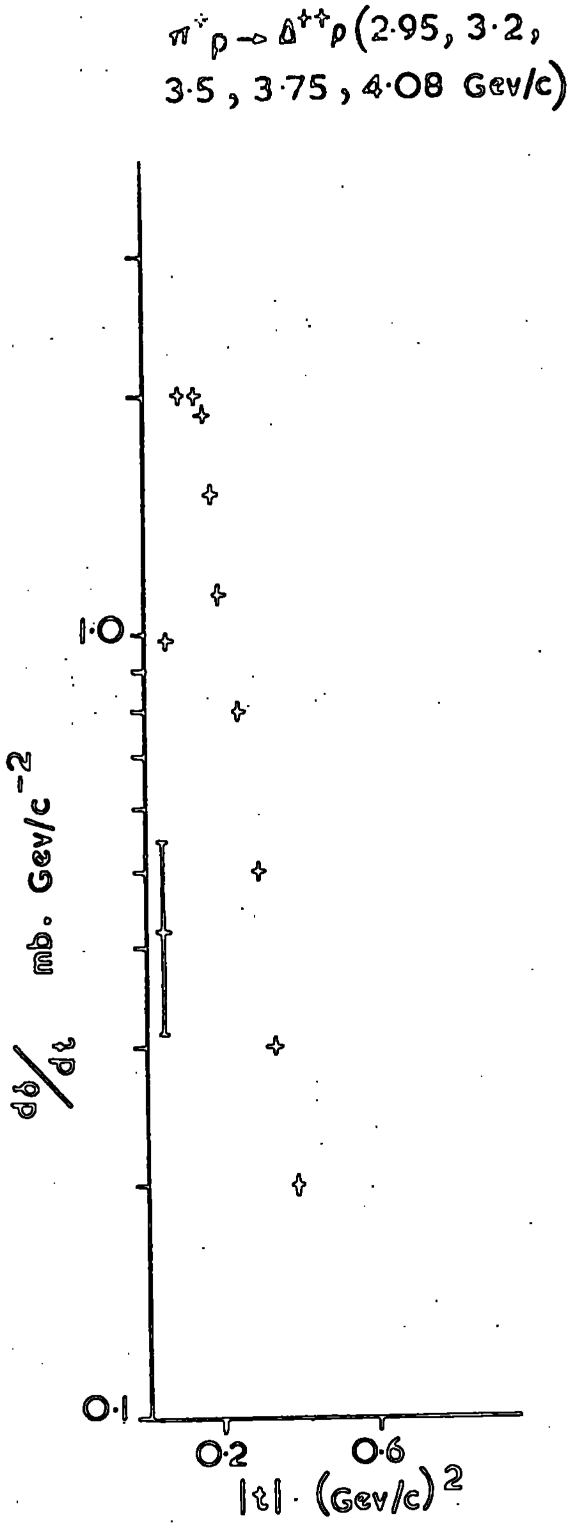

$\pi^+ p \to \Delta^{++} \rho$ (2.95, 3.2, 3.5, 3.75, 4.08 Gev/c)
1.0
0.1
0.2
0.6
$|t|$ (Gev/c)^2
$d\sigma/dt$ mb. Gev/c^{-2}

10[24]

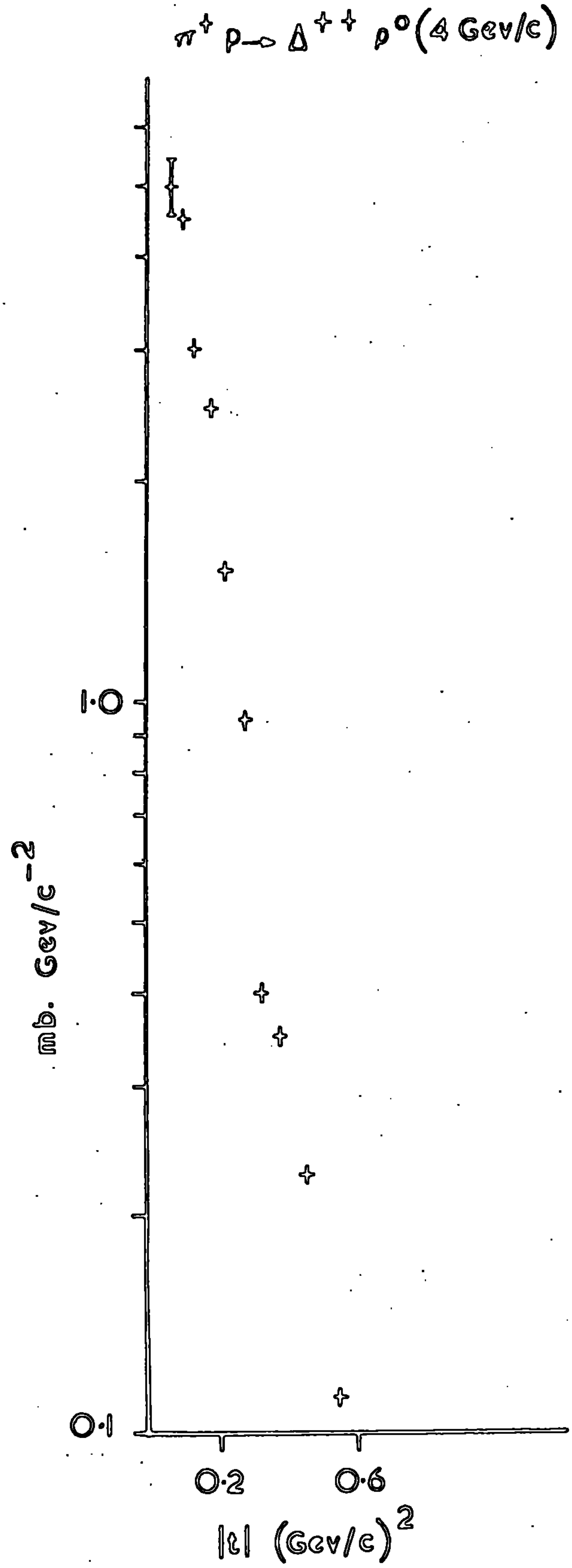

$\pi^+ p \to \Delta^{++} \rho^0$ (4 Gev/c)
1.0
0.1
0.2
0.6
$|t|$ (Gev/c)^2
mb. Gev/c^{-2}

11[25]

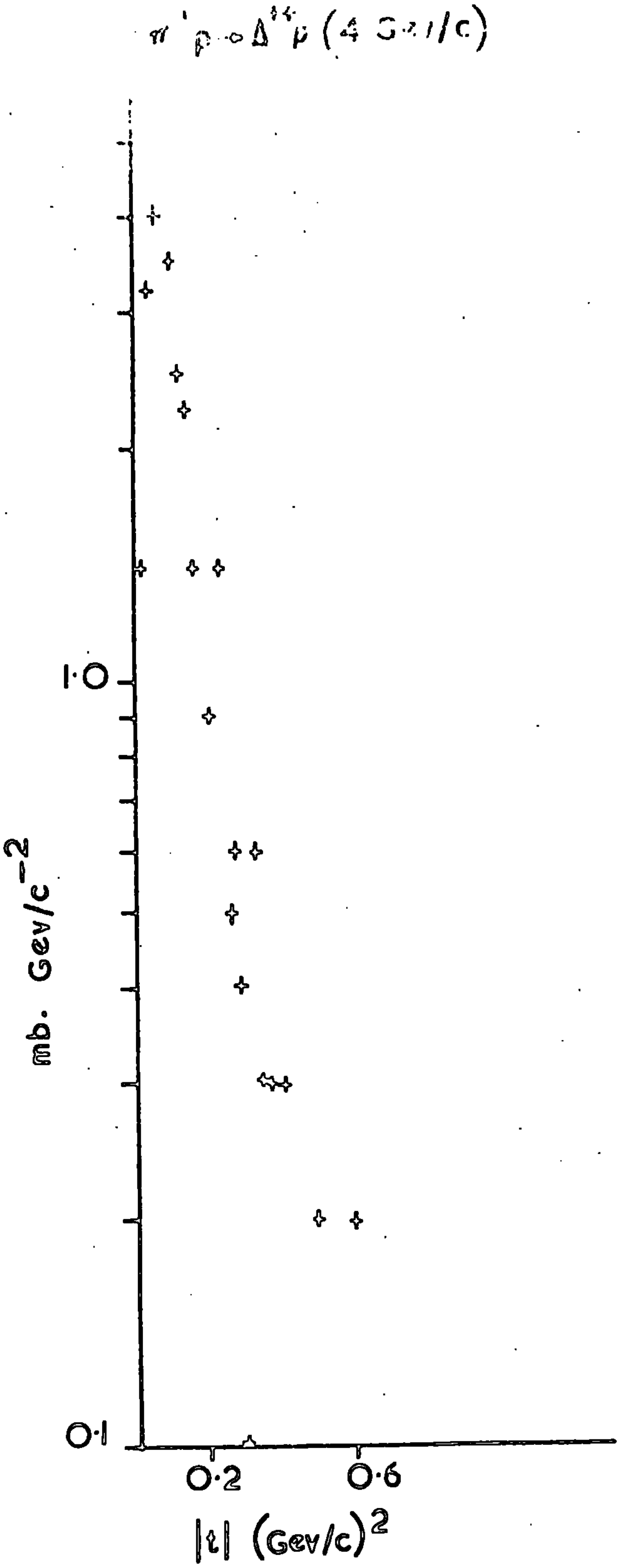
π⁺p → Δ⁺⁺ρ (4 Gev/c)
mb. Gev/c^{-2}
1·0
0·1
0·2
0·6
|t| (Gev/c)^2

12[26]

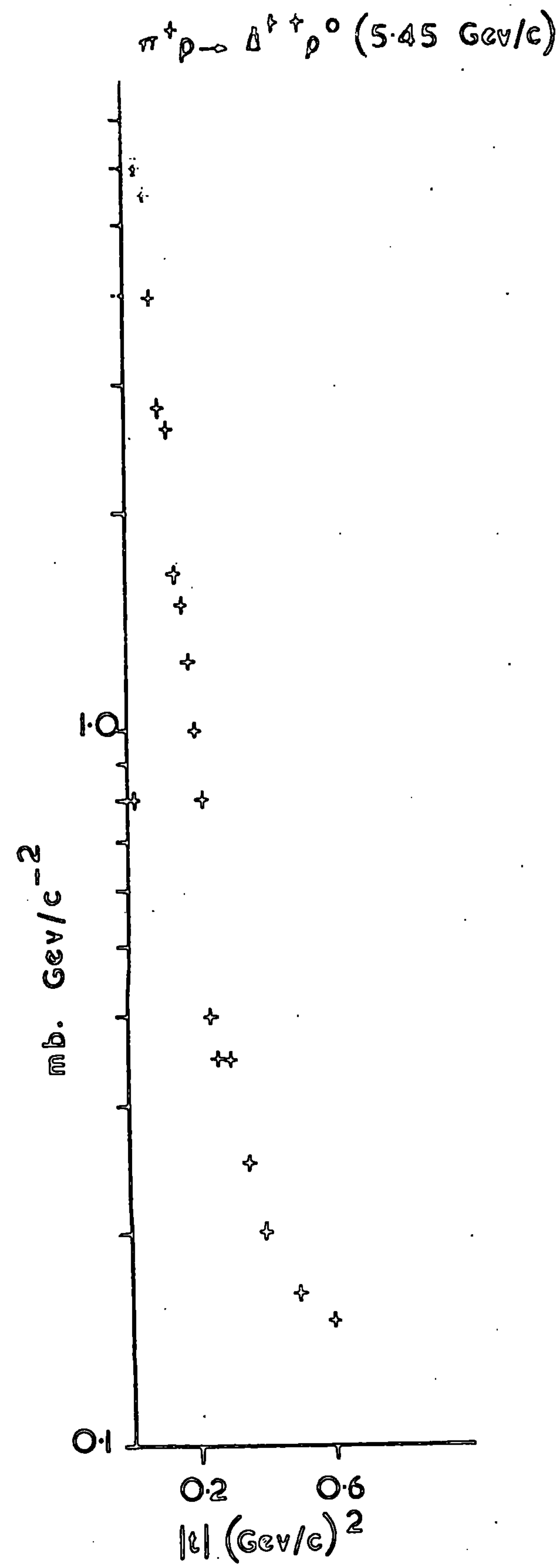
π⁺p → Δ⁺⁺ρ⁰ (5·45 Gev/c)
mb. Gev/c^{-2}
1·0
0·1
0·2
0·6
|t| (Gev/c)^2

13[27]

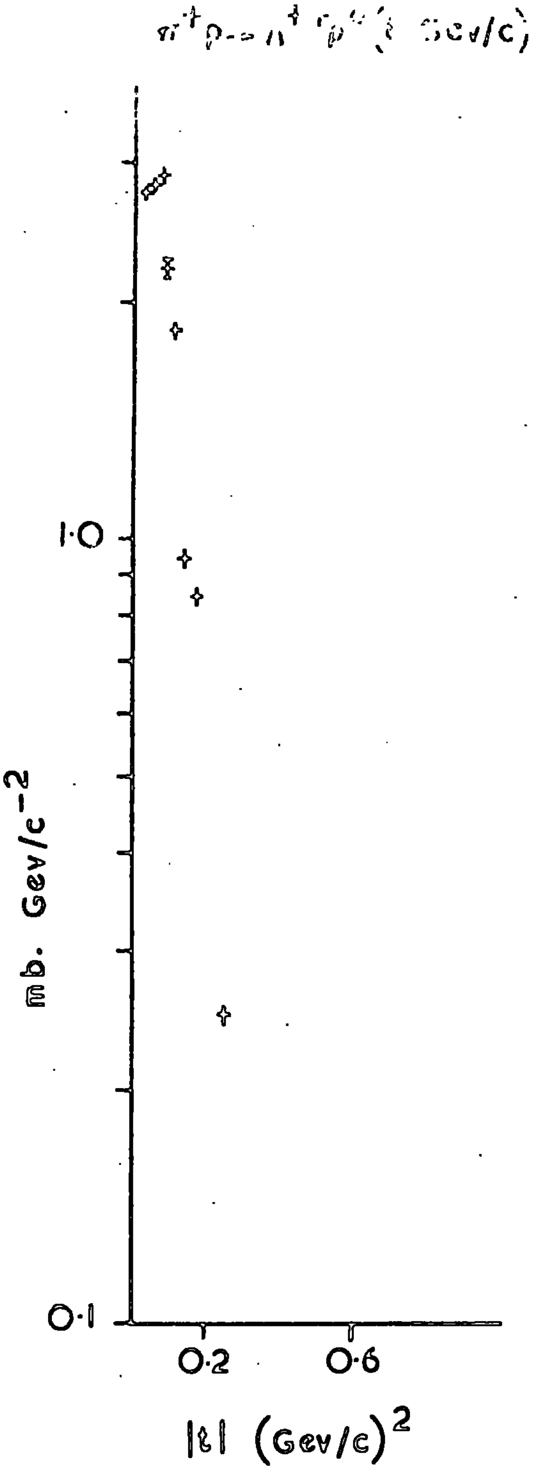

1·0
0·1
mb. Gev/c^{-2}
0·2
0·6
|t| (Gev/c)^2

14[28]

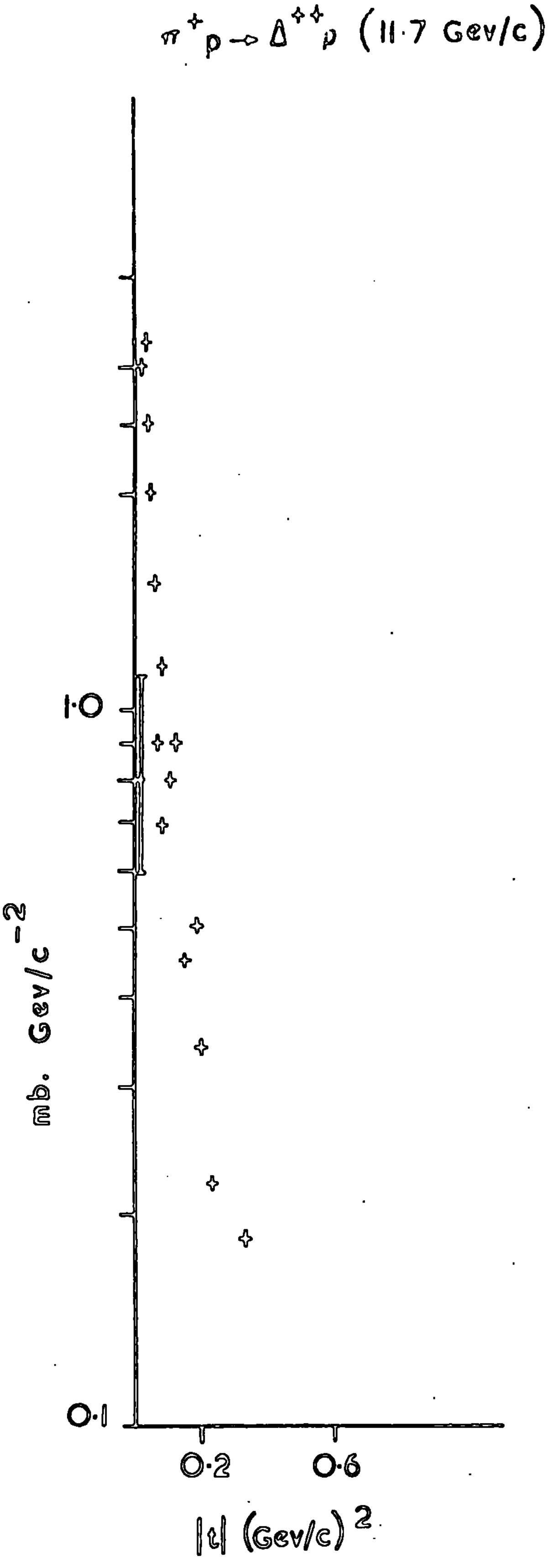

$\pi^+ p \rightarrow \Delta^{++} p$ (11·7 Gev/c)
1·0
0·1
mb. Gev/c^{-2}
0·2
0·6
|t| (Gev/c)^2

15[29]

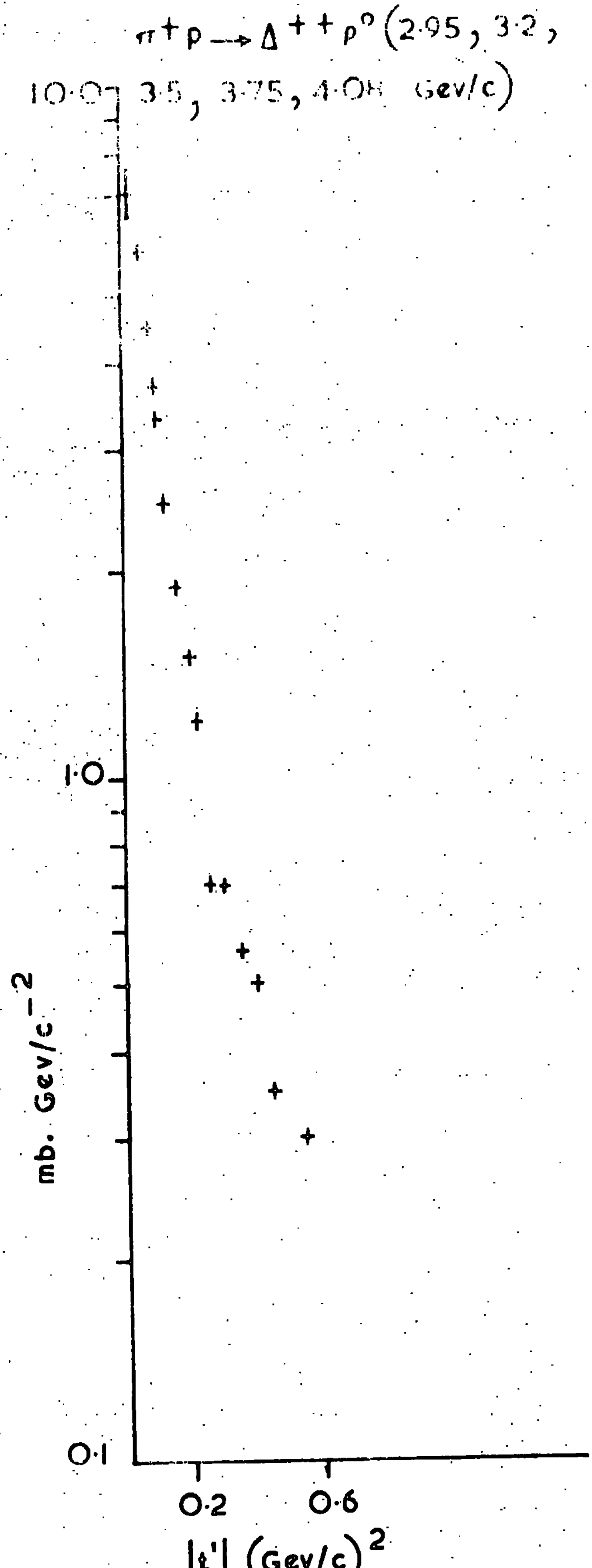

$\pi^+ p \rightarrow \Delta^{++} \rho^0$ (2·95, 3·2, 3·5, 3·75, 4·08 Gev/c)
10·0
1·0
0·1
mb. Gev/c^{-2}
0·2
0·6
$|t'|$ (Gev/c)^2

16[24]

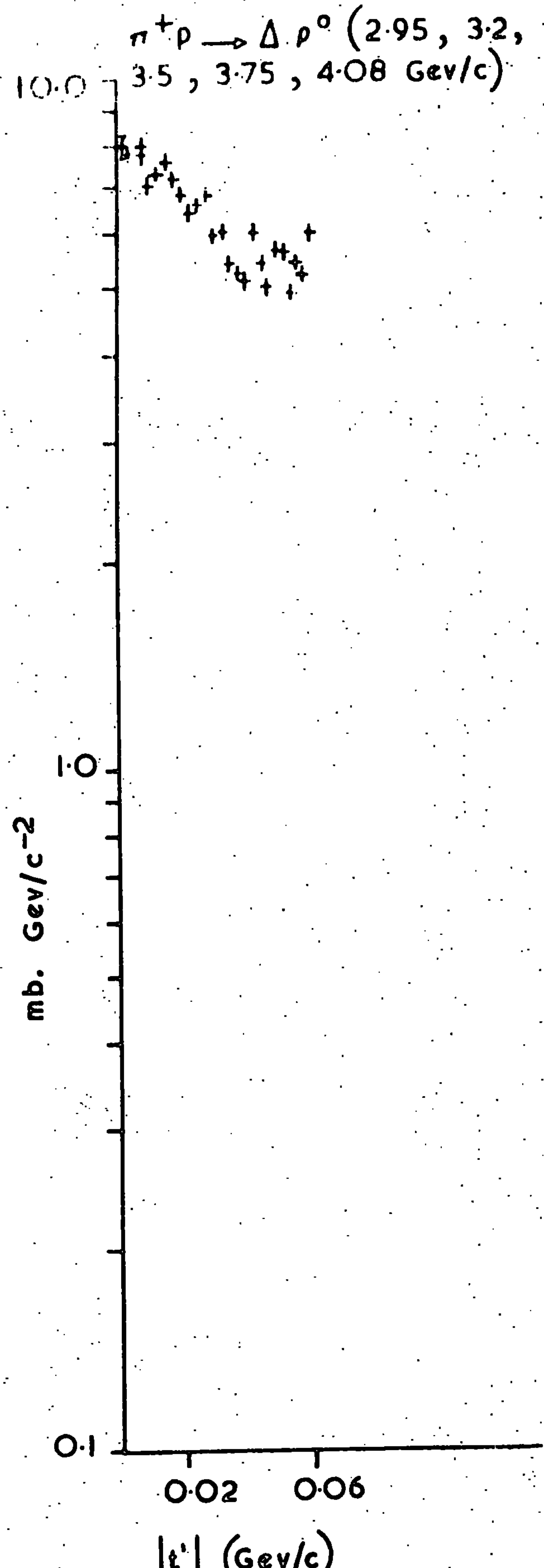

$\pi^+ p \rightarrow \Delta\, \rho^0$ (2·95, 3·2, 3·5, 3·75, 4·08 Gev/c)
10·0
1·0
0·1
mb. Gev/c^{-2}
0·02
0·06
$|t'|$ (Gev/c)

17[24]

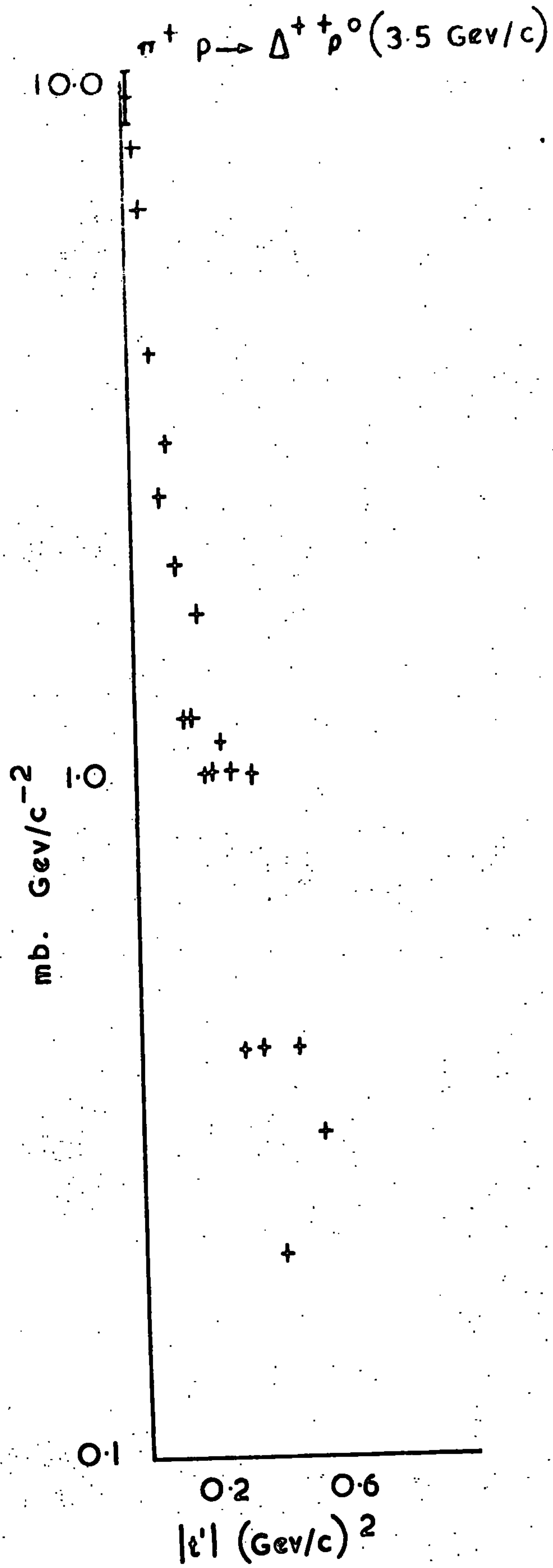

$\pi^+ p \to \Delta^{++} \rho^0$ (3.5 Gev/c)
10.0
1.0
0.1
mb. Gev/c^{-2}
0.2
0.6
$|t'|$ (Gev/c)^2

18[30]

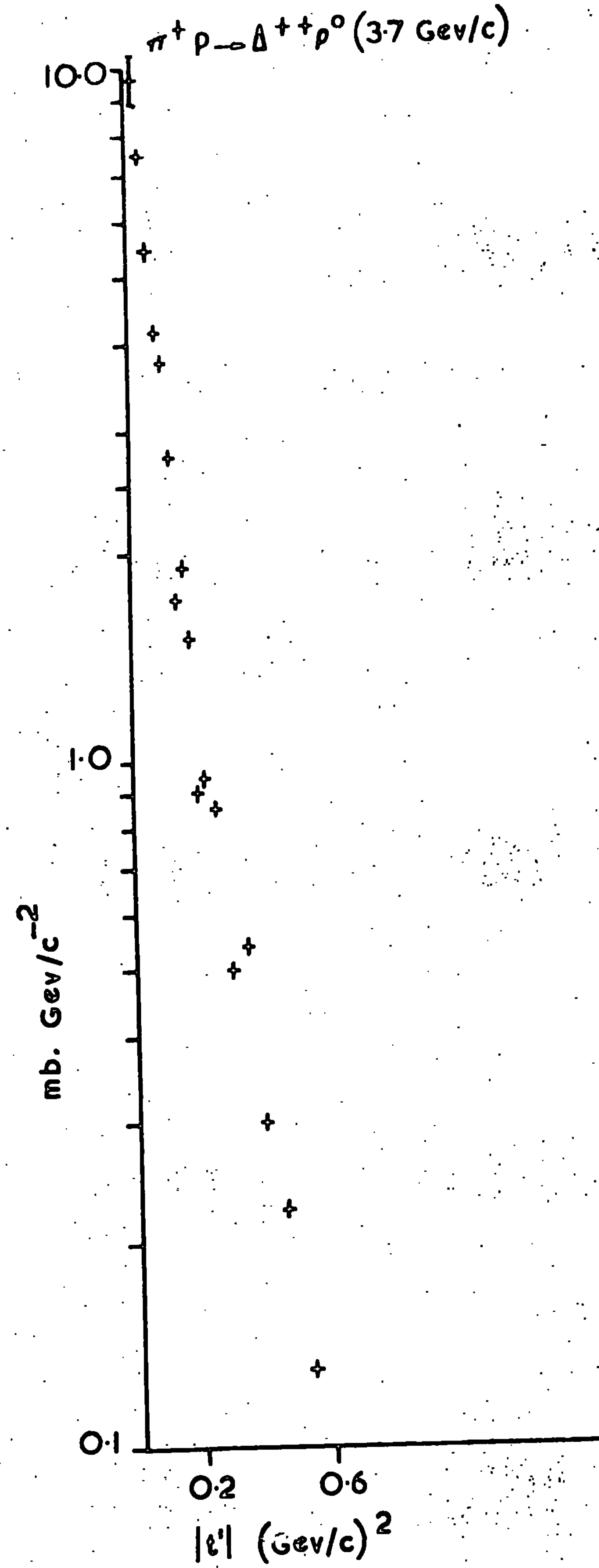

$\pi^+ p \to \Delta^{++} \rho^0$ (3.7 Gev/c)
10.0
1.0
0.1
mb. Gev/c^{-2}
0.2
0.6
$|t'|$ (Gev/c)^2

19[31]

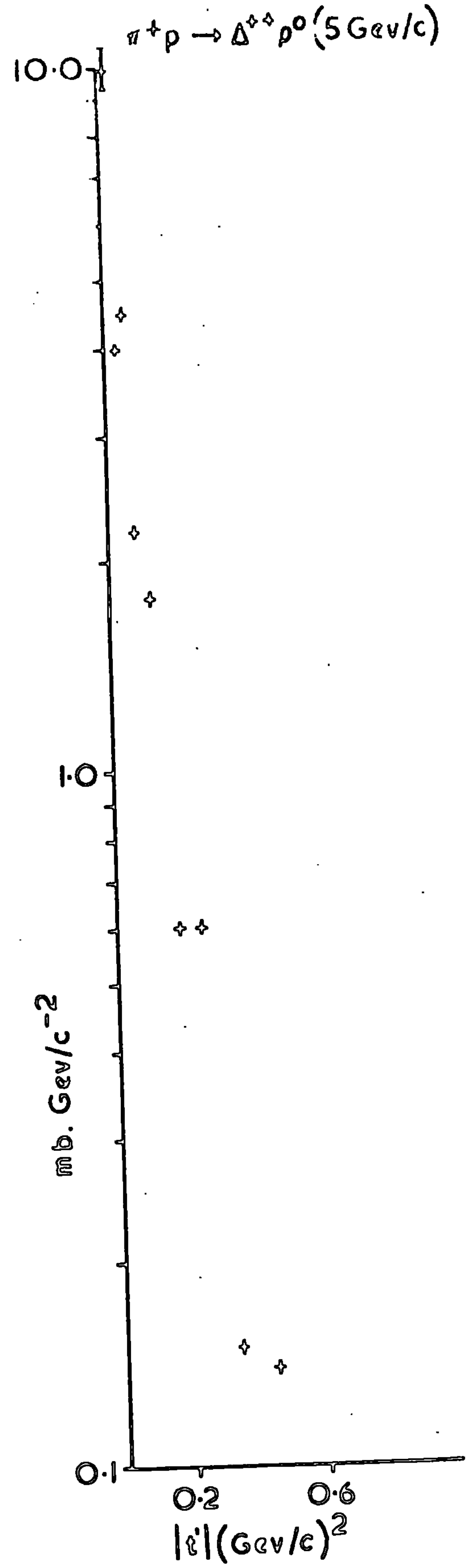

$\pi^+ p \to \Delta^{++} \rho^0$ (5 Gev/c)
10.0
1.0
0.1
mb. Gev/c^{-2}
0.2
0.6
$|t'|$ (Gev/c)^2

20[32]

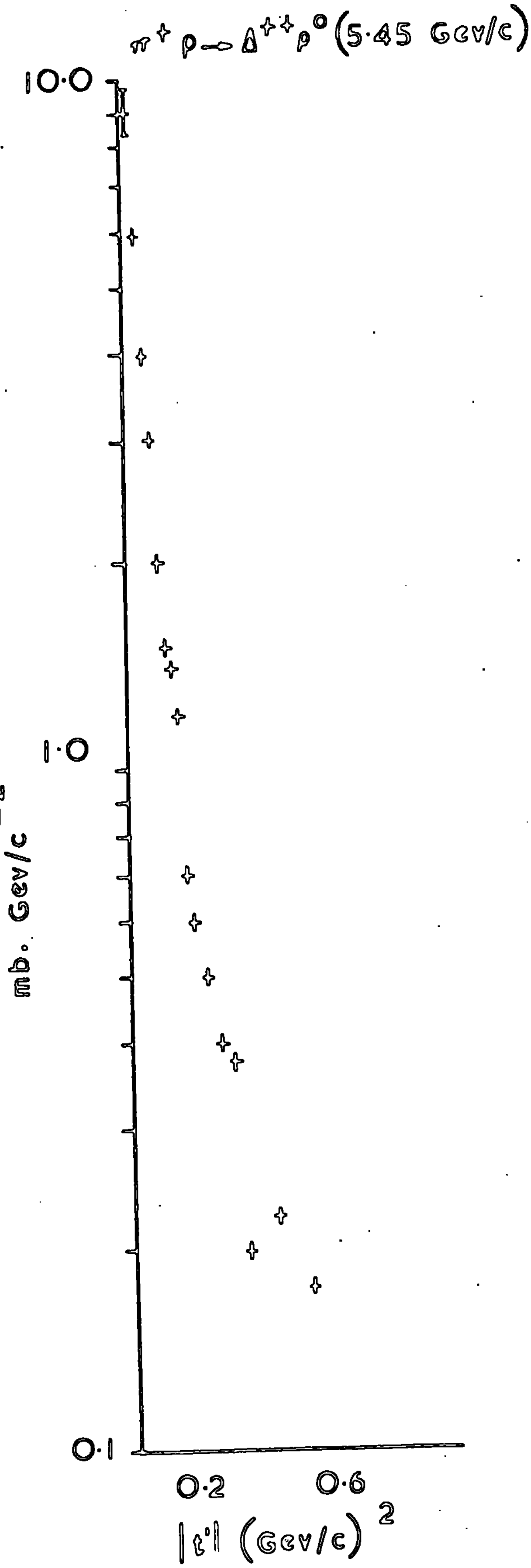

$\pi^+ p \to \Delta^{++} \rho^0$ (5.45 Gev/c)
10.0
1.0
0.1
mb. Gev/c^{-2}
0.2
0.6
$|t'|$ (Gev/c)^2

21[27]

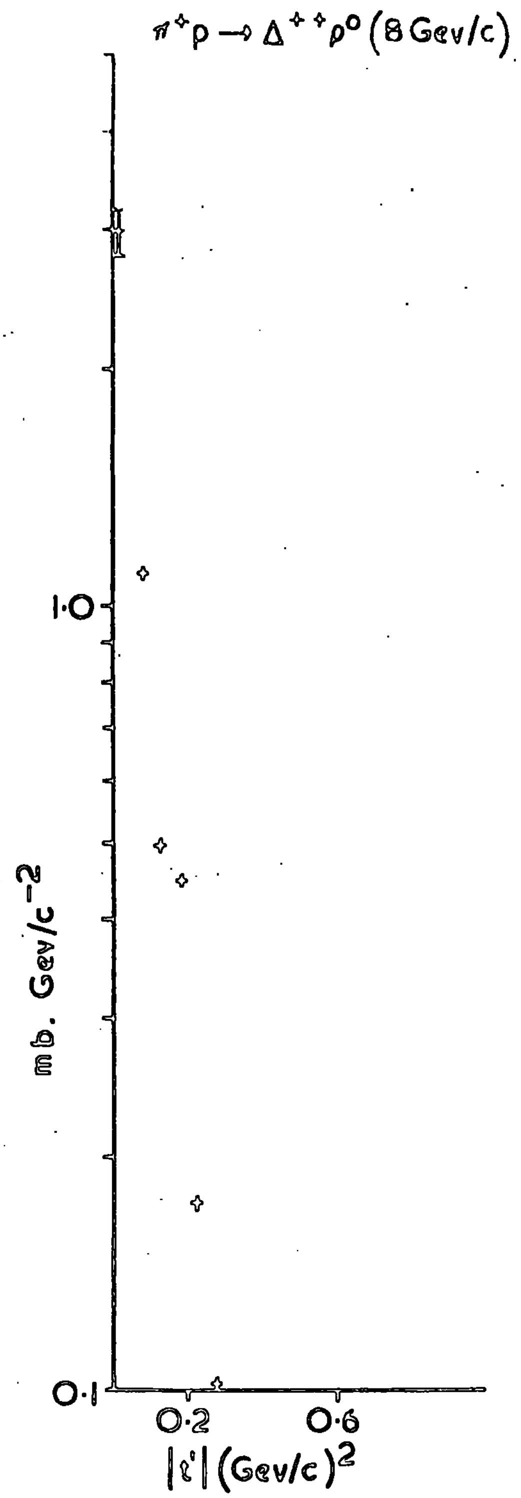
$\pi^+ p \rightarrow \Delta^{++} \rho^0$ (8 Gev/c)
1.0
0.1
mb. Gev/c^{-2}
0.2
0.6
|t'| (Gev/c)^2

22[33]

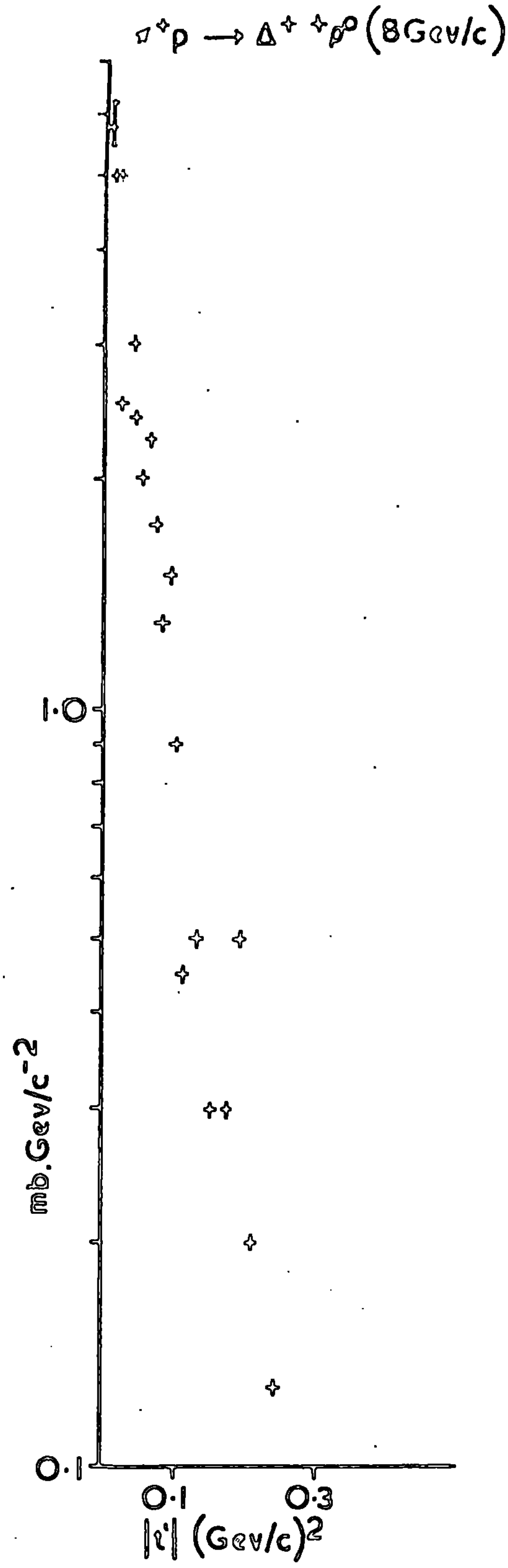
$\pi^+ p \rightarrow \Delta^{++} \rho^0$ (8 Gev/c)
1.0
0.1
mb. Gev/c^{-2}
0.1
0.3
|t'| (Gev/c)^2

23[33]

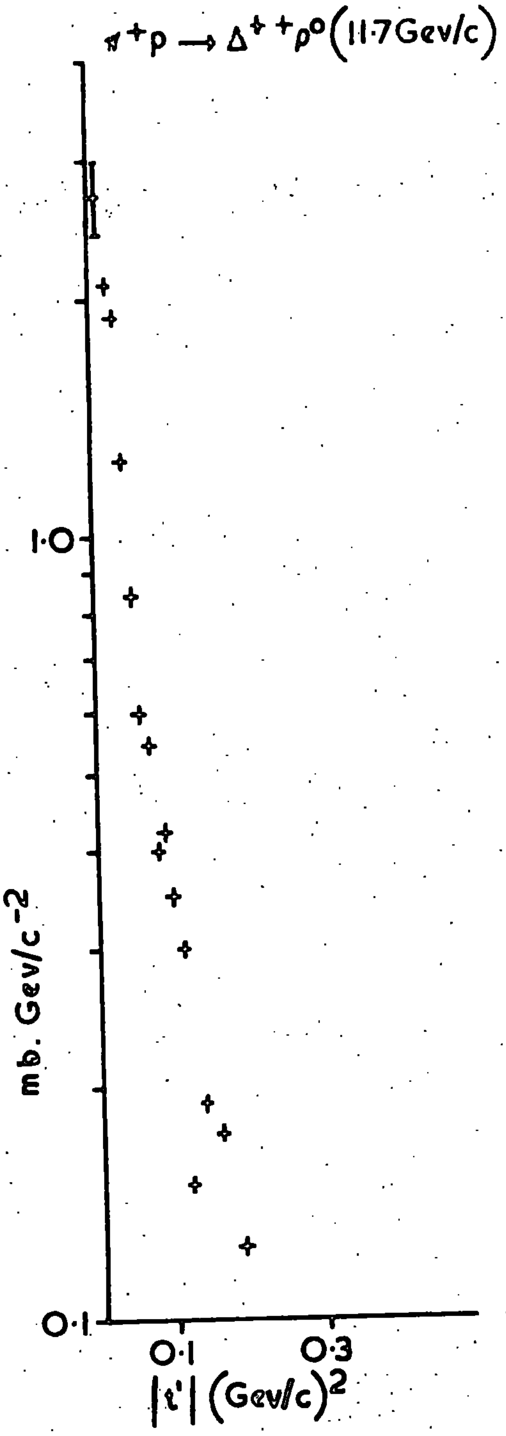

$\pi^+p \rightarrow \Delta^{++}\rho^0$ (11·7 Gev/c)
1·0
0·1
mb. Gev/c^{-2}
0·1
0·3
$|t'|$ (Gev/c)^2

24[29]

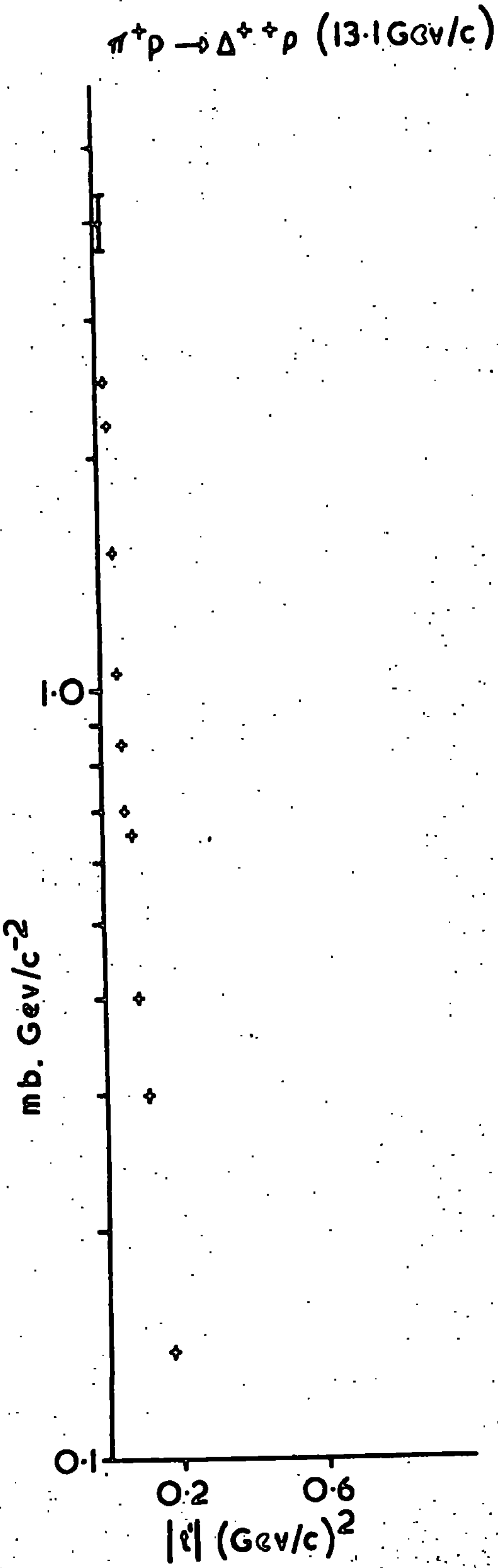

$\pi^+p \rightarrow \Delta^{++}\rho$ (13·1 Gev/c)
1·0
0·1
mb. Gev/c^{-2}
0·2
0·6
$|t'|$ (Gev/c)^2

25[34]

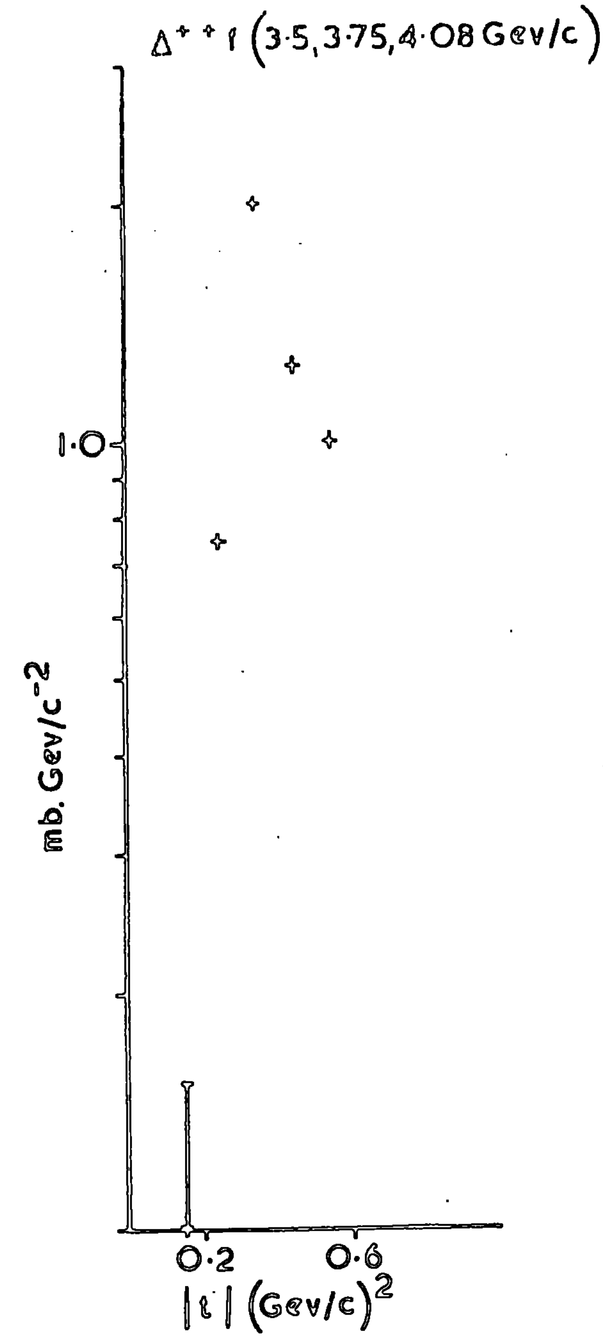
$\Delta^{++}f$ (3.5, 3.75, 4.08 Gev/c)
mb. Gev/c^{-2}
1.0
0.2
0.6
|t| (Gev/c)^2

26[24]

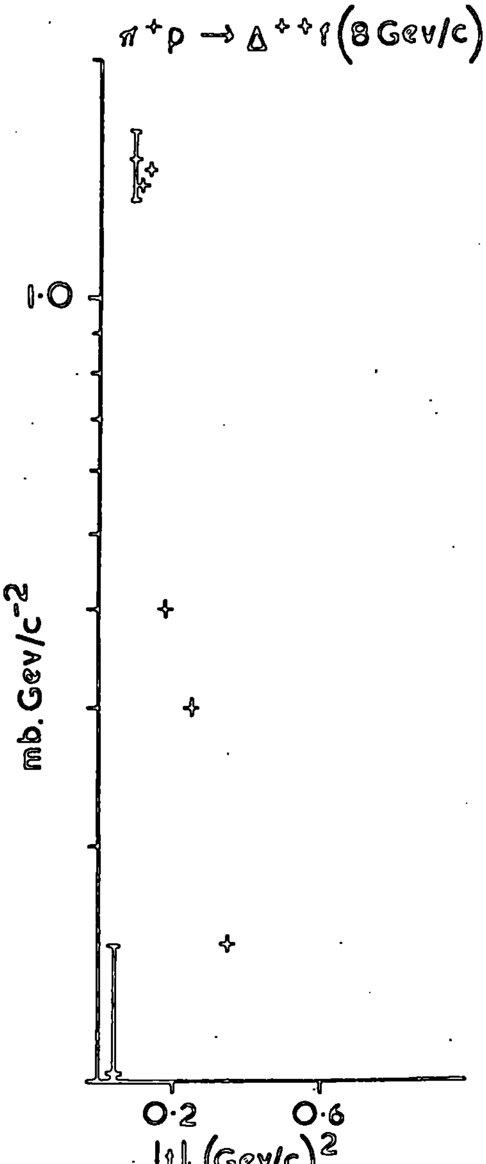
$\pi^+p \to \Delta^{++}f$ (8 Gev/c)
mb. Gev/c^{-2}
1.0
0.2
0.6
|t| (Gev/c)^2

27[28]

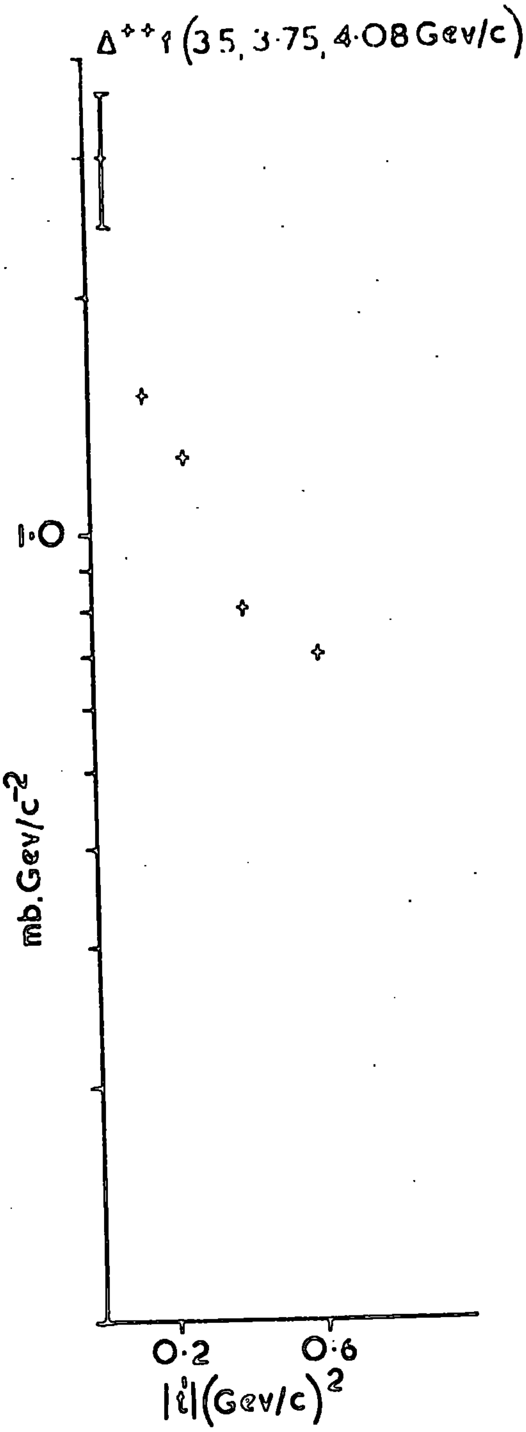
Δ⁺⁺ f (3.5, 3.75, 4.08 Gev/c)
1.0
mb.Gev/c^{-2}
0.2
0.6
|t| (Gev/c)^2

28[24]

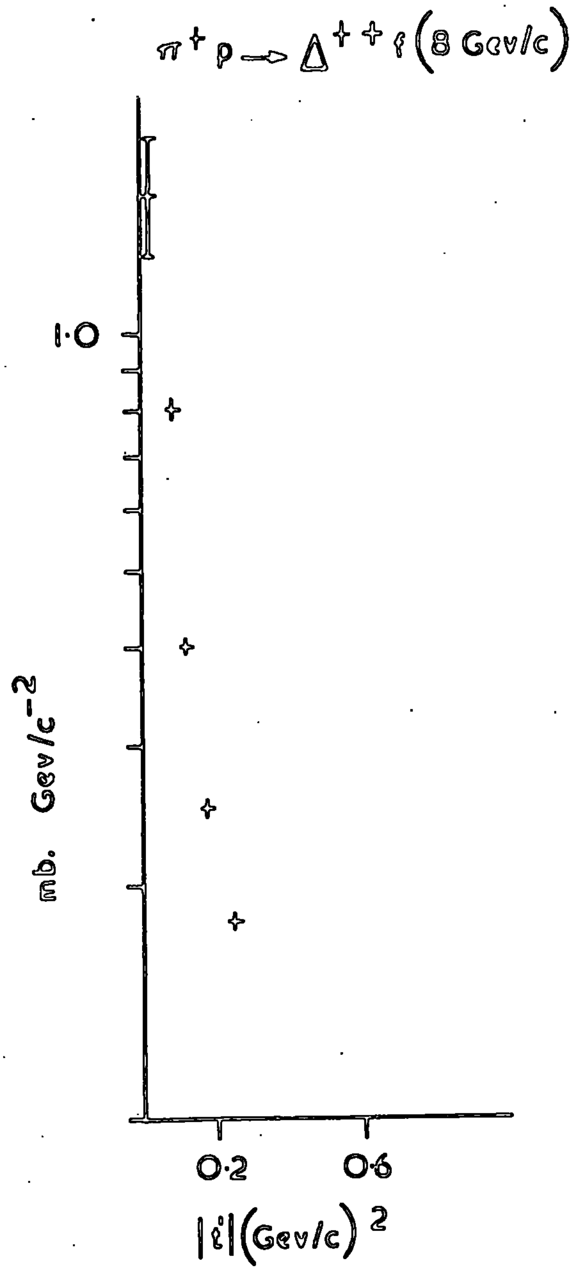
$\pi^+ p \rightarrow \Delta^{++} f$ (8 Gev/c)
1.0
mb. Gev/c^{-2}
0.2
0.6
|t| (Gev/c)^2

29[33]

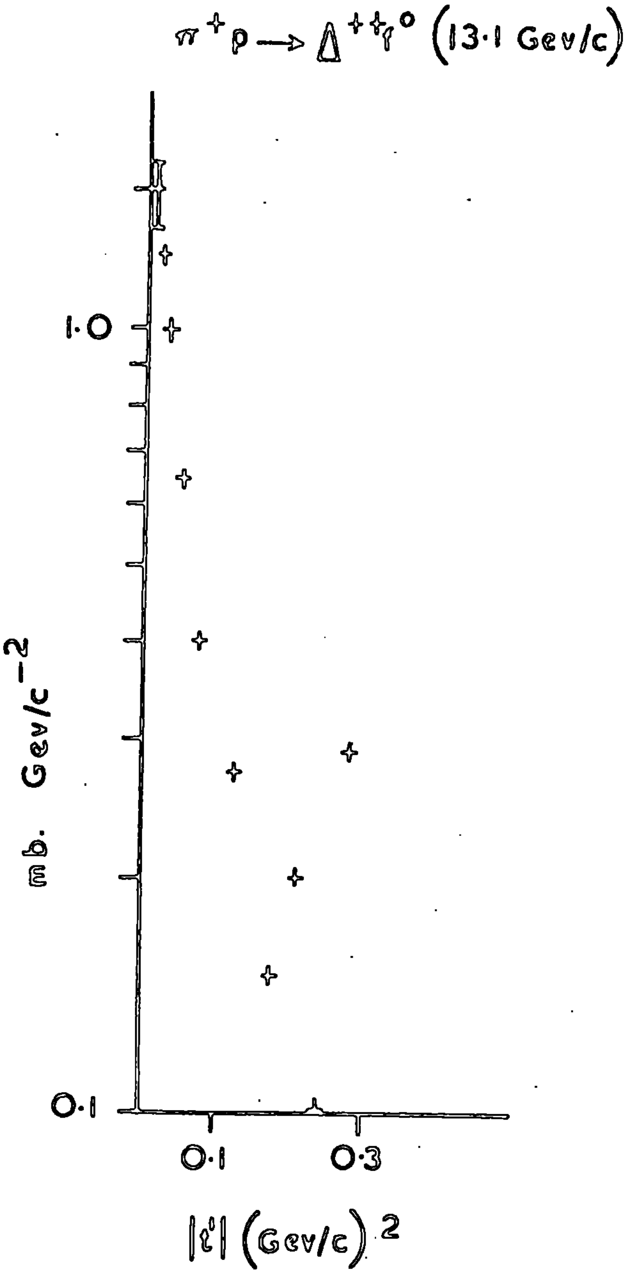

$\pi^+ p \longrightarrow \Delta^{++} \rho^0$ (13·1 Gev/c)
mb. Gev/c^{-2}
1·0
0·1
0·1
0·3
$|t'|$ (Gev/c)^2

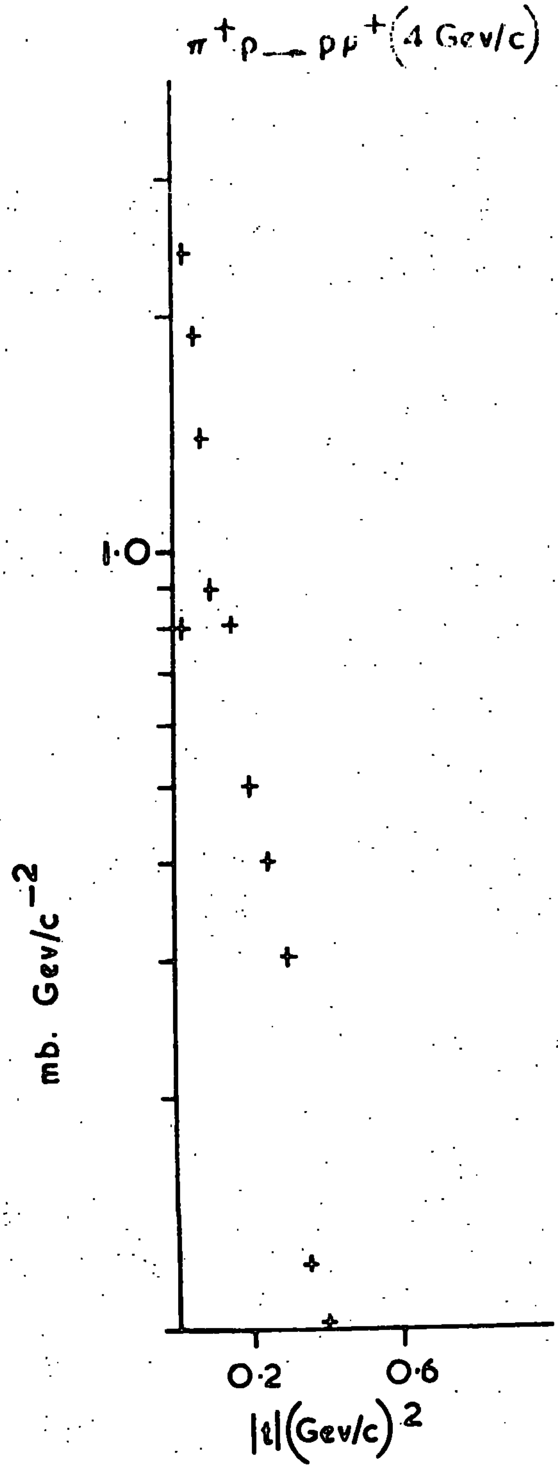
$\pi^+ p \rightarrow p\rho^+$ (4 Gev/c)
1·0
mb. Gev/c^{-2}
0·2
0·6
$|t|$(Gev/c)^2

31[39]

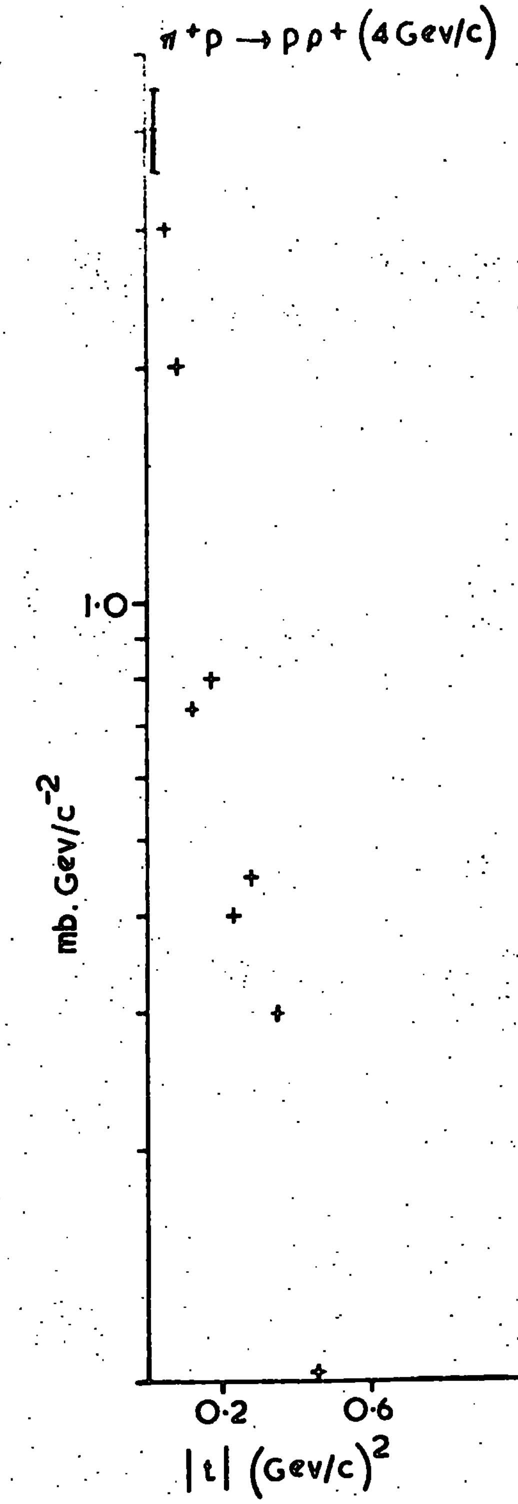
$\pi^+ p \rightarrow p\rho^+$ (4 Gev/c)
1·0
mb. Gev/c^{-2}
0·2
0·6
$|t|$ (Gev/c)^2

32[25]

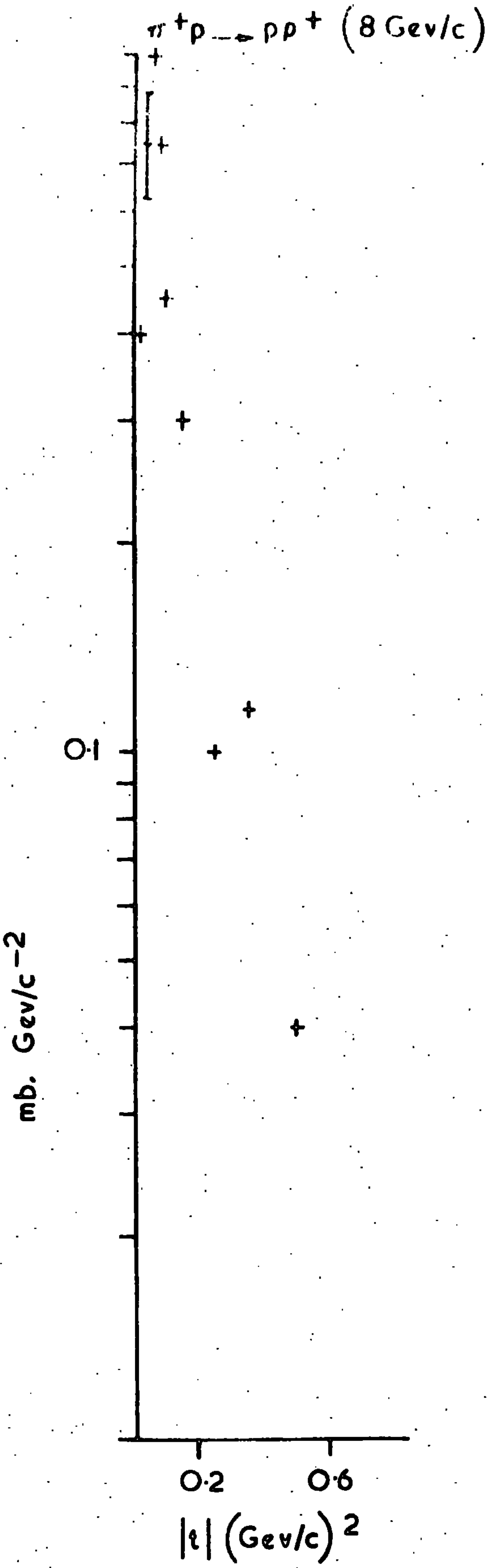
π⁺p → ρρ⁺ (8 Gev/c)
0·1
mb. Gev/c⁻²
0·2
0·6
|t| (Gev/c)²

33[28]

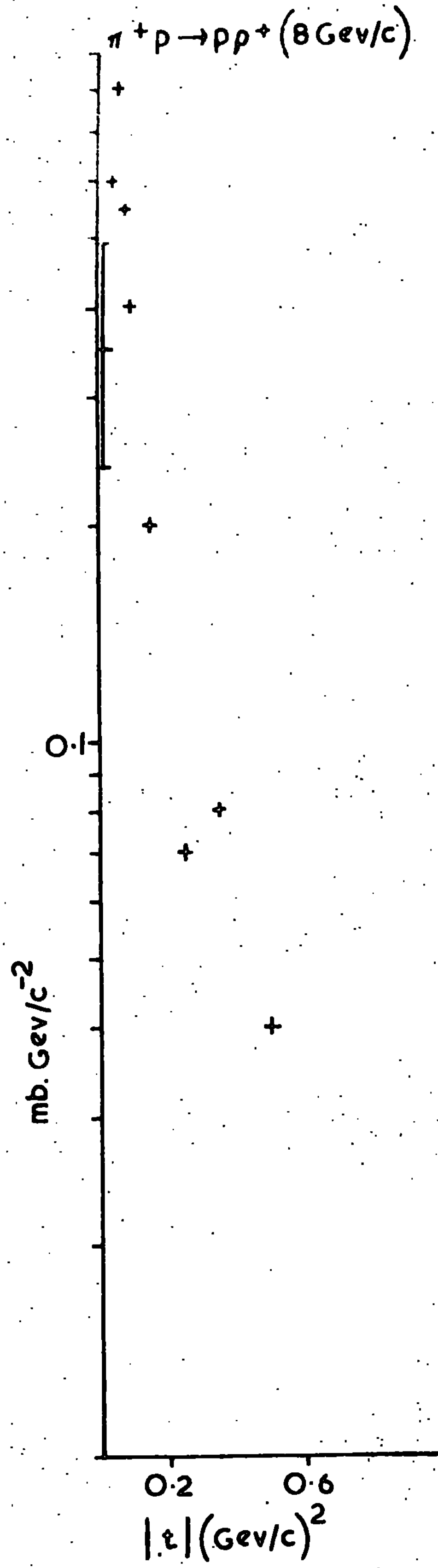
π⁺p → ρρ⁺ (8 Gev/c)
0·1
mb. Gev/c⁻²
0·2
0·6
|t| (Gev/c)²

34[40]

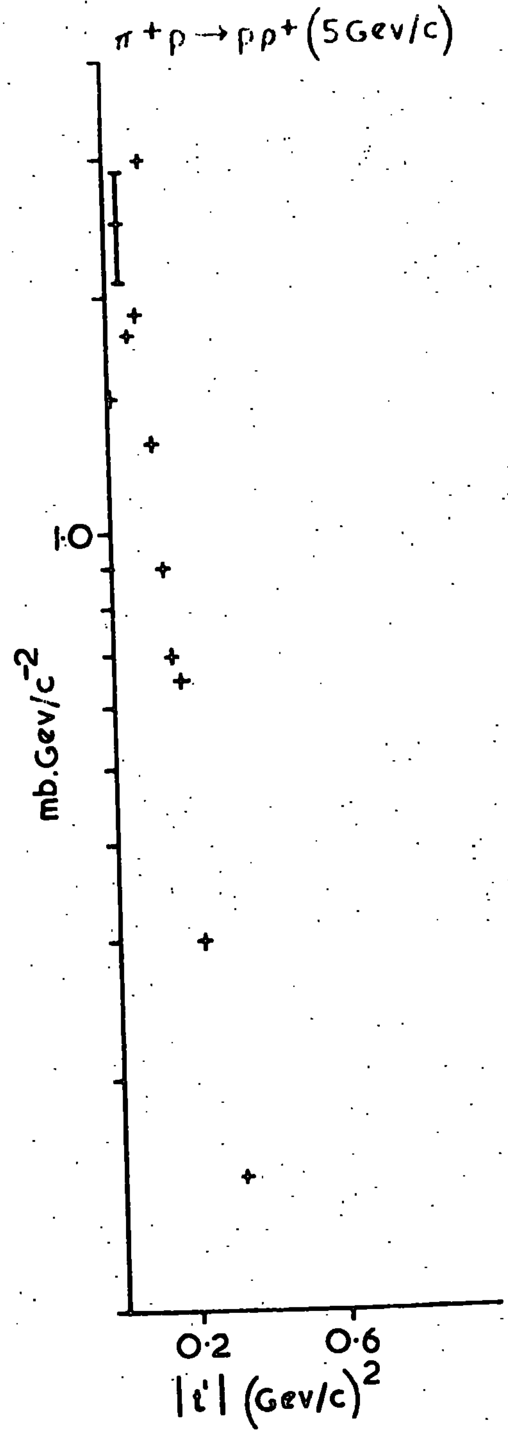
$\pi^+ p \rightarrow p \rho^+$ (5 Gev/c)
1·0
mb.Gev/c^{-2}
0·2
0·6
$|t'|$ (Gev/c)^2

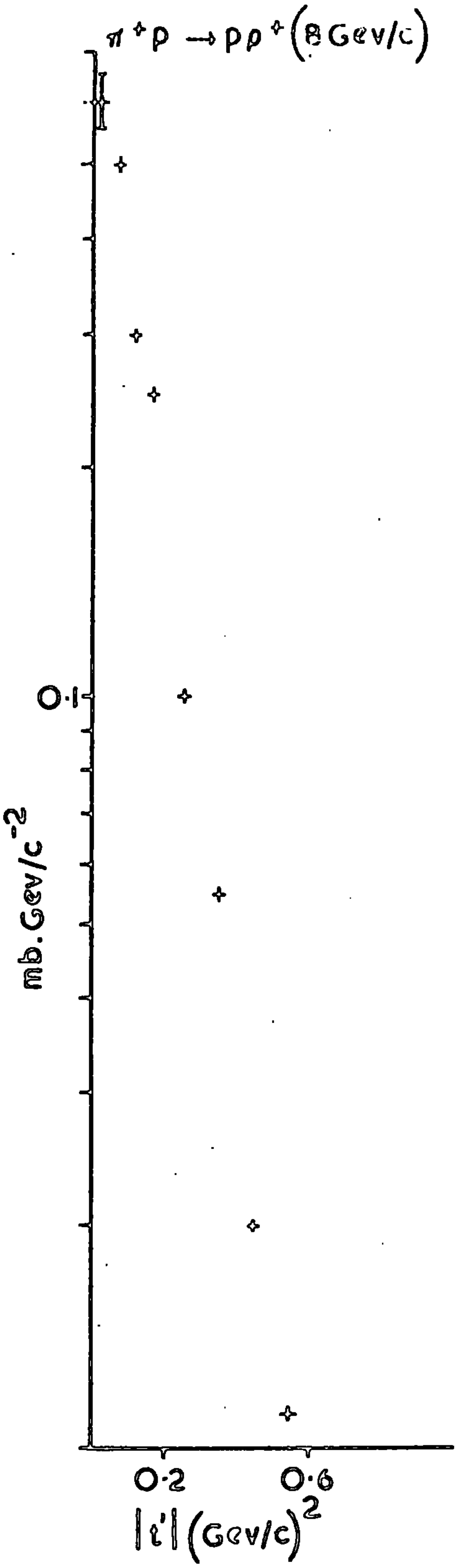

$\pi^+p \rightarrow p\rho^+$ (8 Gev/c)
0·1
mb. Gev/c^{-2}
0·2
0·6
|t'| (Gev/c)^2

36[33]

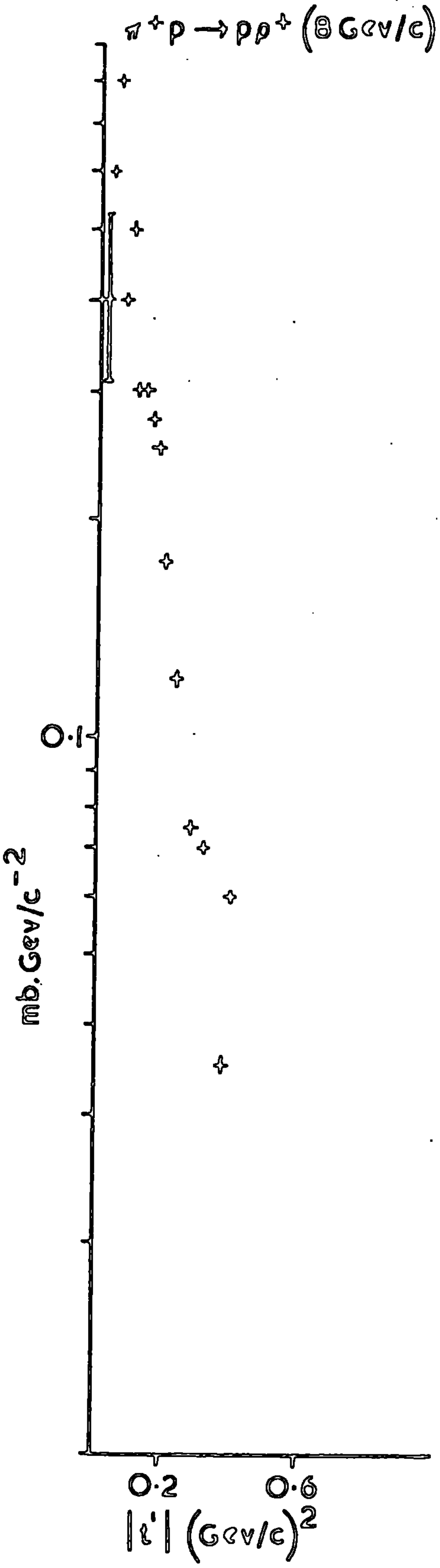

$\pi^+p \rightarrow p\rho^+$ (8 Gev/c)
0·1
mb. Gev/c^{-2}
0·2
0·6
|t'| (Gev/c)^2

37[41]

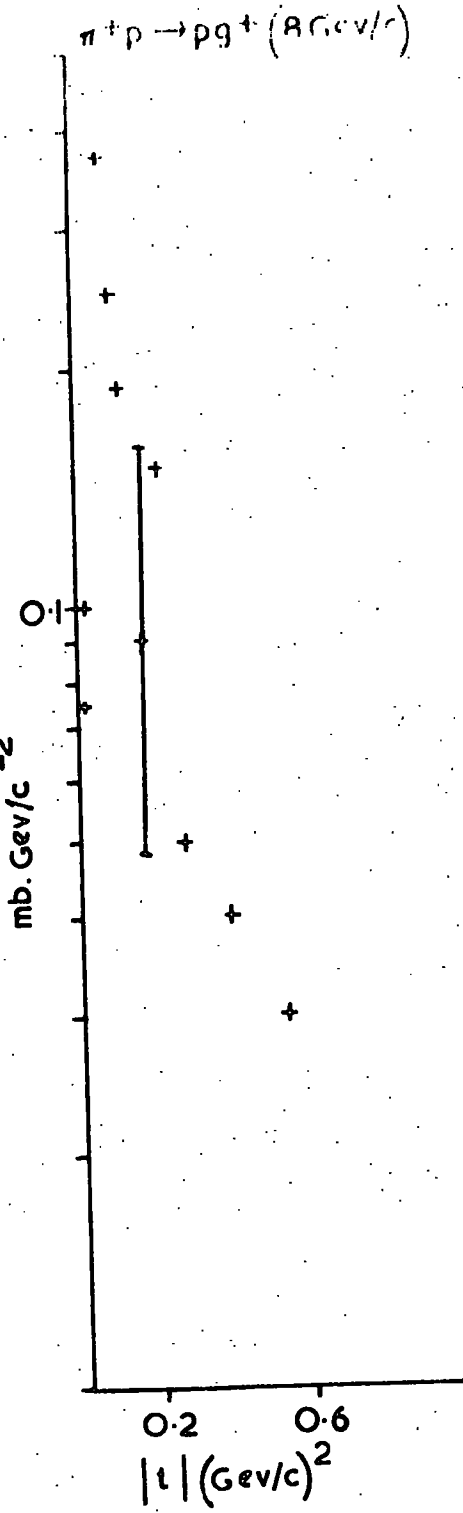

$\pi^+p \rightarrow pg^+$ (8 Gev/c)
0·1
mb. Gev/c^{-2}
0·2
0·6
$|t|$ (Gev/c)^2

38[42]

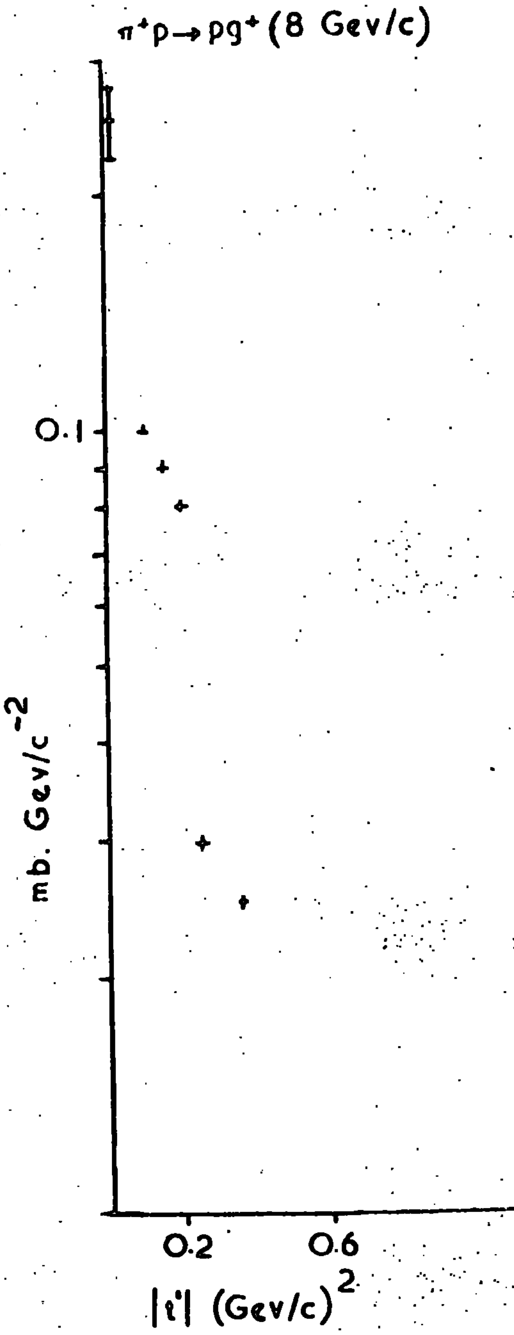

$\pi^+p \rightarrow pg^+$ (8 Gev/c)
0.1
mb. Gev/c^{-2}
0.2
0.6
$|t'|$ (Gev/c)^2

39[33]

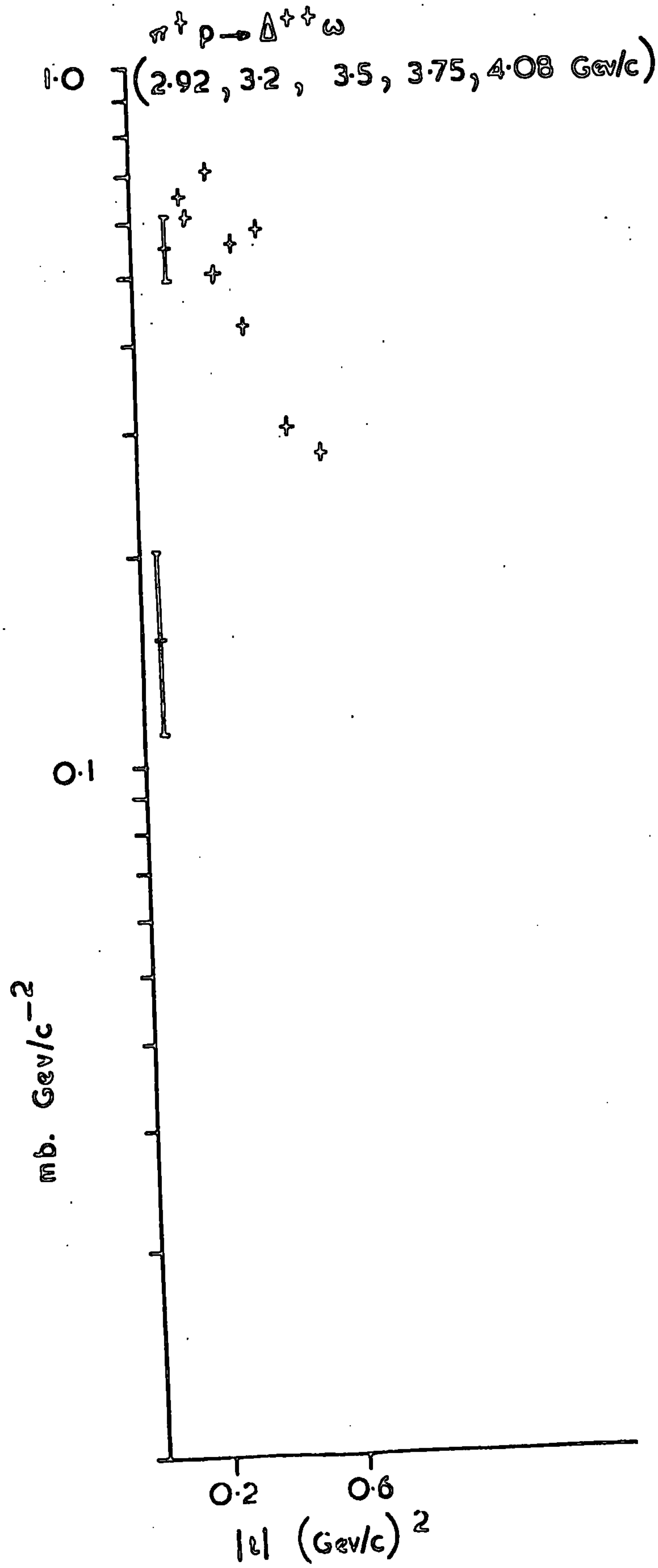

π⁺p → Δ⁺⁺ω
(2.92, 3.2, 3.5, 3.75, 4.08 Gev/c)
1.0
0.1
mb. Gev/c⁻²
0.2
0.6
|t| (Gev/c)²

40[23]

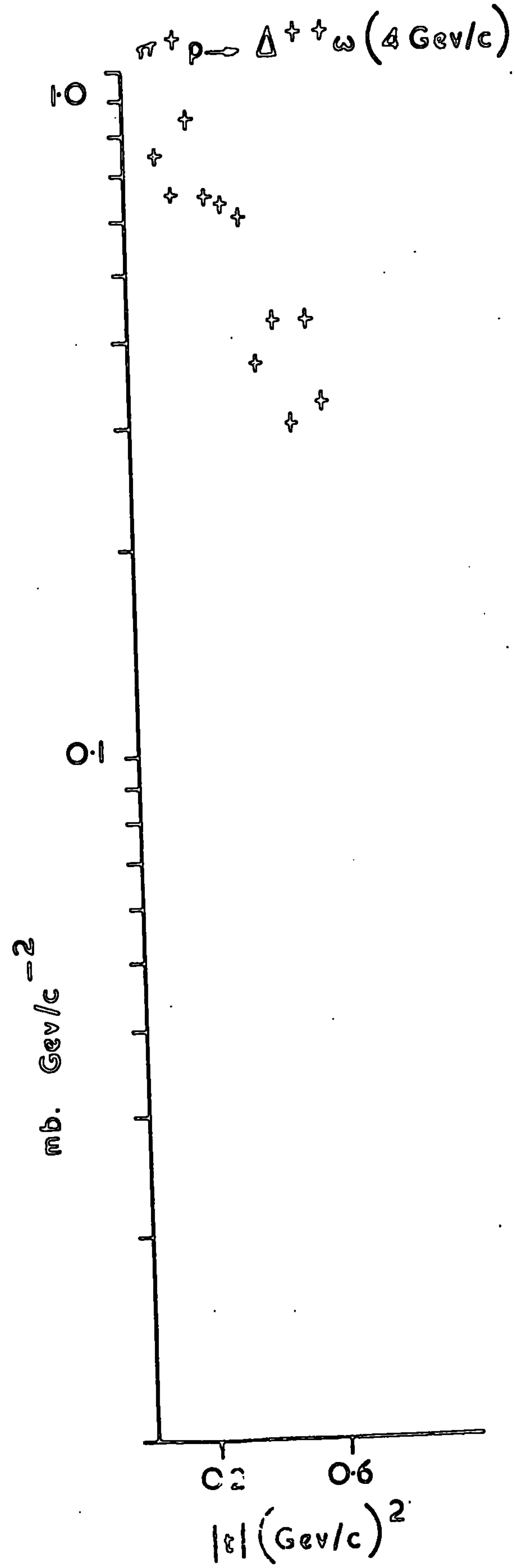

π⁺p → Δ⁺⁺ω (4 Gev/c)
1.0
0.1
mb. Gev/c⁻²
0.2
0.6
|t| (Gev/c)²

41[26]

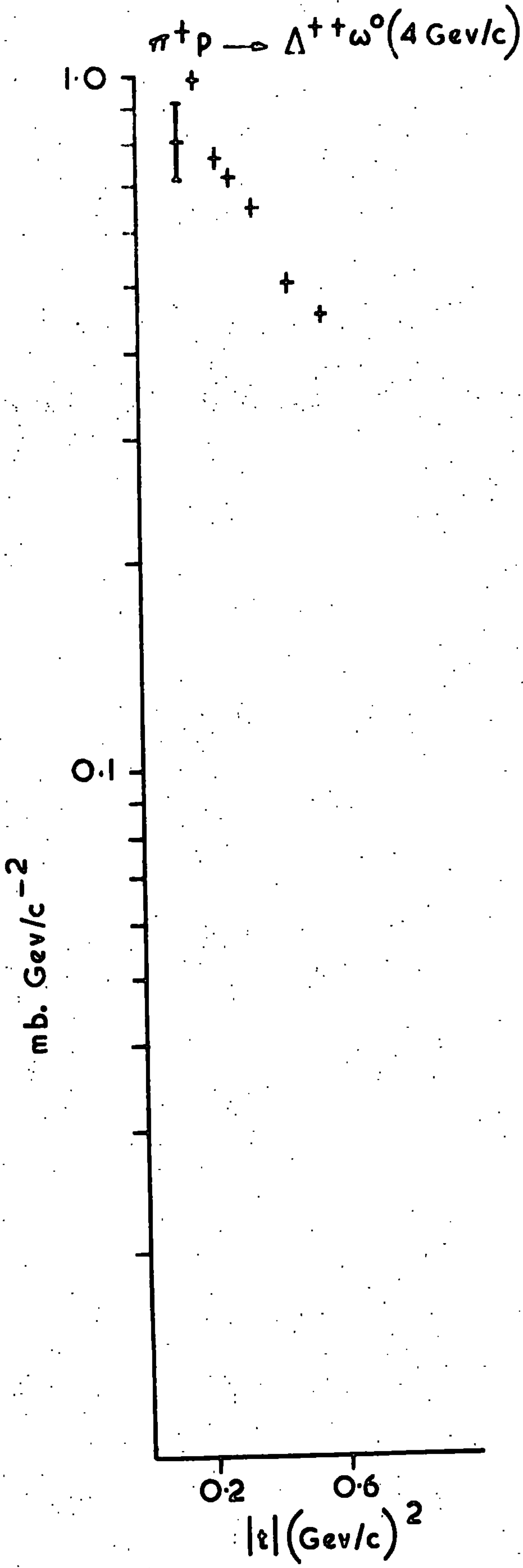

$\pi^+ p \to \Delta^{++}\omega^0$ (4 Gev/c)
1.0
0.1
mb. Gev/c^{-2}
0.2
0.6
$|t|$ (Gev/c)^2

42[25]

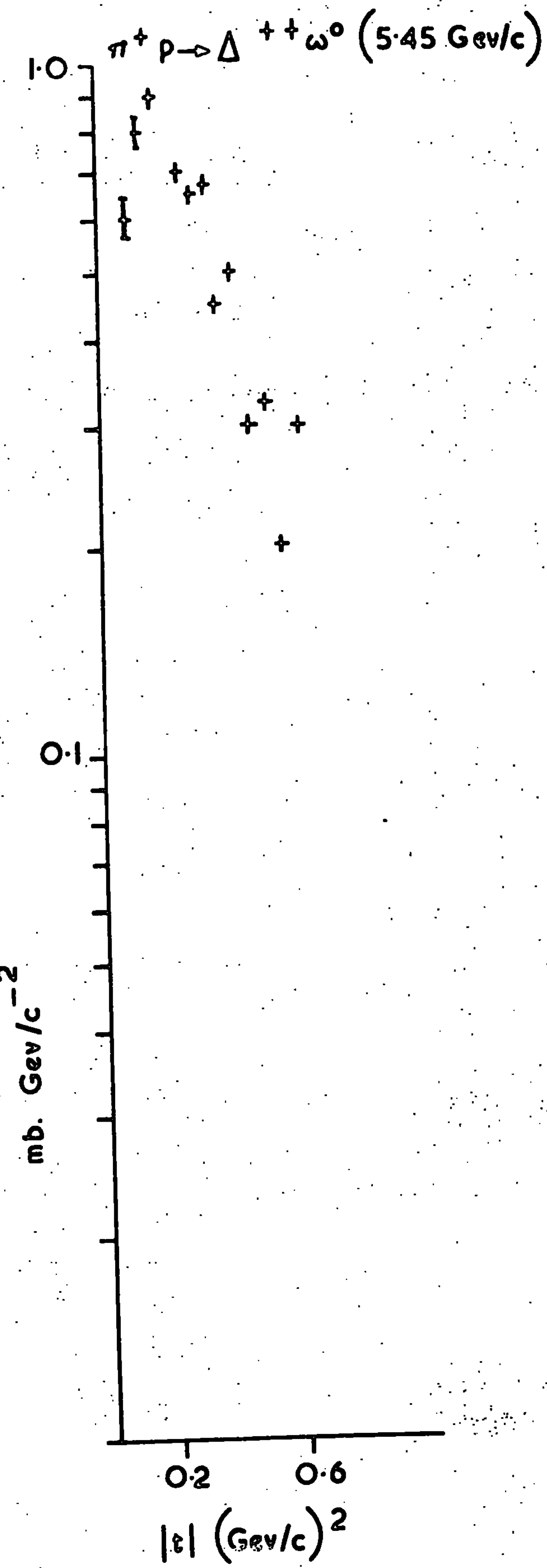

$\pi^+ p \to \Delta^{++}\omega^0$ (5.45 Gev/c)
1.0
0.1
mb. Gev/c^{-2}
0.2
0.6
$|t|$ (Gev/c)^2

43[27]

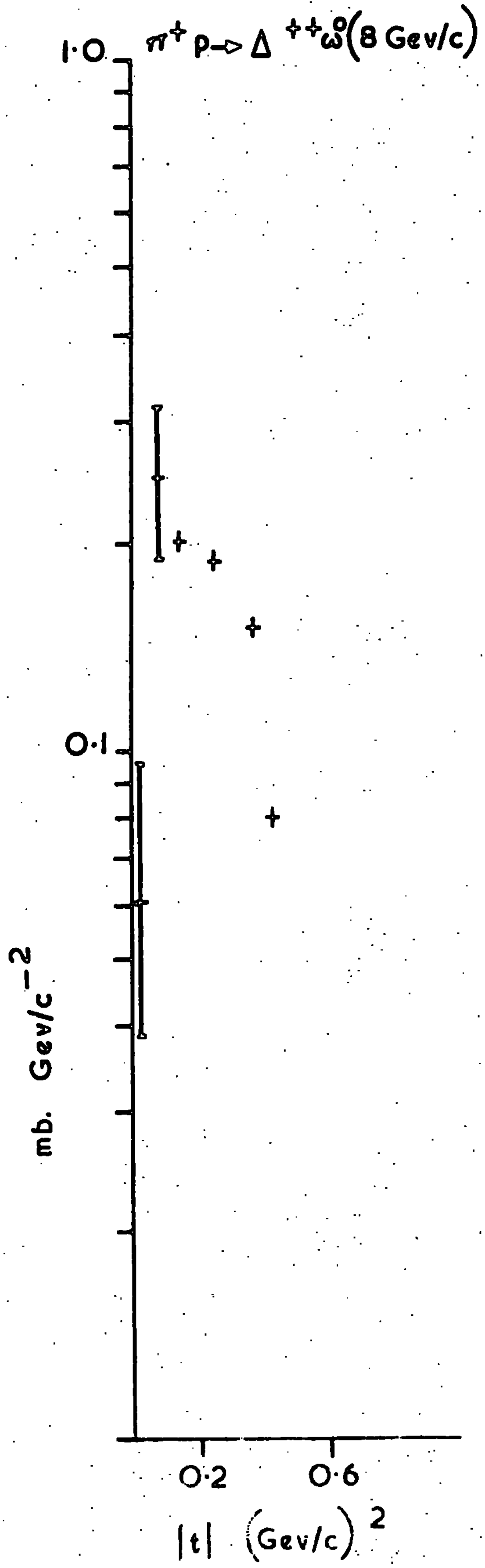

π⁺p → Δ⁺⁺ω⁰(8 Gev/c)
1·0
0·1
mb. Gev/c⁻²
0·2
0·6
|t| (Gev/c)²

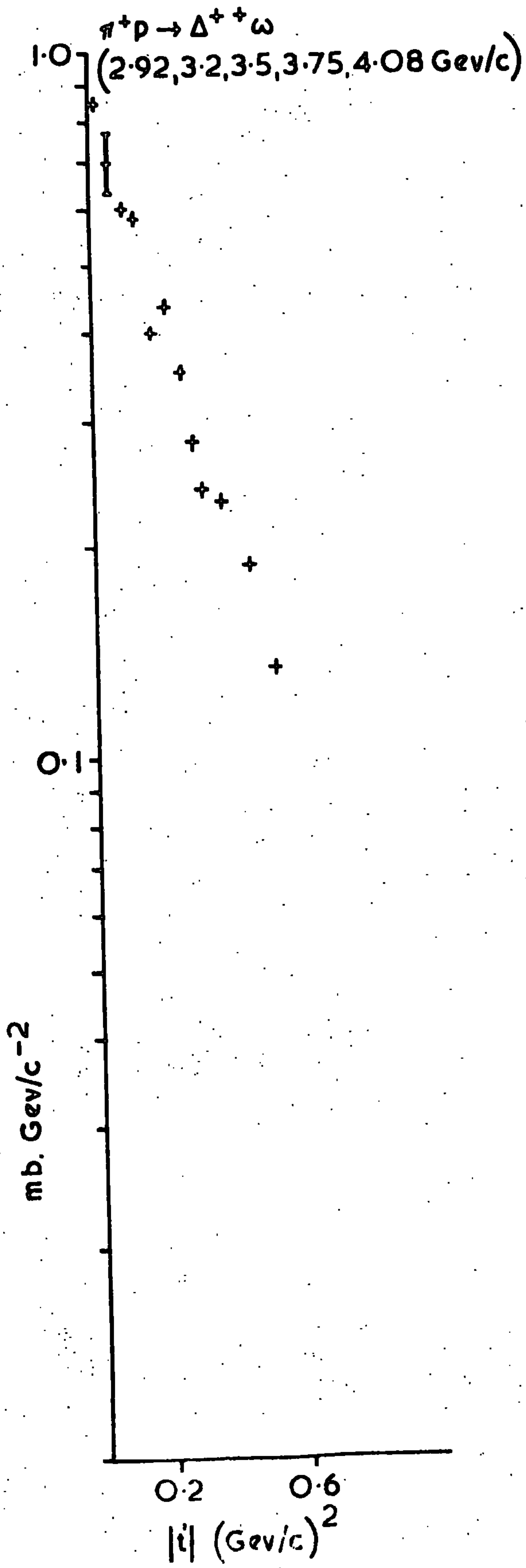

$\pi^+p \to \Delta^{++}\omega$
(2·92, 3·2, 3·5, 3·75, 4·08 Gev/c)
1·0
0·1
mb. Gev/c^{-2}
0·2
0·6
|t'| (Gev/c)^2

45[25]

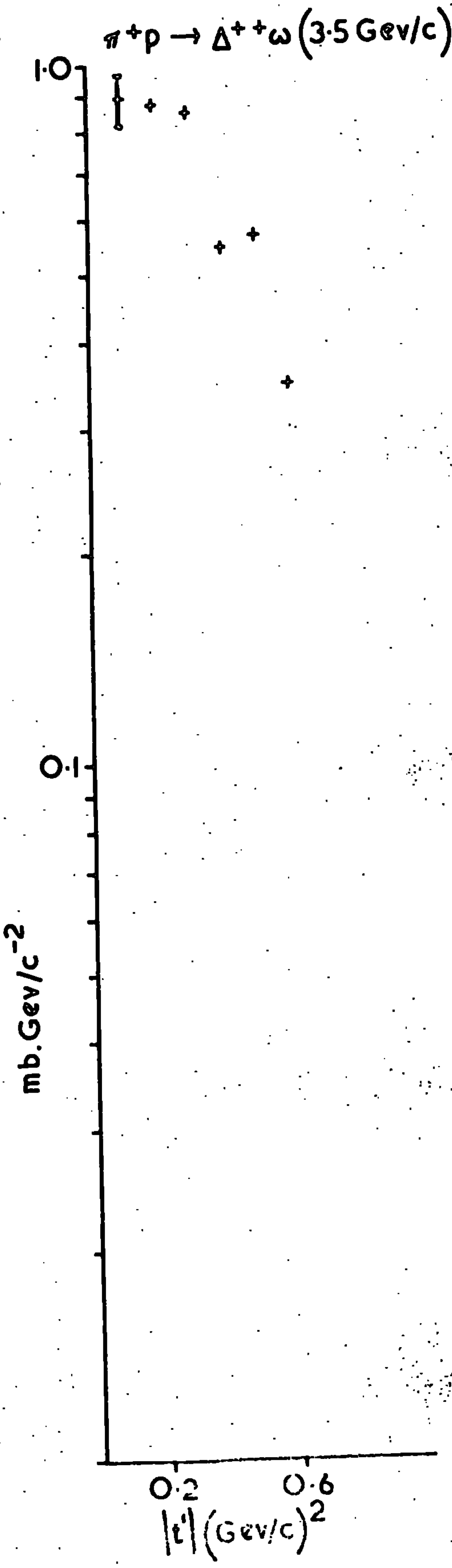

$\pi^+p \to \Delta^{++}\omega$ (3·5 Gev/c)
1·0
0·1
mb. Gev/c^{-2}
0·2
0·6
|t'| (Gev/c)^2

46[30]

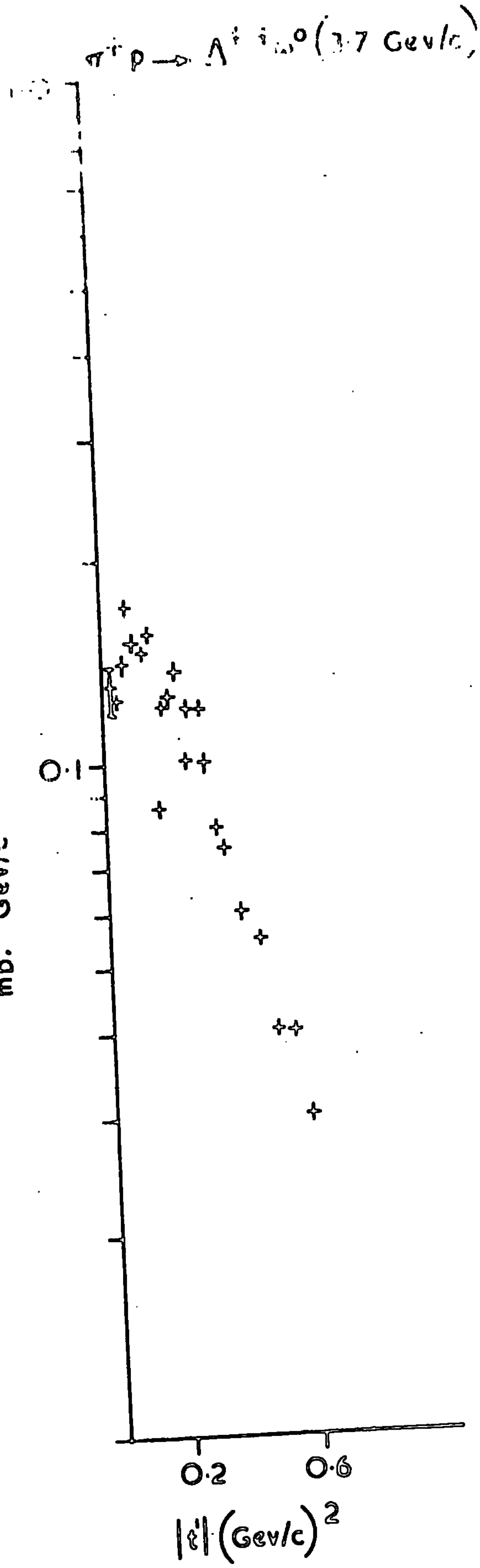

π⁺p → Δ⁺⁺ω⁰ (3.7 Gev/c)
0·1
mb. Gev/c⁻²
0·2
0·6
|t'| (Gev/c)²

47[31]

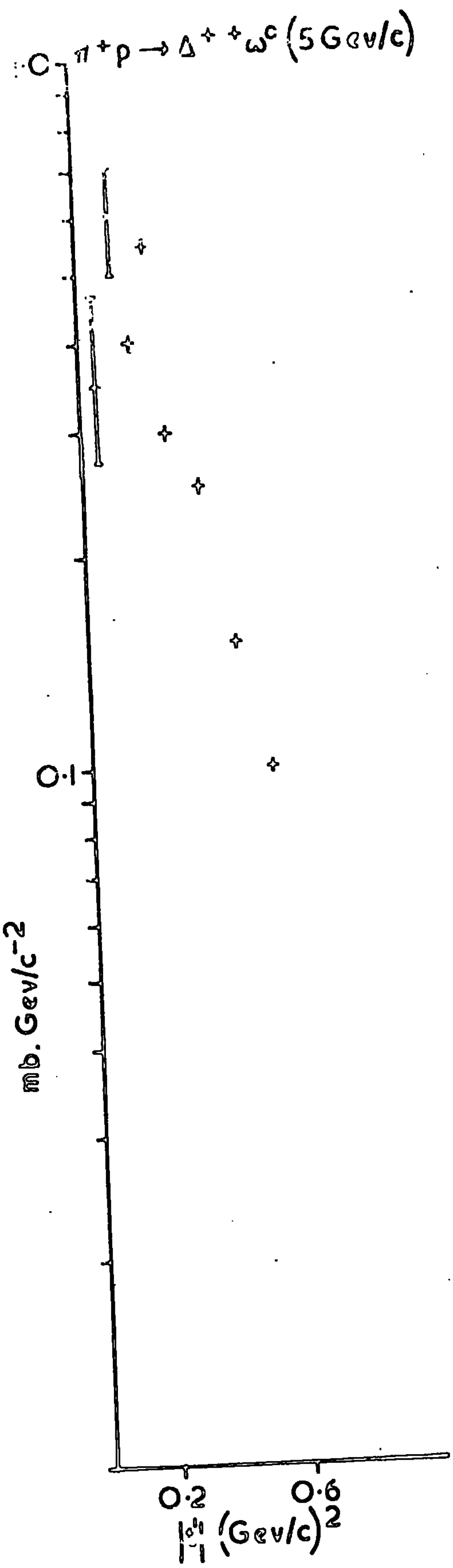

π⁺p → Δ⁺⁺ω⁰ (5 Gev/c)
0·1
mb. Gev/c⁻²
0·2
0·6
(Gev/c)²

48[32]

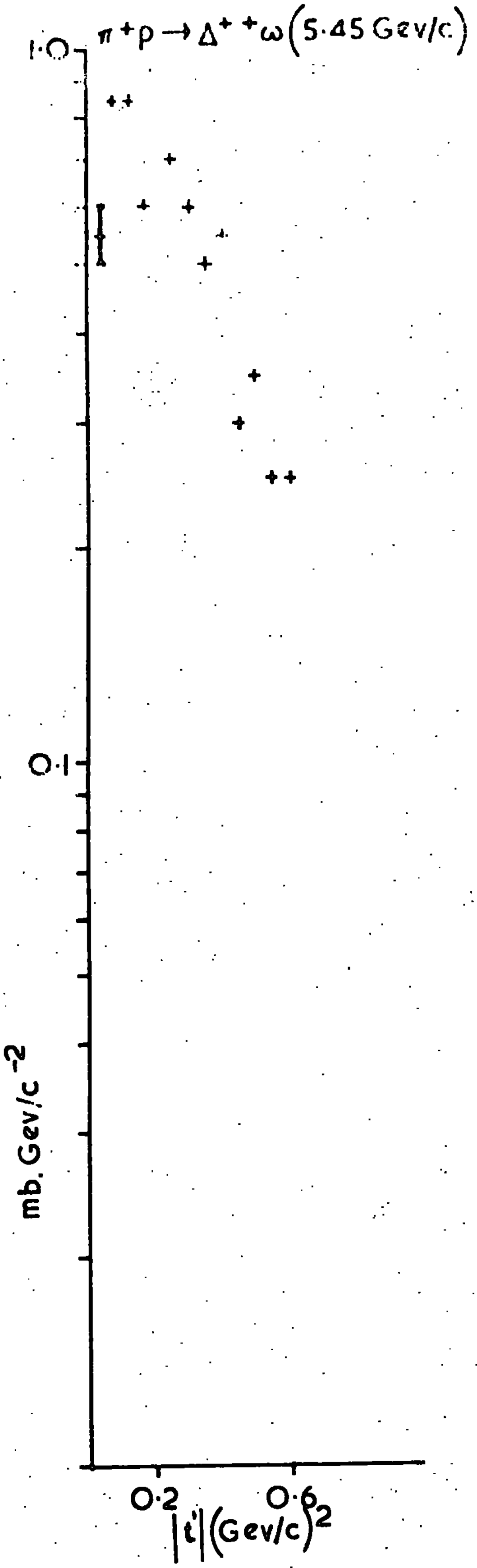

$\pi^+p \to \Delta^{++}\omega$ (5·45 Gev/c)
1·0
0·1
mb. Gev/c^{-2}
0·2
0·6
|t'|(Gev/c)^2

49[27]

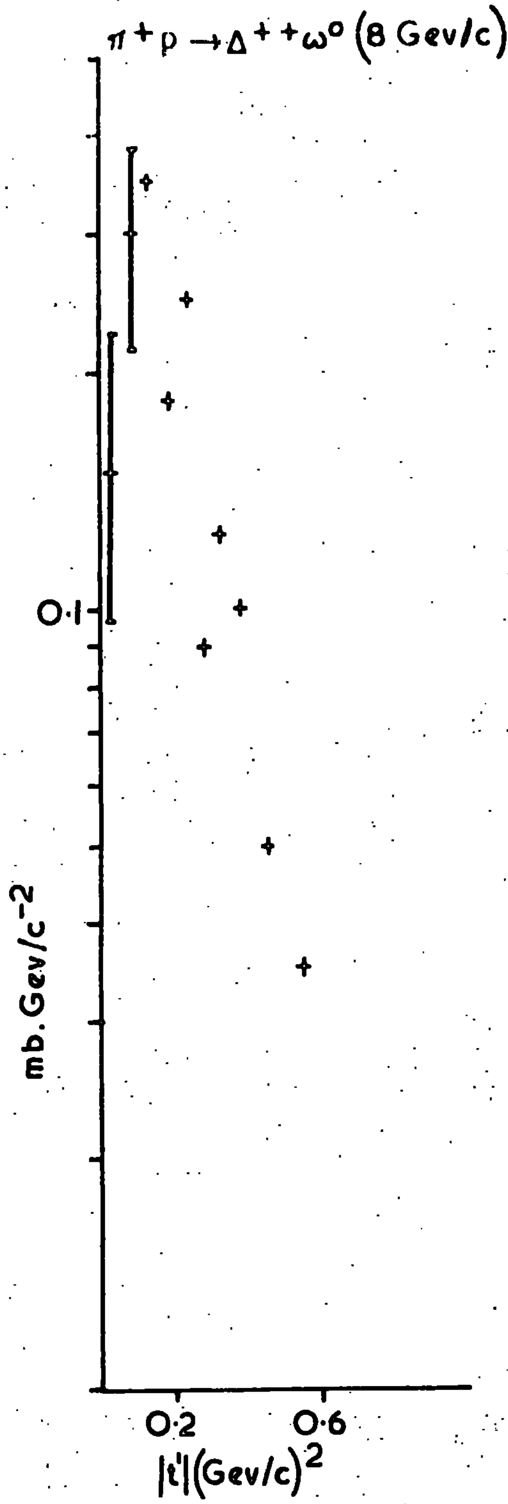

$\pi^+p \to \Delta^{++}\omega^0$ (8 Gev/c)
0·1
mb. Gev/c^{-2}
0·2
0·6
|t'|(Gev/c)^2

50[33]

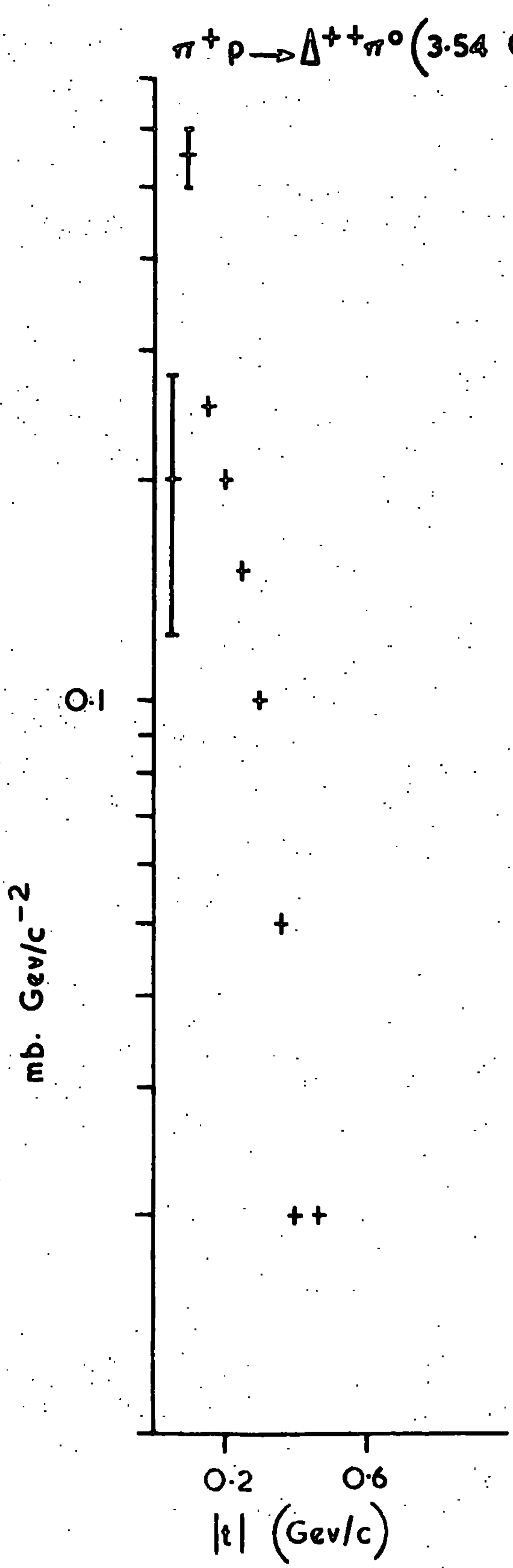

π⁺p → Δ⁺⁺π⁰ (3·54 Gev/c)
0·1
mb. Gev/c⁻²
0·2
0·6
|t| (Gev/c)

51[43]

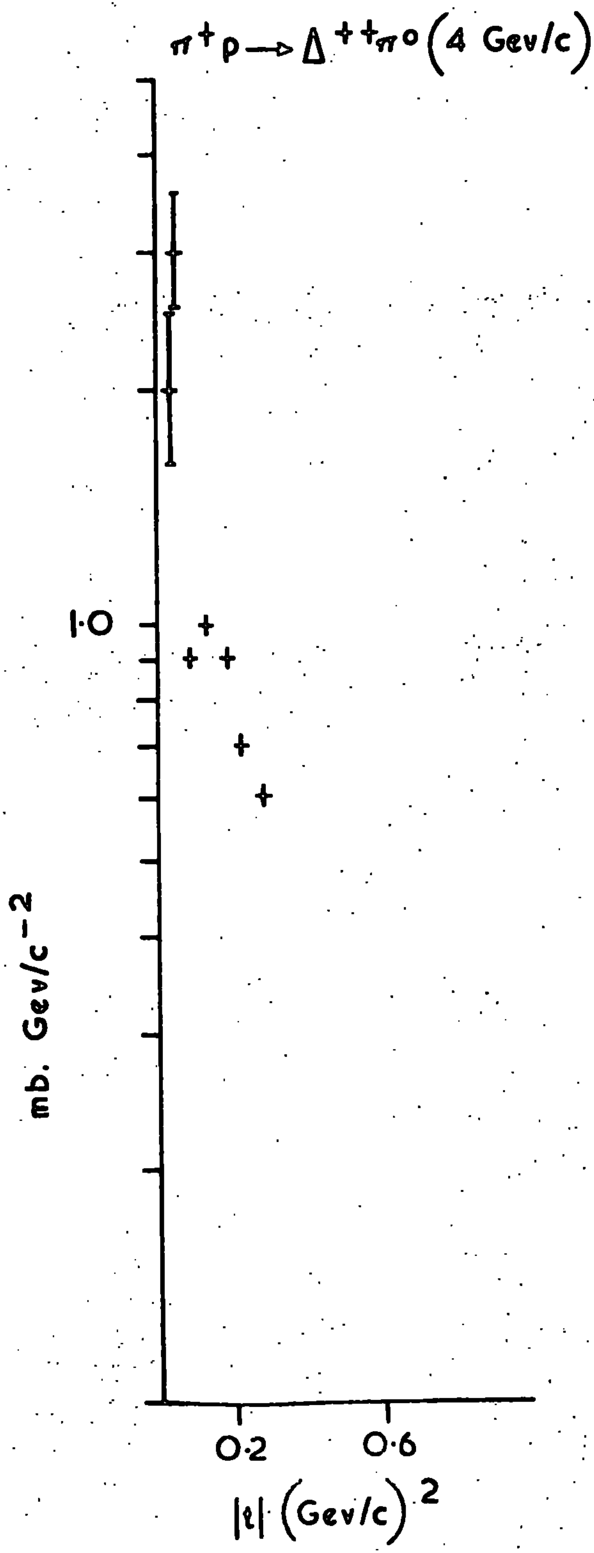

π⁺p → Δ⁺⁺π⁰ (4 Gev/c)
1·0
mb. Gev/c⁻²
0·2
0·6
|t| (Gev/c)²

52[25]

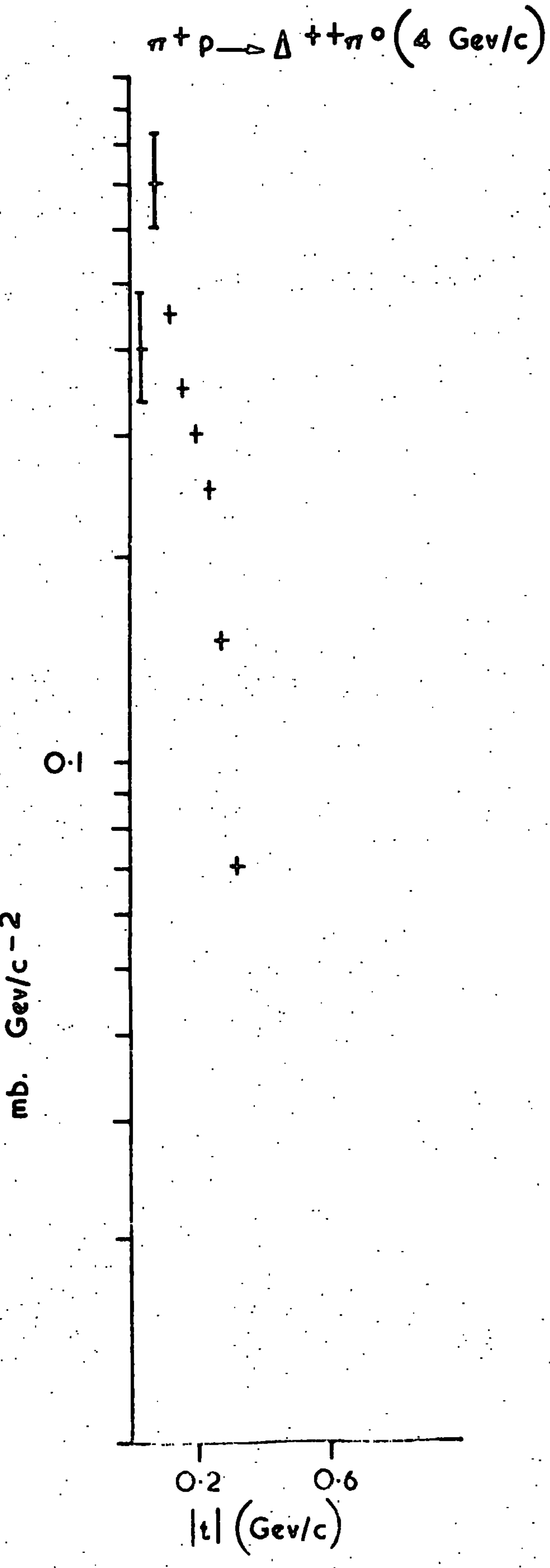

π⁺p → Δ⁺⁺π⁰ (4 Gev/c)
0·1
mb. Gev/c⁻²
0·2
0·6
|t| (Gev/c)

53[44]

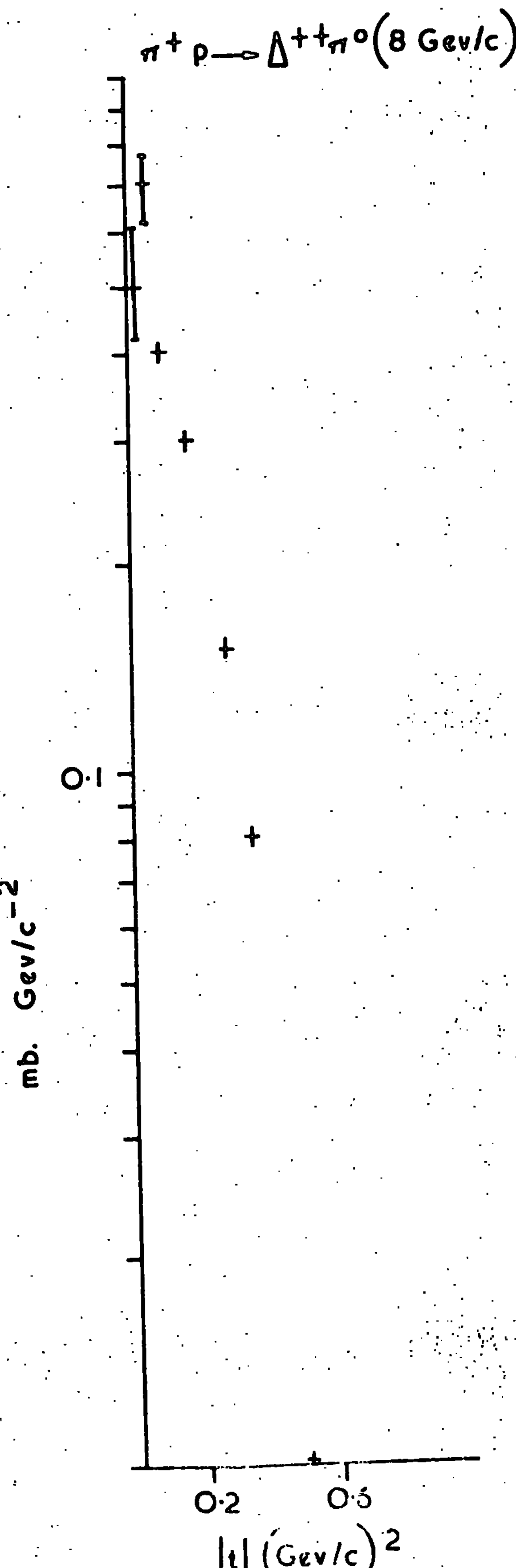

π⁺p → Δ⁺⁺π⁰ (8 Gev/c)
0·1
mb. Gev/c⁻²
0·2
0·5
|t| (Gev/c)²

54[28]

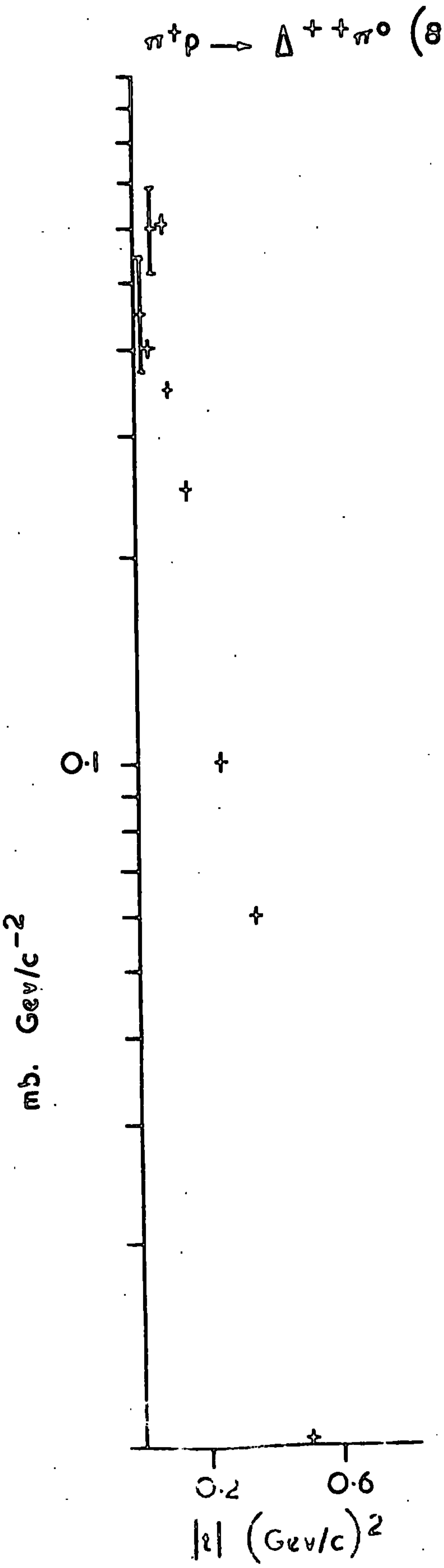

$\pi^+ p \to \Delta^{++}\pi^0$ (8 Gev/c)
0·1
mb. Gev/c^{-2}
0·2
0·6
|t| (Gev/c)^2

55[40]

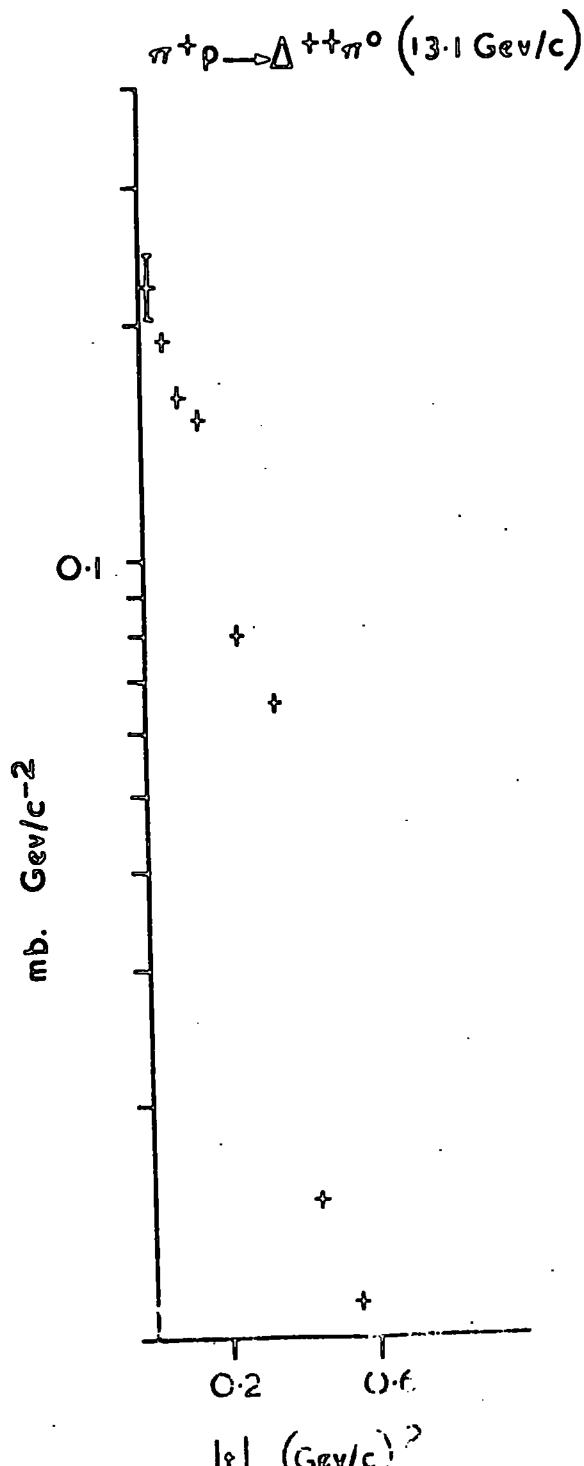

$\pi^+ p \to \Delta^{++}\pi^0$ (13·1 Gev/c)
0·1
mb. Gev/c^{-2}
0·2
|t| (Gev/c)

56[45]

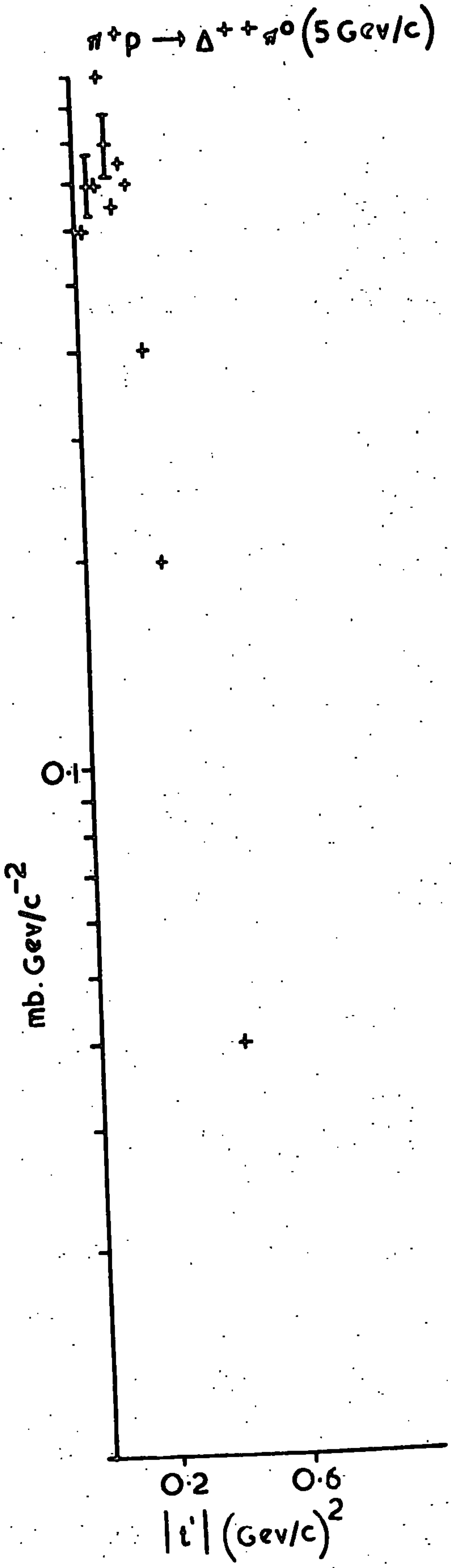

$\pi^+ p \rightarrow \Delta^{++} \pi^0$ (5 Gev/c)
0·1
mb. Gev/c^{-2}
0·2
0·6
$|t'|$ (Gev/c)^2

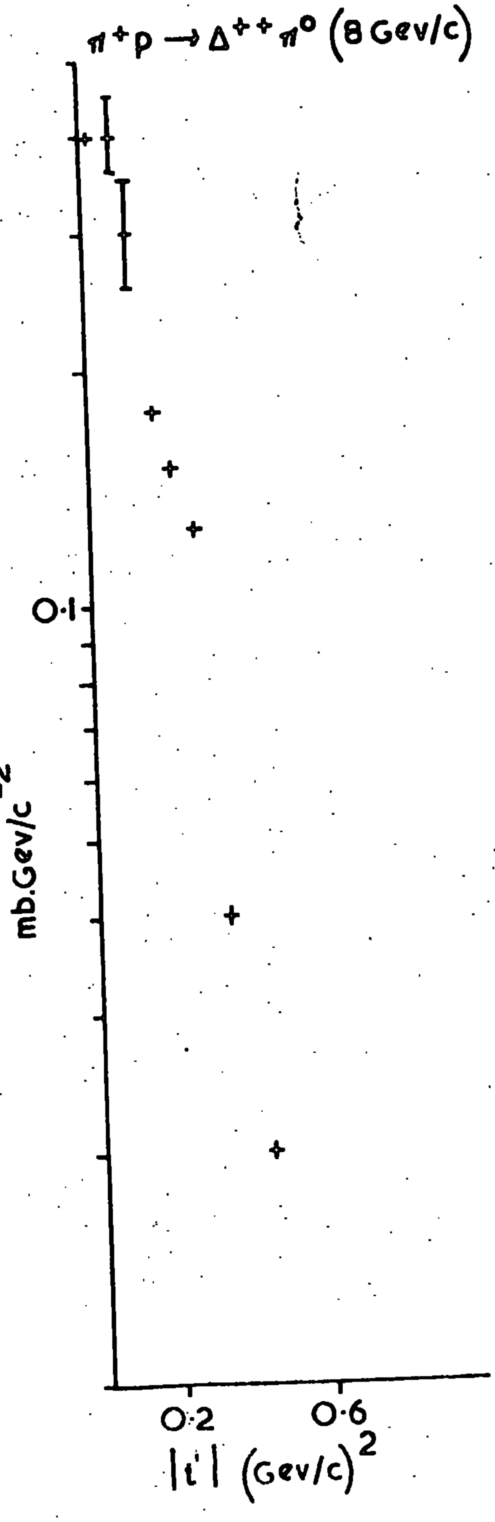

$\pi^+ p \rightarrow \Delta^{++} \pi^0$ (8 Gev/c)
0·1
mb.Gev/c^{-2}
0·2
0·6
$|t'|$ (Gev/c)^2

58[33]

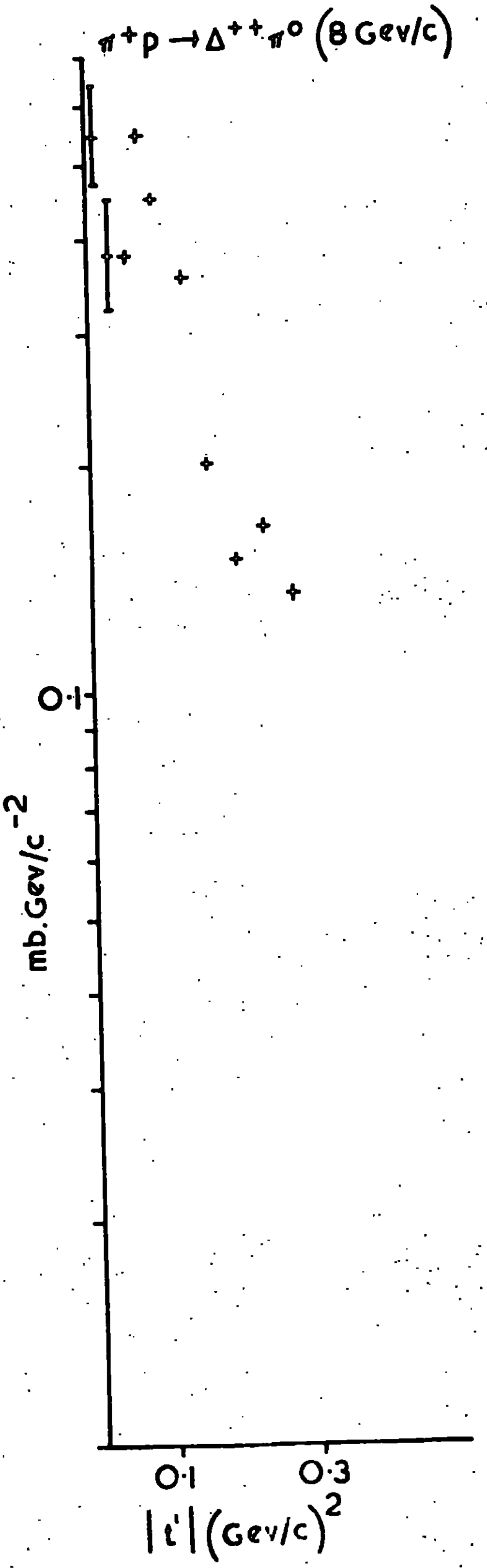

$\pi^+ p \rightarrow \Delta^{++} \pi^0$ (8 Gev/c)
0·1
mb.Gev/c^{-2}
0·1
0·3
$|t'|$ (Gev/c)^2

59[33]

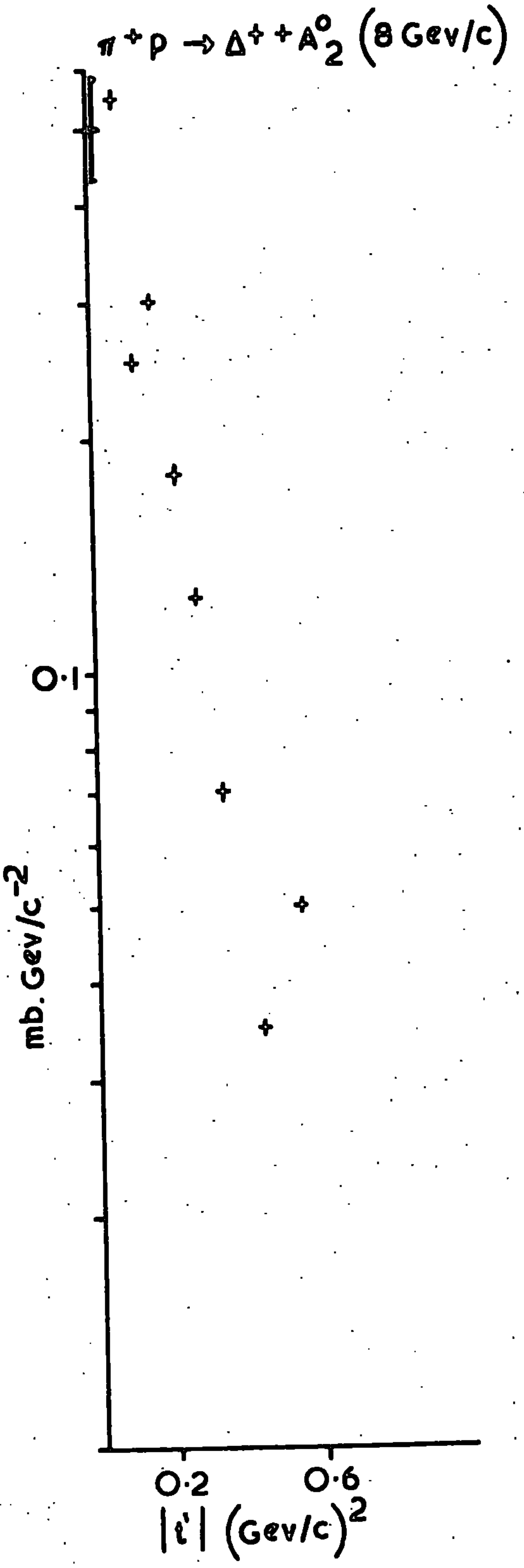

π⁺p → Δ⁺⁺ + A$_2^0$ (8 Gev/c)
0·1
mb.Gev/c^{-2}
0·2
0·6
|t'| (Gev/c)^2

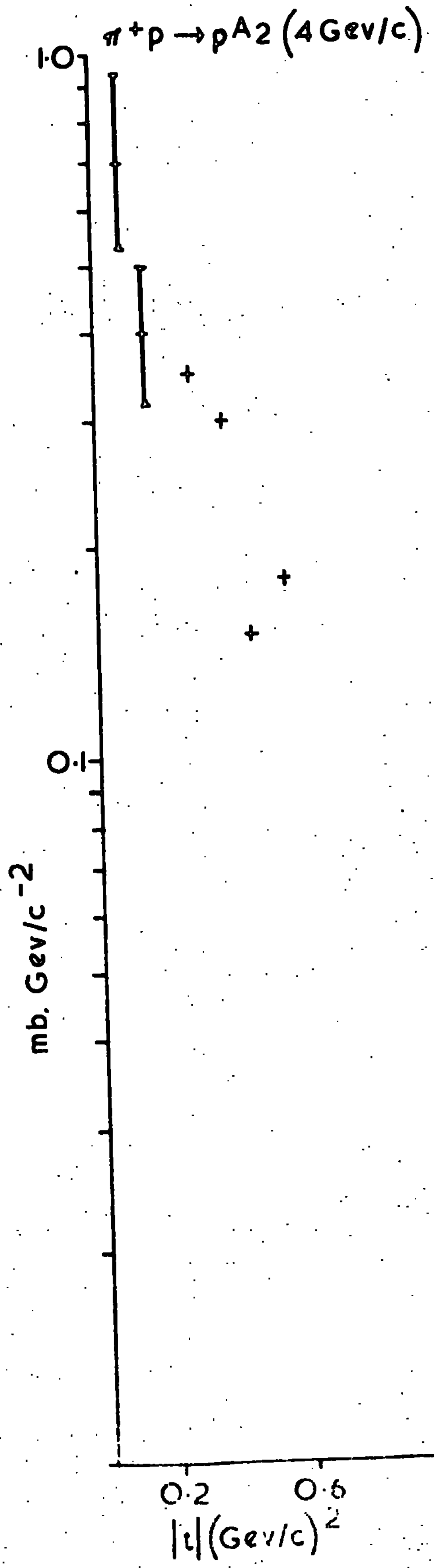

$\pi^+ p \rightarrow p A_2$ (4 Gev/c)
1.0
0.1
mb. Gev/c^{-2}
0.2
0.6
$|t|$ (Gev/c)^2

61[25]

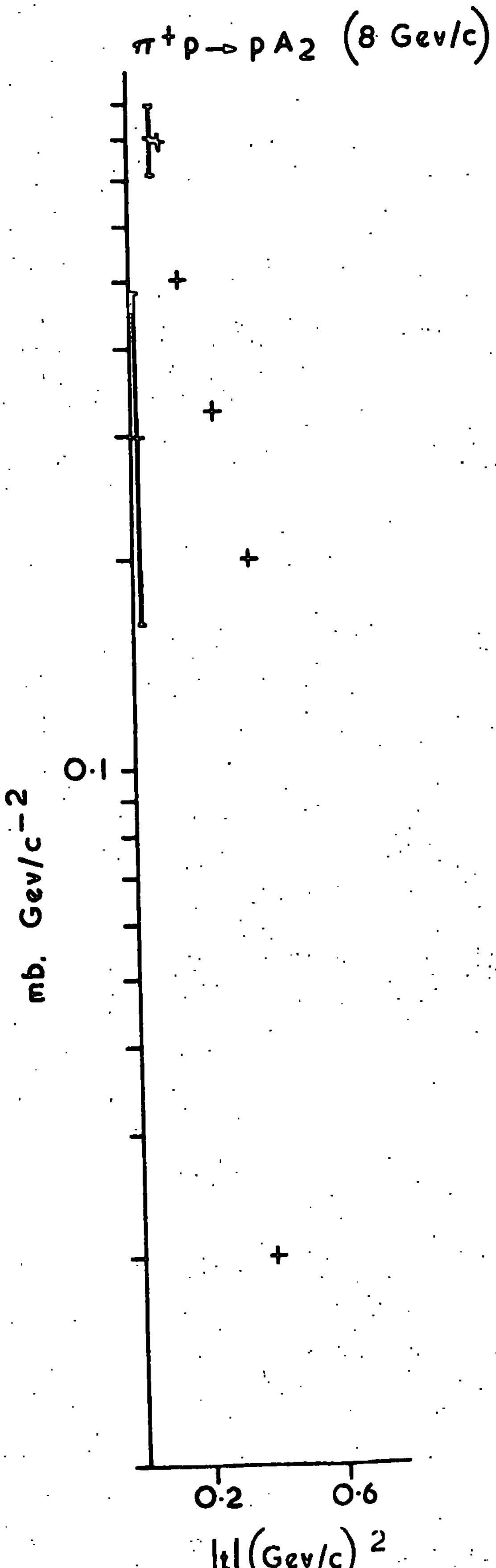

$\pi^+ p \rightarrow p A_2$ (8 Gev/c)
0.1
mb. Gev/c^{-2}
0.2
0.6
$|t|$ (Gev/c)^2

62[28]

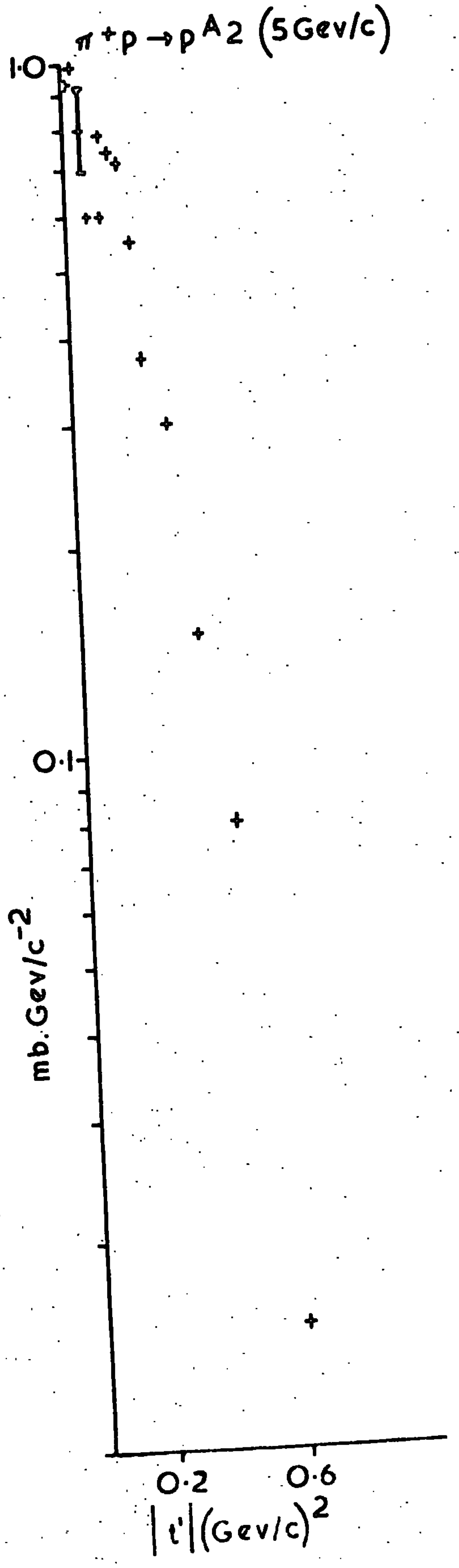
π⁺p → pA2 (5 Gev/c)
1·0
0·1
mb. Gev/c⁻²
0·2
0·6
|t'| (Gev/c)²

63[32]

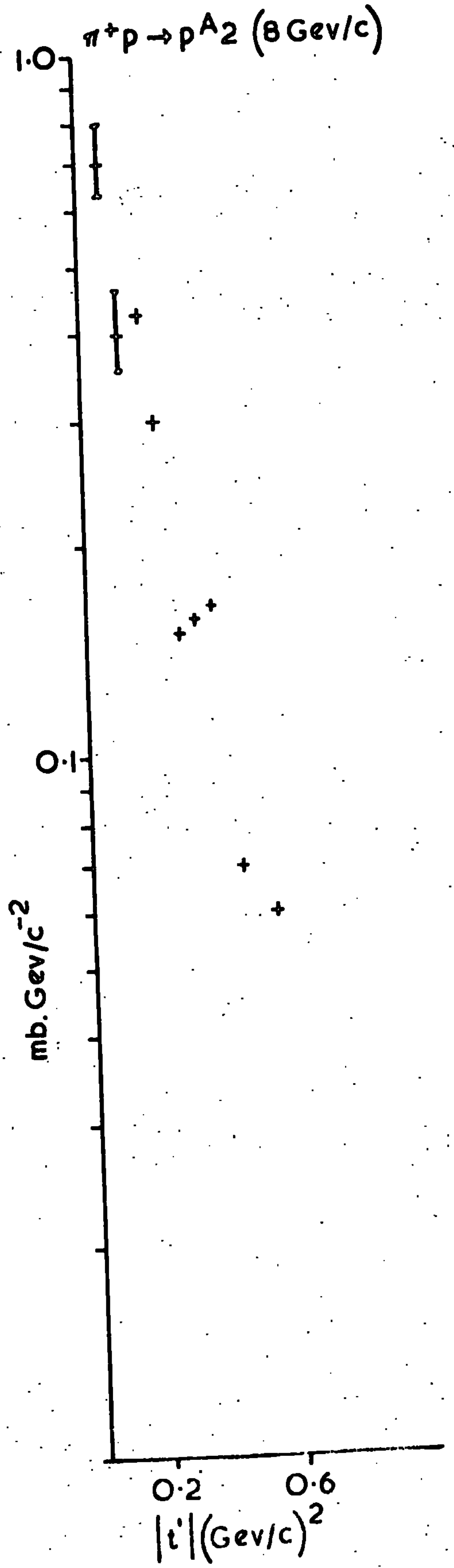
π⁺p → pA2 (8 Gev/c)
1·0
0·1
mb. Gev/c⁻²
0·2
0·6
|t'| (Gev/c)²

64[33]

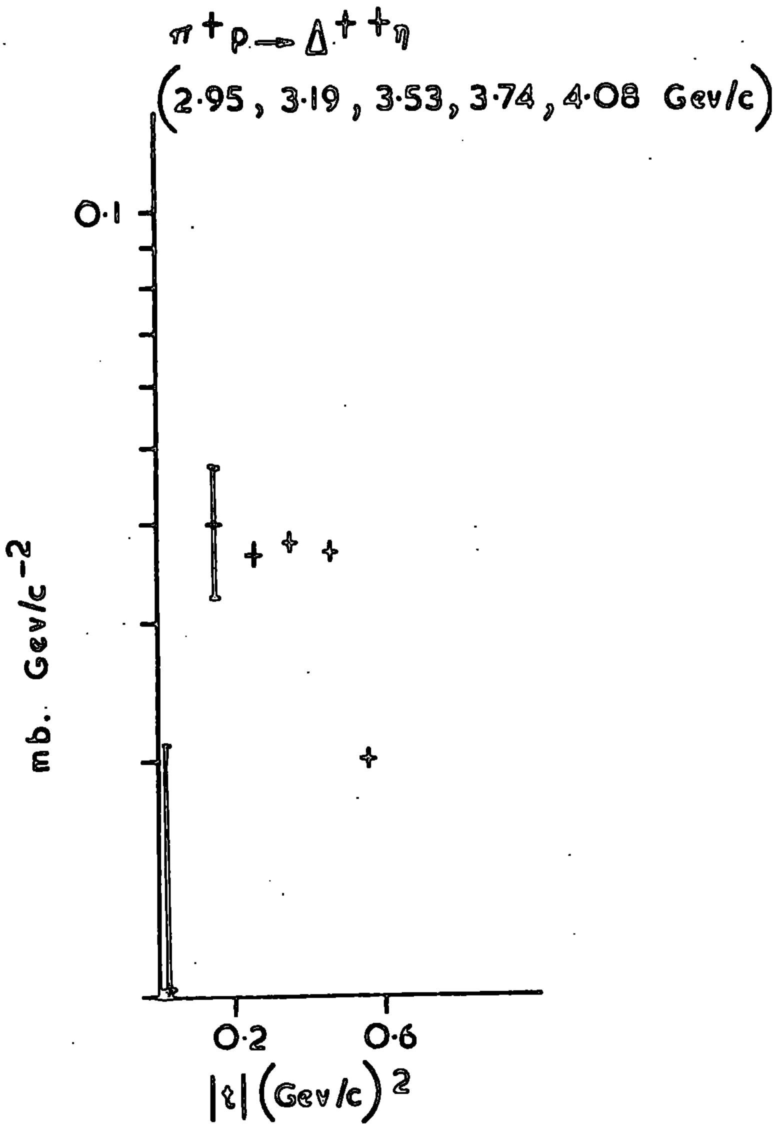

π⁺p → Δ⁺⁺η
(2·95, 3·19, 3·53, 3·74, 4·08 Gev/c)
0·1
mb. Gev/c⁻²
0·2
0·6
|t| (Gev/c)²

65[24]

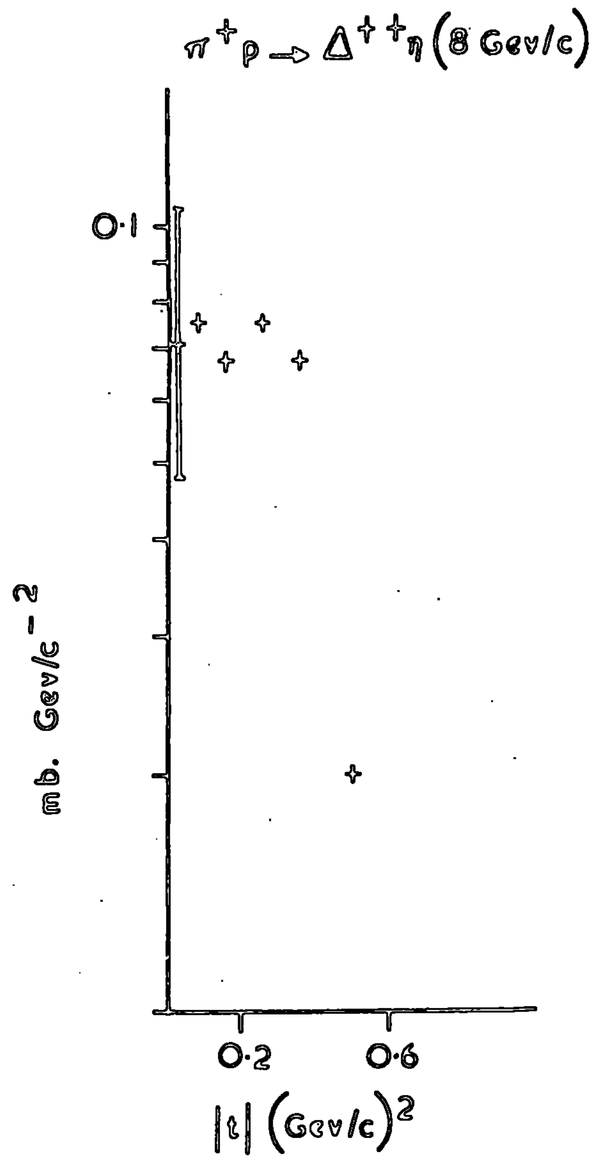

π⁺p → Δ⁺⁺η (8 Gev/c)
0·1
mb. Gev/c⁻²
0·2
0·6
|t| (Gev/c)²

66[28]

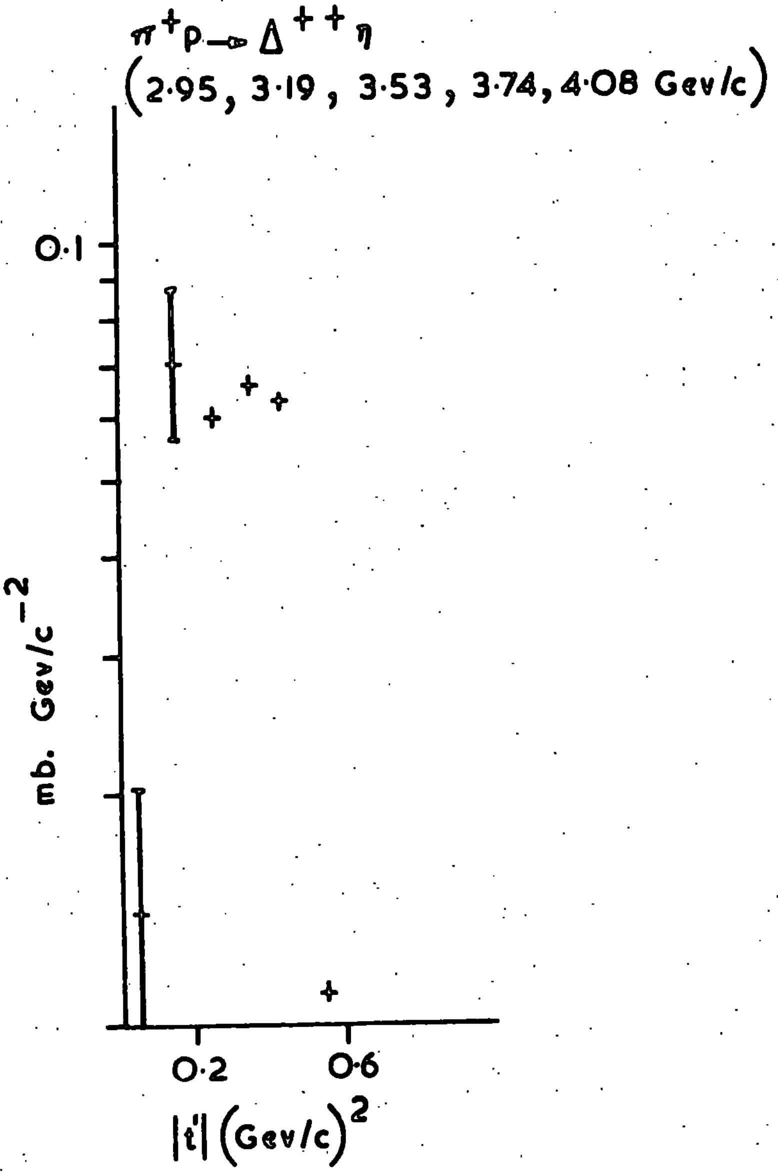

π⁺p → Δ⁺⁺η
(2·95, 3·19, 3·53, 3·74, 4·08 Gev/c)
0·1
mb. Gev/c⁻²
0·2
0·6
|t'| (Gev/c)²

67[24]

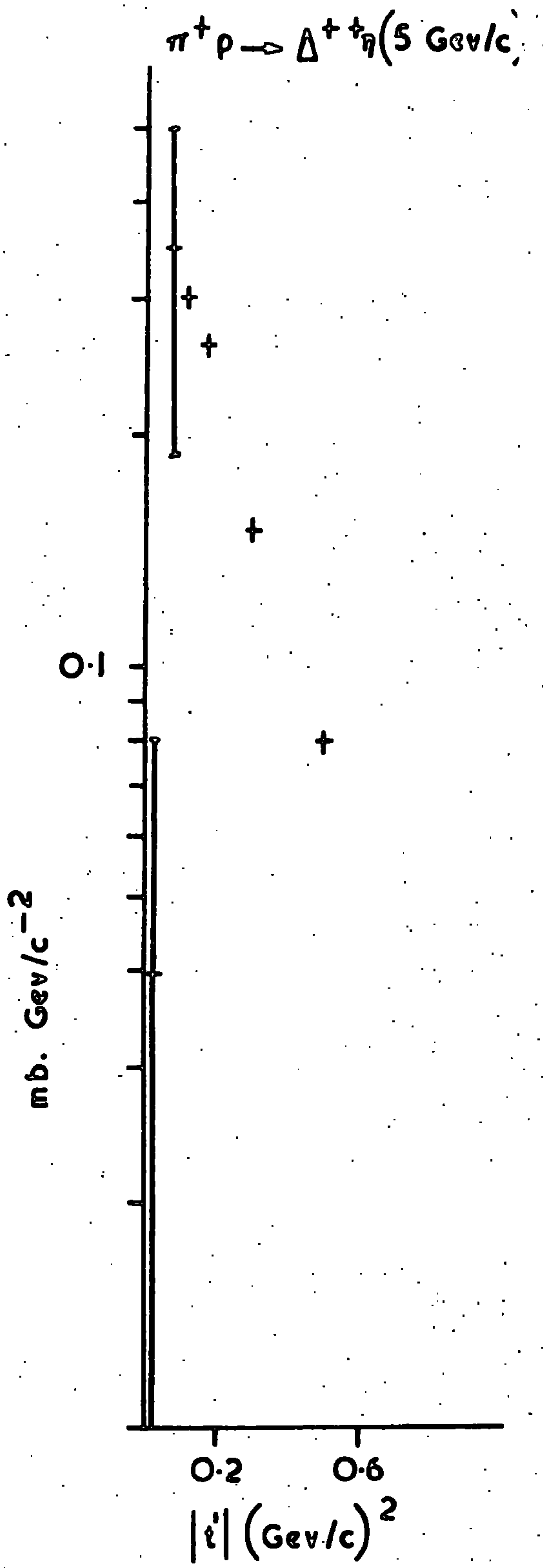

π⁺p → Δ⁺⁺η (5 Gev/c)
0·1
mb. Gev/c⁻²
0·2
0·6
|t'| (Gev/c)²

68[32]

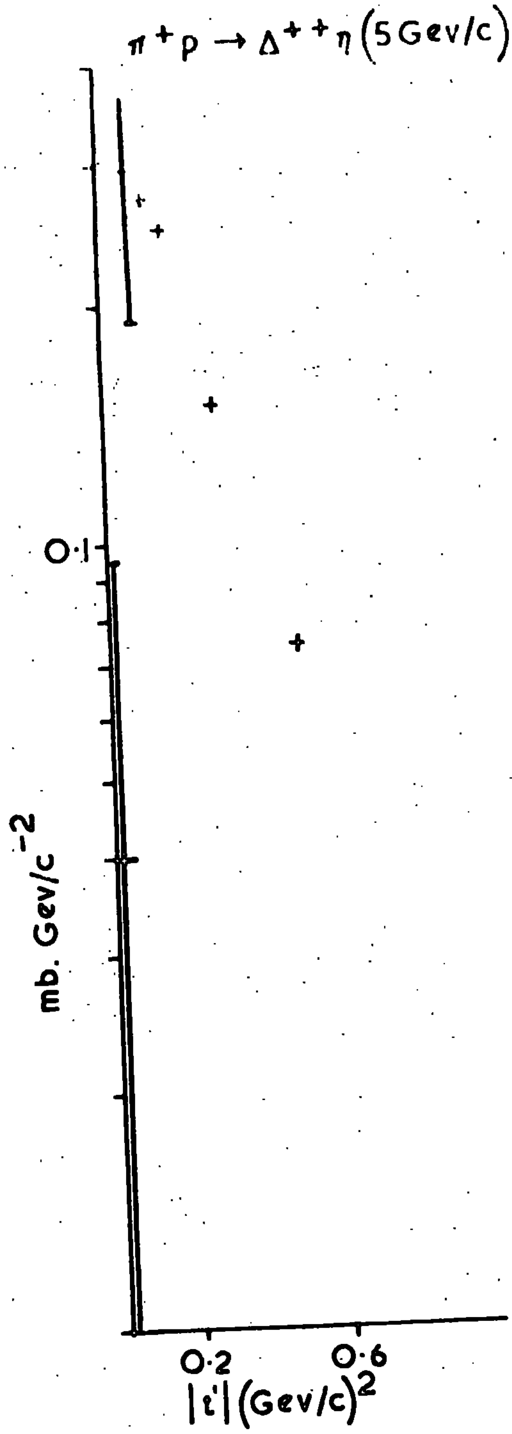
$\pi^+ p \rightarrow \Delta^{++} \eta$ (5 Gev/c)
0·1
mb. Gev/c^{-2}
0·2
0·6
|t'| (Gev/c)^2

69[35]

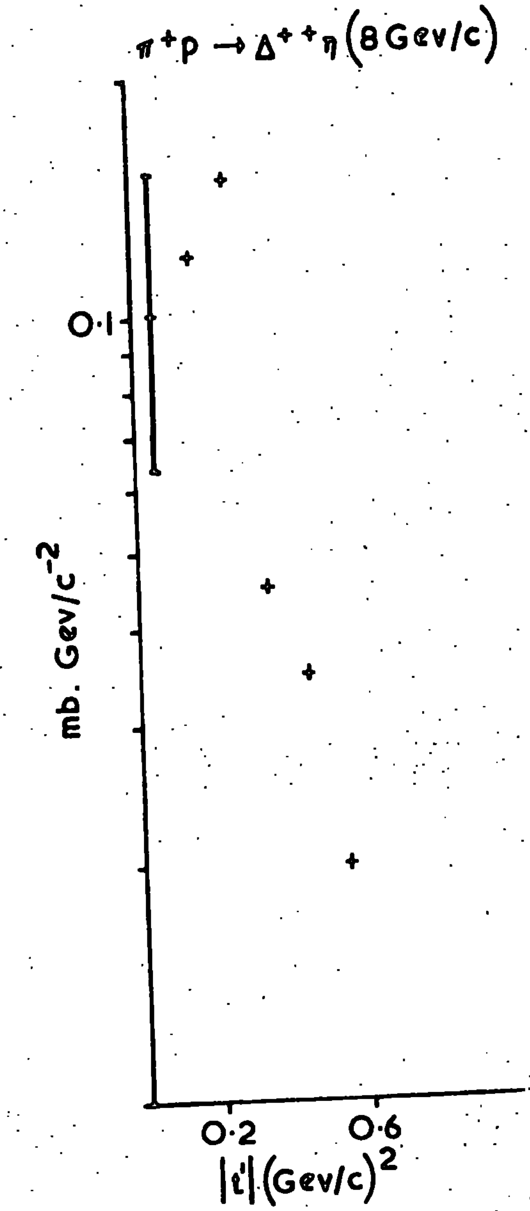
$\pi^+ p \rightarrow \Delta^{++} \eta$ (8 Gev/c)
0·1
mb. Gev/c^{-2}
0·2
0·6
|t'| (Gev/c)^2

70[33]

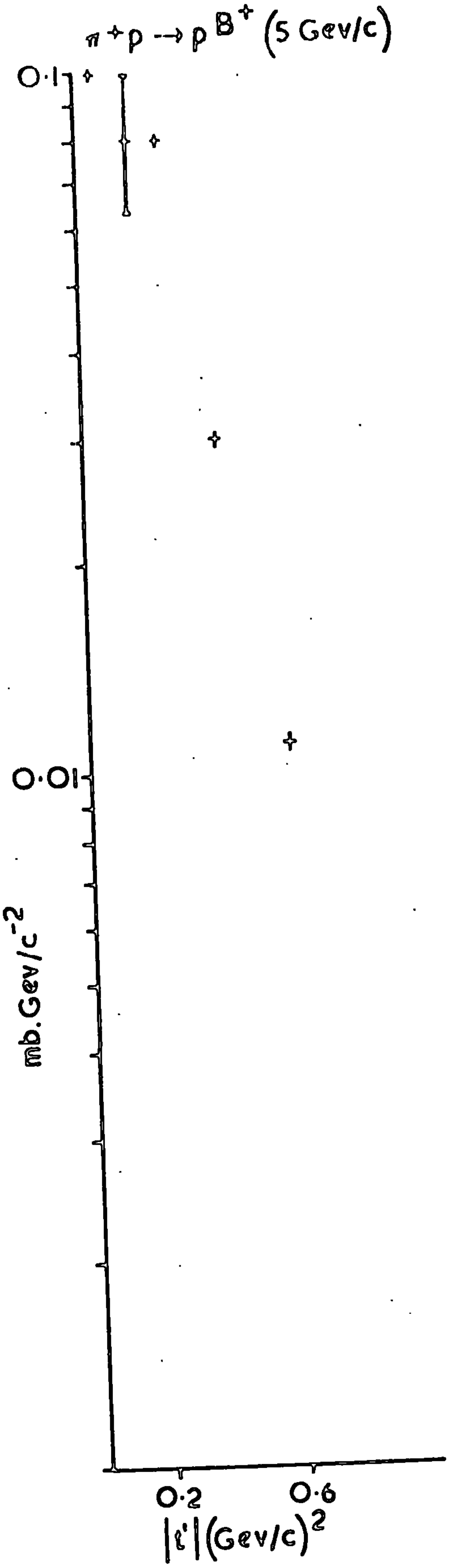

π⁺p → pB⁺ (5 Gev/c)
0·1
0·01
mb.Gev/c⁻²
0·2
0·6
|t'| (Gev/c)²

71[32]

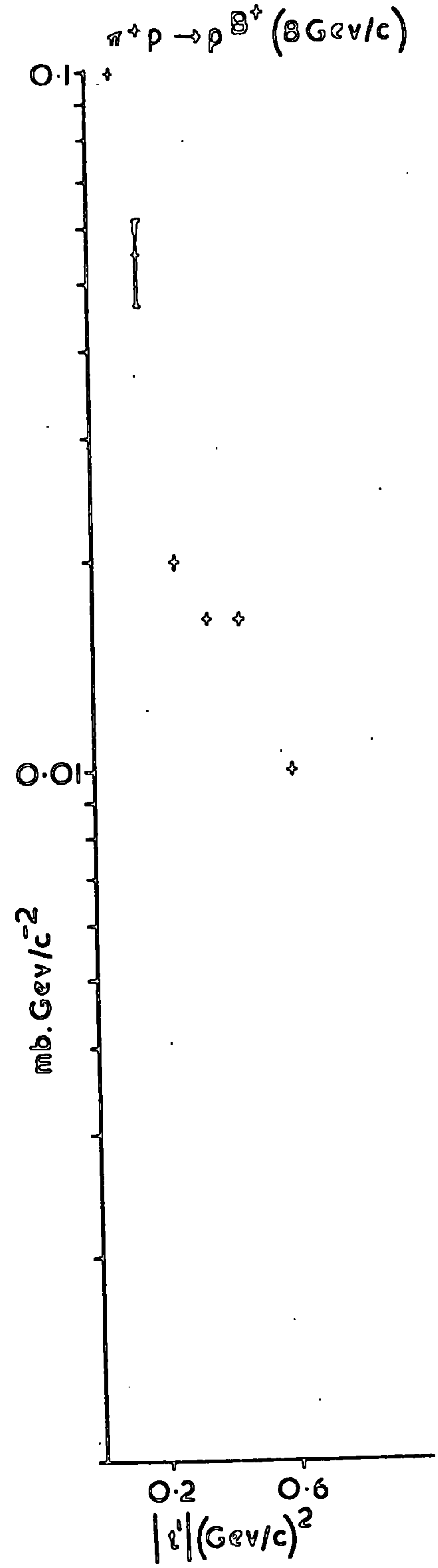

π⁺p → pB⁺ (8 Gev/c)
0·1
0·01
mb.Gev/c⁻²
0·2
0·6
|t'| (Gev/c)²

72[33]

FIGURES

24. t_{min} for a given incident pion momentum for the reaction $\pi^+p \to \Delta^{++}\eta$

25. " " " " " " " " pB^+

26. $d\sigma/d|t|$ vs $|t|$ and $d\sigma/d|t'|$ vs $|t'|$ for the reaction $\pi^+p \to \pi^+p$

27. " " " " " " for the reactions $\pi^+p \to \pi^+p$, pA_1, and pA_3.

28. $d\sigma/d|t|$ vs $|t|$ and $d\sigma/d|t'|$ vs $|t'|$ for the reactions $\pi^+p \to \Delta^{++}\rho^o$

29. " " " " " " " " " $\Delta^{++}f^o$

30. " " " " " " " " " $p\rho^+$

31. " " " " " " " " " pg^+

32. " " " " " " " " " $\Delta^{++}\omega^o$

33. " " " " " " " " " $\Delta^{++}\pi^o$

34. $d\sigma/d|t|$ vs $|t|$ for the reaction $\pi^+p \to \Delta^{++}A_2^o$

35. $d\sigma/d|t|$ vs $|t|$ & $d\sigma/d|t'|$ vs $|t'|$ for the reaction $\pi^+p \to pA_2^+$

36. " " " " " " " $\to \Delta^{++}\eta$

37. $d\sigma/d|t'|$ vs $|t'|$ for the reaction $\pi^+p \to pB^+$.

TABLES

REFERENCES

1. Martin, A.D. and Spearman, T.D., Elementary Particle Theory, North Holland, 1970.

2. Soviet Physics:- J.E.T.P., 34, 1972, p 725.

3. Bethe, H.A. and Jackiw, R., Intermediate Quantum Mechanics, Benjamin Inc. 1968.

4. Goebel, C., 1958, Phys. Rev. Lett., 1, p 337.

5. Bonsignori, F. and Selleri, F., 1960, Nuovo Cim., 15, p 465.

6. Salzman, F. and Salzman, G., 1960, Phys. Rev. Lett., 5, p 377

7. Salzman, F. and Salzman, G., 1960, Phys. Rev. 120, p 599

8. Salzman, F. and Salzman, G., 1961, Phys. Rev. 121, p 1541

9. Drell, 1960, Phys. Rev. Lett. 5, p 278.

10. Drell, 1961, Rev. Mod. Phys. 33, p 458.

11. Pilkuhn, H. The Interactions of Hadrons, North Holland, 1967, p279.

12. Pilkuhn, H., The Interactions of Hadrons, North Holland, 1967, p280

13. Nyborg, R., 1965, Phys. Rev., 140B, p 921.

14. Pilkuhn, H., The Interactions of Hadrons, North Holland, 1967, p290.

15. Ferrari, E. and Selleri, F., 1961, Nuovo Cim. 21, p 1028.

16. Ferrari, E. and Selleri, F., 1962, Suppl. Nuovo Cim. 24, p 453.

17. Ferrari, E. and Selleri, F., 1963, Nuovo Cim. 27, p 1450.

18. Regge, T., 1969, Nuovo. Cim., 14, p 951.

19. Regge, T., 1960, Nuovo Cim., 18, p 947.

20. Morrison, D.R.O., 1968, Phys. Rev. 165, p 1690.

21. Pearson, G., Thesis, Durham University.

22. Collins, P.D.E., 1971. Phys. Reports 1 4, p203.

23. Flaminio, E., Hansen, T.D., Morrison, D.R.O., and Tovey, N., 1970, Compilation of cross-sections IV $\pi^{\mp}$ induced reactions CERN/HERA 70-5.

24. 2.95; 3.19; 3.74 and 4.08 GeV/c Brown, D. 1970, Phys. Rev. D1, p3053.

25. 4.0 GeV/c Aachen-Berlin-Birmingham-Bonn-Hamburg-London (I.C)-Munchen, 1965, Phys. Rev. B138, p897.

26. 4.0 GeV/c Aderholz, 1965, Nuovo Ciment, 35, p659.

27. 5.45GeV/c Bloodworth, 1971, Nucl. Phys. B35, p79.

28. 8.0 GeV/c Deutschmann, 1965, Phys. Lett., 19, p608.

29. 11.7GeV/c Maddock, R.O., 1971, Nuovo Cim., 5A, p433.

30. 3.5 GeV/c Ronat, 1972, Nucl. Phys. B38, p20.

31. 3.7 GeV/c Abrams, 1970, Phys. Rev. Lett., 25, p617.

32. 5.0 GeV/c Pols, C.L., 1970, Nucl. Phys. B25, p109.

33. 8.0 GeV/c Aachen-Berlin-Cern, 1968, Nucl. Phys. B8, p45.

34. 13.10GeV/c Gaidos, 1970, Phys. Rev. D1, p3190

35. 5.0 GeV/c Schotanus, 1970, Nucl. Phys, B22, p45.

36. 13.1 GeV/c Gaidos, 1971, Nucl. Phys. B26, p225.

37. 3.6 GeV/c MacNaughton, 1971, Nucl. Phys. B33, p101.

38. 4.0 GeV/c Aachen-Berlin-Birmingham-Bonn-Hamburg-London (I.C) - Munchen, 1964, Phys. Lett. 10, p248.

39. 4.0 GeV/c Aderholz and Bartsch, 1964, Nuovo Cim. 34, p495.

40. 8.0 GeV/c Deutschmann, 1965, Phys. Lett. 18, p351.

41. 8.0 GeV/c Aderholz and Deutschmann, 1968, Phys. Lett., 27B, p174.

42. 8.0. GeV/c Bartsch, 1970, Nucl. Phys. B22, p109.

43. 3.54 GeV/c Abolins, 1964, Phys. Rev. B136, p195.

44. 4.0 GeV/c Bartisch, 1964, Phys. Lett. 10, p229.

45. 13.1 GeV/c Scharenguivel, 1971, Nucl. Phys. B36, p363.

ACKNOWLEDGEMENTS

I should like to acknowledge the financial support of Durham University for providing a Research Assistantship which enabled me to do the work, the invaluable help of Dr. D. Evans under whose supervision I came, the pains-taking preparation of the numerous graphs and diagrams by Dorothy Pickles, Janet Gibson and Thelma Richardson and also the typing of the end product by Dorothy Anson. To these and to many other people who made less direct contributions, I am most grateful.